SEMI-CLASSICAL DESCRIPTION OF SPINODAL INSTABILITIES OF ASYMMETRIC NUCLEAR MATTER IN A RELATIVISTIC STOCHASTIC MODEL

A THESIS SUBMITTED TO
THE GRADUATE SCHOOL OF NATURAL AND APPLIED SCIENCES
OF
MIDDLE EAST TECHNICAL UNIVERSITY

SELEN SAATCİ

IN PARTIAL FULFILLMENT OF THE REQUIREMENTS
FOR
THE DEGREE OF MASTER OF SCIENCE
IN
PHYSICS

AUGUST 2013

Approval of the thesis:

SEMI-CLASSICAL DESCRIPTION OF SPINODAL INSTABILITIES OF ASYMMETRIC NUCLEAR MATTER IN A RELATIVISTIC STOCHASTIC MODEL

submitted by **SELEN SAATCİ** in partial fulfillment of the requirements for the degree of **Master of Science in Physics Department, Middle East Technical University** by,

Prof. Dr. Canan Özgen _____
Dean, Graduate School of **Natural and Applied Sciences**

Prof. Dr. Mehmet T. Zeyrek _____
Head of Department, **Physics**

Prof. Dr. Osman Yılmaz _____
Supervisor, **Department of Physics, METU**

Prof. Dr. Şakir Ayık _____
Co-supervisor, **Physics Department, Tennessee Tech University**

Examining Committee Members:

Prof. Dr. Şakir Ayık
Physics Department, Tennessee Tech University _____

Prof. Dr. Osman Yılmaz
Department of Physics, METU _____

Prof. Dr. Ayşe Ataç Nyberg
Department of Physics, KTH Royal Institute of Technology _____

Prof. Dr. Ahmet Gökalp
Department of Physics, Bilkent University _____

Prof. Dr. Gürsevil Turan
Department of Physics, METU _____

Date: _____

I hereby declare that all information in this document has been obtained and presented in accordance with academic rules and ethical conduct. I also declare that, as required by these rules and conduct, I have fully cited and referenced all material and results that are not original to this work.

Name, Last Name: SELEN SAATCİ

Signature :

ABSTRACT

SEMI-CLASSICAL DESCRIPTION OF SPINODAL INSTABILITIES OF ASYMMETRIC NUCLEAR MATTER IN A RELATIVISTIC STOCHASTIC MODEL

Saatci, Selen
M.S., Department of Physics
Supervisor : Prof. Dr. Osman Yılmaz
Co-Supervisor : Prof. Dr. Şakir Ayık

August 2013, 95 pages

A hot and dense nuclear matter expands and cools down. It may enter the spinodal region, where uniform matter is mechanically unstable. Small amplitude density fluctuations grow rapidly and leads to formation of nuclear clusters, called nuclear multifragmentation process. It is considered that the spinodal instability provides a dynamical mechanism for liquid-gas phase transformation of nuclear matter. In this work, the spinodal dynamics of the asymmetric nuclear matter is studied within the stochastic extension of the relativistic mean field approximation based on a nonlinear Walecka Model. The early growth of the density fluctuations and the primary size of the condensation regions are investigated in the semi-classical limit. The mediator ρ meson is added to the Walecka model in order to generate the isospin dependence of the nuclear matter. The growth rates of the most unstable modes are determined with the corresponding shortest growth times. In order the specify the temperature and isospin asymmetry dependence of the system, the calculations are implemented for different initial conditions at different asymmetries. The most unstable activity is occurred in the symmetric nuclear matter and decreases as the system becomes richer in neutrons. The baryon density correlation function is also presented as a function of the distance between two space

points and the early size of the condensing regions are determined. The results are found to be consistent with the ranges of the dispersion relation for the most unstable modes. Also, the boundary of the spinodal region is evaluated for the cases with different asymmetries and the isospin dependence of the nuclear matter is observed in this way.

Keywords: Walecka Model, Asymmetric Nuclear Matter, Vlasov Equation, Stochastic Mean Field Approach, Spinodal Instabilities

ÖZ

ASİMETRİK NÜKLEER MADDENİN SPİNODAL KARARSIZLIKLARININ STOKASTİK RELATİVİSTİK MODEL ÇERÇEVESİNDE YARI KLASİK OLARAK İNCELENMESİ

Saatci, Selen
Yüksek Lisans, Fizik Bölümü
Tez Yöneticisi : Prof. Dr. Osman Yılmaz
Ortak Tez Yöneticisi : Prof. Dr. Şakir Ayık

Ağustos 2013 , 95 sayfa

Sıcak ve yoğun olan nükleer madde genişler ve soğumaya başlar. Bu sırada, maddenin homojen ama mekanik olarak dengesiz olduğu spinodal bölgeye girebilir. Düşük genlikli yoğunluk dalgalanmaları hızlı bir şekilde büyür ve nükleer çoklu parçalanma denilen nükleer maddenin kümelere ayrılması durumunu oluşturur. Spinodal kararsızlıkların nükleer madde içindeki sıvı-gaz geçişlerine dinamik bir mekanizma sağladığı düşünülmektedir. Bu çalışmada, yük asimetrik nükleer maddenin spinodal dinamiklerini çalışmak için lineer olmayan Walecka Modeli'ne dayanan ortalama alan yaklaşımının stokastik uzantısı kullanıldı. Yoğunluk dalgalanmalarının erken gelişimi ve yoğunlaşma bölgelerinin ilk büyüklükleri yarı-klasik limitte incelendi. Sistemin izospin bağımlılığını meydana getirmek için Walecka Modeli'ne aracı parçacık olarak ρ mezonu eklendi. Baskın kararsız modların büyüme oranları ve bunlarla ilişkili en kısa büyüme zamanları belirlendi. Sistemin sıcaklık ve izospin asimetrisi bağımlılığını belirtmek için değişik asimetri değerlerinde ve farklı başlangıç koşullarında hesaplar yapıldı. En kararsız aktivite simetrik madde için elde edildi ve sistem nötron bakımından zenginleş-

tikçe bu aktivitenin azaldığı gözlemlendi. Baryon yoğunluğu korelasyon fonksiyonu da iki nokta arasındaki mesafeye bağlı olarak sunuldu ve yoğunlaşma bölgelerinin ilk büyüklükleri belirlendi. Sonuçlar, baskın kararsız modların dağılım bağıntısından elde edilen menzil değerleriyle tutarlı olarak bulundu. Ayrıca, farklı asimetri değerleri için spinodal bölgenin sınırları bulundu ve böylece nükleer maddenin izospin bağımlılığı gözlemlenmiş oldu.

Anahtar Kelimeler: Walecka Modeli, Asimetrik Nükleer Madde, Vlasov Denklemi, Stokastik Ortalama Alan Yaklaşımı, Spinodal Dengesizlikler

To my family

ACKNOWLEDGMENTS

I would like to express my deepest gratitude to my supervisor Prof. Dr. Osman Yılmaz. I have been able to finish this dissertation with his excellent guidance, patience and supportive attitude through my graduate experience. I would like to thank my co-advisor Prof. Dr. Şakir Ayık for providing me help and precious constructive advice on my thesis. This M.Sc. program became an invaluable experience for me with their support.

I am grateful to my colleague Fatma Acar Çakırca for sharing her knowledge, experience and for her friendship. Our fruitful discussions were very useful for me to understand the concepts. Besides, I appreciate the moral motivation that all my friends have provided me in the stressful writing period. I especially thank to Elif Sarıgül for being my companion in the endless hours of studying and to Murat Öztürk, with whom I shared the most comfortable office in the department.

I am deeply thankful to my parents Özlem and Emin Saatci for their trust and for the loving environment they provided all through my life. I have been very fortunate to have their support and sound advice everytime I needed. My brother Murat and my sister Özge are always there with their love and friendship. Also, I owe a special thank to my sister for sparing her time to help me in the writing process. To my family I dedicate this thesis.

Last but not least, I wish to thank Emirhan Postacı, who has been a source of understanding, encouragement and cheer through our graduate program. I feel so lucky to have his love and comforting support in my life.

I acknowledge that this project is partially supported by the Turkish Scientific and Technical Research Council, TUBITAK with grant No. 110T274.

TABLE OF CONTENTS

ABSTRACT v

ÖZ vii

ACKNOWLEDGMENTS x

TABLE OF CONTENTS xi

LIST OF TABLES xiii

LIST OF FIGURES xiv

CHAPTERS

1 INTRODUCTION 1

2 QUANTUM HADRODYNAMICS 7

2.1 Asymmetric Nuclear Matter 7

2.1.1 Nonlinear Walecka Model 7

2.1.2 Formalism 9

2.1.3 Equations of Motion 10

2.1.4 Relativistic Mean Field Theory 10

2.1.5 One-Body Potential 13

2.2 Asymmetric Nuclear Matter Equation of State at Finite Temperature 14

2.2.1 Spinodal Instabilities 17

2.2.2 Chemical Potential 21

3 STOCHASTIC MEAN FIELD APPROACH 27

3.1 The Stochastic Extention of the Mean-Field Theory 27

3.2 Vlasov Equation 28

3.3 Linearization of the Field Equations 31

3.4 Linearization of the Vlasov Equation 33

3.5 Density Fluctuations 37

3.6 Density Correlations 43

4 SPINODAL INSTABILITIES 53

4.1 Growth Rates of the Unstable Collective Modes 53

4.2 The Shortest Growth Time 58

4.3 Phase Diagrams 60

4.4 Spectral Intensities of Baryon Density Correlation Functions 61

4.5 Baryon Density Correlation Functions 65

5 CONCLUSION 73

REFERENCES 77

APPENDICES

A LINHARD FUNCTIONS IN THE SPINODAL REGION 79

B DERIVATIVE OF THE SUSCEPTIBILITY 83

C BARYON DENSITY CORRELATION FUNCTIONS 87

LIST OF TABLES

TABLES

Table 2.1 The parameters of the NL3 set and the predictions for the nuclear matter properties 8

LIST OF FIGURES

FIGURES

Figure 2.1 Effective mass of asymmetric nuclear matter as a function of baryon density ρ_B, for different values of asymmetry parameter, $I = 0.0,\ 0.2,\ 0.5$ and 0.8. . . . 17

Figure 2.2 Energy per nucleon as a function of the baryon density ρ_B, for different values of asymmetry parameter at fixed temperatures $T = 1\ MeV$ in panel (a) and $T = 5\ MeV$ in panel (b). 18

Figure 2.3 Energy per nucleon as a function of the baryon density ρ_B, for fixed asymmetry values $I = 0.0$ in panel (a), $I = 0.5$ in panel (b) and $I = 0.8$ in panel (c), at various temperatures. 20

Figure 2.4 Pressure as a function of the baryon density ρ_B, for fixed asymmetry values $I = 0.0$ in panel (a), $I = 0.2$ in panel (b) and $I = 0.5$ in panel (c), at various temperatures. 21

Figure 2.5 Pressure as a function of the baryon density ρ_B, for different values asymmetry parameter at fixed temperatures $T = 1\ MeV$ in panel (a) and $T = 5\ MeV$ in panel (b). 22

Figure 2.6 Proton and neutron chemical potentials as a function of the baryon density ρ_B, for different values of asymmetry parameter at fixed temperature $T = 5\ MeV$. 24

Figure 2.7 Proton and neutron chemical potentials as a function of the asymmetry parameter I, for fixed values of initial baryon densities $\rho_B = 0.0\rho_0$ in panel (a), $\rho_B = 0.5\rho_0$ in panel (b) and $\rho_B = 0.8\rho_0$ in panel (a), at fixed temperature $T = 5\ MeV$. 24

Figure 2.8 Reduced proton and neutron chemical potentials as a function of the baryon density ρ_B, for different values of asymmetry parameter at fixed temperature $T = 5\ MeV$ 25

Figure 4.1 Growth rates of the most unstable modes as a function of wave number with an initial baryon density $\rho_B = 0.2\rho_0$ for different values of asymmetry parameters $I = 0.0,\ 0.2,\ 0.5,\ 0.8$ in panels (a), (b), (c) and (d) at various temperatures. The dashed lines indicate the presence of the Coulomb interaction. 54

Figure 4.2 Growth rates of the most unstable modes as a function of wave number with an initial baryon density $\rho_B = 0.4\rho_0$ for different values of asymmetry parameters $I = 0.0,\ 0.2,\ 0.5,\ 0.8$ in panels (a), (b), (c) and (d) at various temperatures. The dashed lines indicate the presence of the Coulomb interaction. 55

Figure 4.3 Growth rates of the most unstable modes as a function of wave number with an initial baryon densities $\rho_B = 0.2\rho_0$ for panel (a) and $\rho_B = 0.4\rho_0$ for panel (b), for different values of asymmetry parameters $I = 0.0,\ 0.2,\ 0.5,\ 0.8$ at fixed temperature $T = 1\ MeV$. The dashed lines indicate the presence of the Coulomb interaction. 56

Figure 4.4 Growth rates of the most unstable modes as a function of wave number with an initial baryon densities $\rho_B = 0.2\rho_0$ for panel (a) and $\rho_B = 0.4\rho_0$ for panel (b), for different values of asymmetry parameters $I = 0.0,\ 0.2,\ 0.5,\ 0.8$ at fixed temperature $T = 5\ MeV$. The dashed lines indicate the presence of the Coulomb interaction. 57

Figure 4.5 Growth rates of the most unstable modes as a function of baryon density ρ_B for different values of asymmetry parameters $I = 0.0,\ 0.2,\ 0.5,\ 0.8$, at fixed temperatures $T = 1\ MeV$ for panel (a) and $T = 5\ MeV$ for panel (b). The dashed lines indicate the presence of the Coulomb interaction. 57

Figure 4.6 Shortest growth times for the most unstable modes as a function of baryon density for different values of asymmetry parameters $I = 0.0,\ 0.2,\ 0.5,\ 0.8$ for panel (a) at $T = 1\ MeV$ and $I = 0.0,\ 0.2,\ 0.5$ for panel (b) at $T = 5\ MeV$. The dashed lines indicate the presence of the Coulomb interaction. 58

Figure 4.7 Shortest growth times for the most unstable modes as a function of baryon density for various temperatures at fixed values of asymmetry parameters $I = 0.0,\ 0.2,\ 0.5,\ 0.8$ respectively for panels (a), (b), (c) and (d). The dashed lines indicate the presence of the Coulomb interaction. 59

Figure 4.8 Phase Diagrams for asymmetric nuclear matter with asymmetry values $I = 0.0,\ 0.2\ 0.5$ and $I = 0.8$ in panels (a), (b), (c) and (d) respectively. The dashed lines are for the initial wavelength $\lambda = 9\ fm$, while the solid lines represent the initial case with $\lambda = 12\ fm$. 61

Figure 4.9 Phase Diagram for asymmetric nuclear matter with $\lambda = 9\ fm$, for different asymmetry values $I = 0.0,\ 0.2,\ 0.5$ and $I = 0.8$. The dashed lines indicate the presence of the Coulomb interaction. 62

Figure 4.10 Phase Diagram for asymmetric nuclear matter with $I = 0.8$, for different wavelength values $\lambda = 9\ fm,\ 12\ fm,\ 15\ fm$ and $18\ fm$. 62

Figure 4.11 Spectral intensity of baryon density correlation function as a function of wave number at $T = 1\ MeV$, initial baryon density $\rho_B = 0.4\rho_0$ and at different asymmetry parameters $I = 0.0,\ 0.2,\ 0.5,\ 0.8$ respectively in panels (a), (b), (c) and (d). 63

Figure 4.12 Spectral intensity of baryon density correlation function as a function of wave number at $T = 5\ MeV$, initial baryon density $\rho_B = 0.4\rho_0$ and at different asymmetry parameters $I = 0.0,\ 0.2,\ 0.5$ respectively in panels (a), (b) and (c). . . 64

Figure 4.13 Spectral intensity of baryon density correlation function as a function of wave number at $T = 1\ MeV$, initial baryon density $\rho_B = 0.2\rho_0$ and at different asymmetry parameters $I = 0.0,\ 0.2,\ 0.5,\ 0.8$ respectively in panels (a), (b), (c) and (d). 66

Figure 4.14 Spectral intensity of baryon density correlation function as a function of wave number at $T = 5\ MeV$, initial baryon density $\rho_B = 0.2\rho_0$ and at different asymmetry parameters $I = 0.0,\ 0.2,\ 0.5,\ 0.8$ respectively in panels (a), (b), (c) and (d). 67

Figure 4.15 Baryon density correlation $\sigma_{BB}(\vec{x}, t)$ as a function of distance between two space points at $T = 1\ MeV$, initial baryon density $\rho_B = 0.4\rho_0$ and at different asymmetry parameters $I = 0.0,\ 0.2,\ 0.5,\ 0.8$ respectively in panels (a), (b), (c) and (d). 68

Figure 4.16 Baryon density correlation $\sigma_{BB}(\vec{x}, t)$ as a function of distance between two space points at $T = 5\ MeV$, initial baryon density $\rho_B = 0.4\rho_0$ and at different asymmetry parameters $I = 0.0,\ 0.2,\ 0.5,\ 0.8$ respectively in panels (a), (b), (c) and (d). 69

Figure 4.17 Baryon density correlation $\sigma_{BB}(\vec{x}, t)$ as a function of distance between two space points at $T = 1\ MeV$, initial baryon density $\rho_B = 0.2\rho_0$ and at different asymmetry parameters $I = 0.0,\ 0.2,\ 0.5,\ 0.8$ respectively in panels (a), (b), (c) and (d). 70

Figure 4.18 Baryon density correlation $\sigma_{BB}(\vec{x}, t)$ as a function of distance between two space points at $T = 5\ MeV$, initial baryon density $\rho_B = 0.2\rho_0$ and at different asymmetry parameters $I = 0.0,\ 0.2,\ 0.5$ respectively in panels (a), (b) and (c). . . 71

Figure 4.19 Baryon density correlation $\sigma_{BB}(\vec{x}, t)$ as a function of distance between two space points at $T = 5\ MeV$, initial baryon density $\rho_B = 0.4\rho_0$ and at different asymmetry parameters $I = 0.0,\ 0.2,\ 0.5$ respectively in panels (a), (b) and (c). The Coulomb interaction is neglected. 72

CHAPTER 1

INTRODUCTION

The study of atomic nuclei and nucleons have always been a challenging subject. Extensive studies are carried out in nuclear physics nearly for a century, from the discovery of protons to the heavy ion collisions with accelerators in new generation laboratories. As the knowledge concentrated through the years, nuclear matter has become an important subject to understand the nuclear interactions and structure. Being a hypothetical infinite system of neutrons and protons, nuclear matter is studied as a many body problem in non relativistic framework. In this traditional approach, the nuclear structure can be explained in terms of a phenomenological two-body potential and the dynamics are described by the Schrodinger equation [1, 2].

The development of new accelerator facilities, such as the LHC (Large Hadron Collider) at CERN, or RHIC (Relativistic Heavy Ion Collider) at Brookhaven National Laboratory, allows us to produce nuclear matter at extreme conditions via the heavy ion collisions. The non-relativistic many body formalism is inadequate to explain this new physics and many applications of nuclear matter require a more complete and consistent theoretical framework to include relativistic effects, such as the spin dependence or the relativistic motion of nucleons [1]. For example, the evolution of the universe in very early stages includes the quark gluon plasma phase that can only be studied and simulated in high energy heavy ion reactions [3]. Also, the properties of neutron stars or the formation of stellar objects after the supernova explosions are studied through the nuclear equation of state at much higher temperatures and densities than those of the ordinary nuclei [1]. The knowledge of the equation of state is a very important key point in nuclear physics and can be studied at the intermediate energy heavy ion collisions, as well as the other aspects such as the multifragmentation process or the isospin physics. At the collisions with beam energies in the order of tens of MeV, the

nuclear matter is compressed and heated, leading to the formation of small fragments which is called multifragmentation [3].

In recent years, studies based on the effective quantum field theories and renormalizable models have gained great achievements in explaining the nuclear dynamics and the interacting relativistic many body systems. In this manner the relativistic mean field theory, proposed by John Dirk Walecka, describes the interaction between the nucleons via the meson exchange [4]. In this thesis, the asymmetric nuclear matter is studied within the nonlinear Walecka Model including the ρ meson coupling and the self interaction terms of the scalar meson to have a more realistic approach. Also, the electromagnetic interaction between the protons is taken into account by including the coupling of the nucleons to the photon field, which is an important addition in order to describe the structure of the crusts of the neutron stars [5].

Our aim is to study the dynamics of the spinodal region and the multifragmentation process through the asymmetric nuclear matter equation of state. The liquid gas phase transition is predicted for nuclear matter as a result of the similarity between the nuclear equation of state and the classical van der Waals equation [8]. The van der Waals fluid enters the spinodal region at subcritical temperatures because of the short range repulsive and otherwise attractive nature of the intermolecular forces [5, 9]. Likewise, at low temperatures and ordinary densities, the nuclear matter is said to be in the liquid phase and tends to shift to a gas state with increasing temperature. From the theoretical point of view, the phase coexistence region can be determined from the mechanical and chemical equilibrium states of the system. Therefore, besides the equation of state, the isospin and ρ meson coupling dependence of the chemical potential has a significant role in studying the phase transitions of asymmetric nuclear matter [10]. The liquid-gas phase transition is found to take place at subsaturation densities, with a critical temperature between $10 - 15\ MeV$ for infinite nuclear matter without Coulomb interactions in different models. Experimental findings of the intermediate energy heavy-ion collisions verify that the compressed and heated nuclear matter breaks up into several fragments [11]. The formation of the massive clusters in the nuclear matter at low densities is thought to be a possible signature of the phase transition.

The cluster formation in hot nuclear matter can possibly be explained by the spinodal instability mechanism. The spinodal decomposition can be defined as the small amplitude density fluctuations that grow rapidly around an equilibrium point in a short time interval that cause

the system to resolve into an ensemle of various sized fragments [12]. The hot and compressed matter at $10 - 15\ MeV$ that is produced during the heavy-ion reaction, starts to cool down and enters to a mechanically unstable region at densities below the ordinary density of nuclear matter, $\rho_0 = 0.15\ fm^{-3}$. In this so called spinodal instability region, the decomposition is possible up to a critical temperature, where the derivative of the pressure becomes negative, the frequencies are imaginary and the system breaks up eventually [13, 14].

The liquid-gas phase coexistence exists at the crusts of the neutron stars, in which the baryon densities appear to be between $(\rho_B = 0.3 - 0.5\rho_0)$. At low temperatures around $T = 1\ MeV$, the isospin asymmetric nuclear matter with $I = 0.8$ corresponds to the conditions in such regions and therefore, the asymmetric nuclear matter equation of state is directly related with the key points of astrophysics as well as the structure of exotic nuclei.

Furthermore, isospin physics is a recently developing topic and a lot of activity is conducted to describe the isospin dependence of the in-medium nuclear interaction [3, 6]. The yet poorly known isospin dependence of finite nuclear matter is studied in the laboratories with the low and intermediate energy heavy-ion collisions [6, 7], however there are several critical difficulties in making the measurements. The reactions take place in the order of 10^{-21} seconds and it is not possible to make a direct observation of the clusters. Besides, proper observables should be introduced to identify the spinodal region [11].

There are also a variety of studies in order to develop a theoretical description to the nuclear matter dynamics. The microscopic approach of the Dirac-Brueckner-Hartree-Fock Model (DBHF) with the asymmetric matter extension, the Self-Consistent Green Functions or the variational methods are used as many-body techniques that provide a way to investigate the thermal behaviour of nuclear matter. However, calculations based on the mean field approximations have certain advantages in both relativistic and non-relativistic cases. For example, the numeric calculation period is shorter and the mean field parameters are extracted from the experimental observations of nuclear structure [11].

In that sense, the mean field transport models can include the isospin degrees of freedom and are useful to study the dynamics of the isospin asymmetric nuclear matter at low energies, such as the semi-classical Boltzmann-Uehling-Ulenbeck (BUU) Model and the time dependent Hartree-Fock (TDHF) theory, which is based on an effective Lagrangian density. Furthermore, the mean field models based on a phenomenological approach are useful to de-

scribe the nuclear properties at subsaturation and ordinary densities and can provide succesful explanations in the average effects of the collision process at low energies [15, 16]. However, the common point of these different mean field models is that they fail to describe the fluctuation dynamics and consequently the spinodal region. Density fluctuations can be categorized in two different mechanisms; fluctuations as a result of two-body collisions and the one-body dissipation mechanisms or the mean field fluctuations. At low energy regime which is also treated in this work, the mean field fluctuations are the dominant mechanisms in nuclear dynamics and the collisional fluctuations need not to be taken into account [17]. The TDHF involves the one-body dissipations, however the associated fluctuations can not be explained with this model [18]. Therefore, it should be extended in such a way that both the dissipation mechanisms and the resulting fluctuations are included in the models.

The Stochastic Mean Field (SMF) Theory is a powerful tool to investigate the fluctuation dynamics at low energy nuclear systems. This approach can generate the density fluctuations resulting from the one-body dissipations and presents results that are in accordance with the quantal dissipation-fluctuation relation [16, 18]. Furthermore, the spinodal instabilities and the liquid gas phase transitions can be described by implementing the stochastic extension to the mean field theory.

In the previous works [12, 13, 19, 20], the symmetric nuclear matter is investigated within the nonlinear Walecka Model, by using both the point and the density dependent couplings. Different parameter sets are utilized and compared to obtain the most realistic results and to show that the spinodal dynamics have the same trend in all cases. Also, the results from the relativistic mean field approximation are compared with the non-relativistic calculations including the Skyrme type effective calculations and the quantum statistical effects. It has been verified that the physics behind the nuclear matter studies is model independent.

In this thesis, the spinodal instability region and the early growth of the small amplitude density fluctuations are studied through the Stochastic Mean Field Theory for asymmetric nuclear matter, in a semi-classical limit of the relativistic mean field theory [21]. Isospin asymmetry and the electromagnetic interaction between the protons are included to the system with the addition of ρ meson and photon field couplings to the effective Lagrangian density of the nonlinear Walecka Model. Hence, the isospin dependence of the growth rates and the size of clusters are investigated as well as the effects of the Coulomb interaction in the system.

For calculations, we utilized the NL3 parameter set including the self interaction terms κ and λ, of the scalar meson [22].

In chapter 2, the equation of state for asymmetric nuclear matter at finite temperature is derived after a brief explanation of nonlinear Walecka Model. The phase coexistence region is determined and the influence of the isospin asymmetry in the state variables are observed. The density fluctuations are introduced after the linearization of the field equations in Chapter 3. The two coupled Vlasov equations for protons and neutrons are derived and linearized in order to investigate the early time evolution of the phase space distribution function. The dispersion relation is obtained and the expressions for the small amplitude density fluctuations are given. In chapter 4, the results of the numerical calculations are presented. We investigated the growth rates of the most unstable modes and the corresponding shortest growth times for different temperatures and initial densities of the system. The effect of the initial isospin asymmetry is demonstrated for different initial conditions. The size of the primary clusters and the boundaries of the spinodal region for different wave numbers are also estimated for asymmetric nuclear matter. The conclusion is given in Chapter 5.

CHAPTER 2

QUANTUM HADRODYNAMICS

2.1 Asymmetric Nuclear Matter

2.1.1 Nonlinear Walecka Model

Quantum Hadrodynamics (QHD) is a general name for the effective quantum field theories that have been introduced to provide a theoretical description to the relativistic nuclear many-body problem. It is proposed by John Dirk Walecka in early seventies and is based on an effective Lagrangian with hadronic degrees of freedom. It describes the strong interaction between nucleons via the exchange of mesons [2, 4].

The research conducted within QHD aims to describe the many baryon systems at low energy regime. This choice is an appropriate framework to study the bulk properties of infinite nuclear matter. Within this framework, there are several models that can describe symmetric and charge asymmetric nuclear matter. The simplest model is QHD-I, also referred as the Walecka Model, includes the neutral scalar σ and the neutral vector ω mesons as the mediator particles. The calculations do not contain the pion field since the parity is well defined in the ground state and there is spherical symmetry. The fundamental property of the strong nuclear force is produced within this simple model, the vector meson creates the short range repulsion while the scalar meson is responsible for the attractive force in the larger distances [1, 2, 4].

However, only the symmetric nuclear matter can be investigated within QHD-I since the model does not contain the contribution of isovector mesons which specifies the only difference between proton and neutron, their isospin projection. A more realistic model can be obtained by modifying the original theory, by inserting additional terms to the Lagrangian for

Table2.1: The parameters of the NL3 set and the predictions for the nuclear matter properties

The NL3 Parameter Set	
$m_s(MeV)$	508.194
$m_{\mathrm{v}}(MeV)$	782.501
g_s	10.217
g_{v}	12.868
$\kappa(fm^{-1})$	10.431
λ	-28.885
Nuclear Matter Properties	
$\rho_0(fm^{-3})$	0.148
E/A (MeV)	-16.299
K (MeV)	271.76
M^*/M	0.60

the coupling of the isovector-vector meson field. This extended model is called QHD-II and it includes the nucleons, the scalar meson σ, the vector meson ω, the isovector meson ρ and the photon γ as the quanta of the electromagnetic field [1]. With this extension, the nucleon has the isospin degree of freedom where the baryon field is an isospin doublet, $\psi = \begin{pmatrix} \psi_p \\ \psi_n \end{pmatrix}$.

The isospin operator is denoted by t and it has two values of projection on the third component, $t_3 = \frac{1}{2}$ for proton and $t_3 = -\frac{1}{2}$ for neutron. The nuclear matter is said to be asymmetric if the neutron and proton densities are not the same and in this case, the isospin asymmetry parameter is defined as $I = \frac{\rho_n - \rho_p}{\rho_n + \rho_p}$, where ρ_n and ρ_p are the neutron and proton densities respectively [6, 23]. τ_3 denotes the third Pauli isospin matrix and $\frac{1}{2}(1 + \tau_3)$ is the isospin projection operator, with the values $\tau_3 = 1$ for proton and $\tau_3 = -1$ for neutron. [1]

QHD is a renormalizable theory which implies that the models within QHD can be characterized by a finite set of phenomenological constants; the masses of the mesons and the strong coupling constants (g_s, g_{v}, g_ρ for the scalar, vector and isovector fields) [1, 2]. These parameters are determined to reproduce the experimental data and obtained by fitting the bulk properties of some spherical nuclei [23]. In this work, NL3 parameter set is used where the nucleon mass is taken to be 939 MeV, the mass of ρ meson is fixed to the empirical value of 763 MeV and the other parameters are determined by fitting the properties of several spherical nuclei such as charge radii, the binding energy and the neutron radii. The values of the masses and the coupling constants for NL3 set are given in Table 2.1 including the nuclear matter properties that the set produces. In the table, the coupling constants are given as the

standard expressions however in our calculations they are utilized in the form $g_s \rightarrow g_s\sqrt{\hbar c}$, $g_{\rm v} \rightarrow g_{\rm v}\sqrt{\hbar c}$, $\kappa \rightarrow \kappa/\sqrt{\hbar c}$ and $\lambda \rightarrow \lambda/\hbar c$. With the use of this parameter set, the saturation of the nuclear matter is given at the Fermi momentum of $k_f = 1.30\ fm^{-1}$ and the binding energy is found to be approximately $16.3\ MeV$ for symmetric nuclear matter [22, 23].

2.1.2 Formalism

The Lagrangian density for a system of nucleons, represented by the nucleon field ψ with mass M, that interact through the exchange of the scalar field ϕ with mass m_s, the vector field V_μ with mass $m_{\rm v}$, the isovector field b_μ with mass m_ρ and the massless photon field A_μ can be written as

$$\begin{aligned} L \;=\; & \overline{\psi}[\gamma^\mu i\hbar\partial_\mu - Mc^2]\psi + \frac{1}{2}\partial_\mu\phi\partial^\mu\phi - (\frac{1}{2}\mu_s^2\phi^2 + \frac{\kappa}{3!}\phi^3 + \frac{\lambda}{4!}\phi^4) + g_s\overline{\psi}\psi\phi \\ & -\frac{1}{4}\Omega_{\mu\nu}\Omega^{\mu\nu} + \frac{1}{2}\mu_{\rm v}^2 V_\mu V^\mu - g_{\rm v}\overline{\psi}\gamma^\mu\psi V_\mu \\ & -\frac{1}{4}\vec{G_{\mu\nu}}\vec{G^{\mu\nu}} + \frac{1}{2}\mu_\rho^2\vec{b_\mu}\vec{b^\mu} - \frac{1}{2}g_\rho\overline{\psi}\gamma^\mu\vec{\tau}\vec{b_\mu}\psi \\ & -\frac{1}{4}F_{\mu\nu}F^{\mu\nu} - \frac{e}{2}(1+\tau_3)\overline{\psi}\gamma^\mu A_\mu\psi \end{aligned} \tag{2.1}$$

where the short hand notations are used for $\mu_s \equiv (m_s c/\hbar)$, $\mu_{\rm v} \equiv m_{\rm v}c/\hbar$ and $\mu_\rho \equiv (m_\rho c/\hbar)$. The field tensors for the vector, isovector and photon fields are given as $\Omega_{\mu\nu} = \partial_\mu V_\nu - \partial_\nu V_\mu$, $\vec{G_{\mu\nu}} = \partial_\mu\vec{b_\nu} - \partial_\nu\vec{b_\mu}$ and $F_{\mu\nu} = \partial_\mu A_\nu - \partial_\nu A_\mu$ respectively.

In the standard Walecka Model, the self interaction coupling constants (κ and λ) of the scalar field are not included in the calculations. However, this yields to a theoretical value of compressibility $K = 540\ MeV$ which deviates from the experimentally observed value of $200\ MeV$, approximately [12]. The nonlinear self interaction terms of the scalar meson field are added to the Lagrangian density in the form of a scalar potential $U(\phi) = \frac{1}{2}\mu_s^2\phi^2 + \frac{\kappa}{3!}\phi^3 + \frac{\lambda}{4!}\phi^4$, in order to provide a more accurate compressibility value at $K = 271\ MeV$, which better explains the experimental results [22, 23]. Also, the nonlinear model yields to a critical temperature about $14\ MeV$ which is reasonably close to the results of the experimental findings around $13\ MeV$ [24].

2.1.3 Equations of Motion

By using the Euler-Lagrange equation, the equations of motion for the meson fields are found as follows;

$$(\partial_\mu \partial^\mu + \mu_{\rm s}^2)\phi + \frac{\kappa}{2}\phi^2 + \frac{\lambda}{6}\phi^3 = g_{\rm s}\bar{\psi}\psi \tag{2.2}$$

$$(\partial_\mu \partial^\mu + \mu_{\rm v}^2)V^\mu = g_{\rm v}\bar{\psi}\gamma^\mu\psi \tag{2.3}$$

$$(\partial_\mu \partial^\mu + \mu_\rho^2)\vec{b^\nu} = \frac{1}{2}g_\rho\overline{\psi}\gamma^\mu\vec{\tau}\psi \tag{2.4}$$

$$\partial_\mu \partial^\mu A^\nu = e\left[\overline{\psi}\gamma^\nu\frac{1}{2}(1+\tau_3)\psi\right] . \tag{2.5}$$

The first three equations are the Klein Gordon equations for the scalar, neutral vector and the charged isovector fields with the source terms $g_{\rm s}\bar{\psi}\psi$, $g_{\rm v}\bar{\psi}\gamma^\mu\psi$ and $\frac{1}{2}g_\rho\overline{\psi}\gamma^\mu\vec{\tau}\psi$. The fourth equation is the field equation for the electromagnetic field.

The Dirac equation for the nucleon field includes the interaction with the meson and the photon fields and can be obtained as;

$$\left[\gamma^\mu(i\hbar\partial_\mu - g_{\rm v}V_\mu - \frac{1}{2}g_\rho\vec{\tau}\vec{b_\mu} - e\frac{1}{2}(1+\tau_3)A_\mu) - (Mc^2 - g_{\rm s}\phi)\right]\psi \;=\; 0 . \tag{2.6}$$

Furthermore, the energy momentum tensor which can be related to the energy and pressure densities is defined as [1]

$$T^{\mu\nu} = \frac{\partial L}{\partial\frac{\partial q_i}{\partial x_\mu}}\frac{\partial q_i}{\partial x_\nu} - g_{\mu\nu}L \tag{2.7}$$

with the corresponding energy and pressure densities of the form

$$\epsilon \;=\; < T_{00} > \tag{2.8}$$

$$p \;=\; \frac{1}{3} < T_{ii} > . \tag{2.9}$$

It is a conserved quantity since the Lagrangian density does not explicitly depend on the space-time coordinates.

2.1.4 Relativistic Mean Field Theory

The Klein Gordon equations in Eq. (2.2-2.5) are nonlinear coupled field equations and the exact solutions cannot be obtained in simple manners [1]. Also, the strong coupling constants are large and the perturbative approaches are not useful. The appropriate approach is

the use of the relativistic mean field theory which is the most valid approximation as the nuclear density increases for a uniform system of B baryons in a volume V [4]. As the baryon density increases, the source terms on the right hand side of the equations become large and consequently the meson field operators can be replaced by their classical representations;

$$\begin{aligned}
\phi &\rightarrow \langle\phi\rangle \equiv \phi_0 \\
V^\mu &\rightarrow \langle V^\mu\rangle \equiv V_0 g^{\mu 0} \\
b_a^\mu &\rightarrow \langle b_a^\mu\rangle \equiv g^{\mu 0}\delta_{a3} b_0 \\
A^\mu &\rightarrow \langle A^\mu\rangle \equiv g^{\mu 0} A_0 \ .
\end{aligned} \tag{2.10}$$

This follows from the fact that for a static, infinite system at equilibrium, the vector, isovector and the photon fields can only develop a fourth component since there is no spatial direction in the system and the classical fields ϕ_0, V_0, b_0 and A_0 are constants that are independent of space and time x^μ [1].

Furthermore, in the mean field approximation the baryon field operators in the field equations are also replaced by their ground state expectation values as follows;

$$\begin{aligned}
\overline{\psi}\psi &\rightarrow \langle\overline{\psi}\psi\rangle = \rho_s \\
\overline{\psi}\gamma^\mu\psi &\rightarrow \langle\overline{\psi}\gamma^\mu\psi\rangle = g^{\mu 0}\rho_B \\
\overline{\psi}\gamma^\mu\tau_a\psi &\rightarrow \langle\overline{\psi}\gamma^\mu\tau_a\psi\rangle = g^{\mu 0}\delta_{a3}\rho_3 \\
\overline{\psi}\gamma^\mu\frac{1}{2}(1+\tau_3)\psi &\rightarrow \langle\overline{\psi}\gamma^\mu\frac{1}{2}(1+\tau_3)\psi\rangle = g^{\mu 0}\rho_p \ .
\end{aligned} \tag{2.11}$$

Here, the densities can be given as the sum of the corresponding proton and neutron densities as;

$$\begin{aligned}
\rho_s &= \rho_{s,p} + \rho_{s,n} \\
\rho_B &= \rho_{B,p} + \rho_{B,n} \\
\vec{\rho}_{\rm v} &= \vec{\rho}_{{\rm v},p} + \vec{\rho}_{{\rm v},n} \\
\rho_3 &= \rho_{B,p} - \rho_{B,n} \ .
\end{aligned} \tag{2.12}$$

After imposing the classical fields and the ground state expectation values, the effective mean

field Lagrangian density becomes

$$
\begin{aligned}
L_{RMF_{II}} &= \overline{\psi}[\gamma^{\mu} i\hbar\partial_{\mu} - Mc^2]\psi + \frac{1}{2}\partial_{\mu}\phi_0\partial^{\mu}\phi_0 - (\frac{1}{2}\mu_s^2\phi_0^2 + \frac{\kappa}{3!}\phi_0^3 + \frac{\lambda}{4!}\phi_0^4) + g_s\overline{\psi}\psi\phi_0 \\
&+\frac{1}{2}\mu_{\mathrm{v}}^2 V_0^2 - g_{\mathrm{v}}\overline{\psi}\gamma^0\psi V_0 \\
&+\frac{1}{2}\mu_{\rho}^2 b_0^2 - \frac{1}{2}g_{\rho}\overline{\psi}\gamma^0\tau_3 b_{3,0}\psi \\
&-\frac{e}{2}(1+\tau_3)\overline{\psi}\gamma^0 A_0\psi \; . \qquad (2.13)
\end{aligned}
$$

Thus, the field equations for a static, charge asymmetric infinite nuclear matter at equilibrium reduces to

$$
\begin{aligned}
\phi_0 &= \frac{1}{\mu_s^2}\left[g_s(\rho_{s,p}^0 + \rho_{s,n}^0) - \frac{\kappa}{2}\phi_0^2 - \frac{\lambda}{6}\phi_0^3\right] \\
V_0^0 &= \frac{g_{\mathrm{v}}}{\mu_{\mathrm{v}}^2}(\rho_{B,p}^0 + \rho_{B,n}^0) \\
\vec{V_0} &= 0 \\
b_3^0 &= \frac{1}{2}\frac{g_{\rho}}{\mu_{\rho}^2}(\rho_{B,p}^0 - \rho_{B,n}^0) \\
\vec{b_3} &= 0 \\
A_0^0 &= 0 \\
\vec{A_0} &= 0 \qquad (2.14)
\end{aligned}
$$

where the zero sub indices denotes the equilibrium state of the system. In the mean field limit, the problem can exactly be solved and the relativistic nuclear many body system can be described [1]. Furthermore, the energy momentum tensor for the charge asymmetric nuclear matter becomes,

$$
T^{\mu\nu} = \overline{\psi}\gamma i\hbar\partial_{\nu}\psi + g_{\mu\nu}\left[U(\phi_0) - \frac{1}{2}\mu_{\mathrm{v}}^2 V_0^2 - \frac{1}{2}\mu_{\rho}^2 b_0^2\right] \qquad (2.15)
$$

with the corresponding energy and pressure densities;

$$
\epsilon = \langle T_{00}\rangle = \langle\overline{\psi}\gamma^0 i\hbar\partial_0\psi\rangle + U(\phi_0) - \frac{1}{2}\mu_{\mathrm{v}}^2 V_0^2 - \frac{1}{2}\mu_{\rho}^2 b_0^2 \; , \qquad (2.16)
$$

$$
p = \frac{1}{2}\langle T_{ii}\rangle = \frac{1}{3}\langle\overline{\psi}\gamma^i i\hbar\partial_i\psi\rangle - U(\phi_0) + \frac{1}{2}\mu_{\mathrm{v}}^2 V_0^2 + \frac{1}{2}\mu_{\rho}^2 b_0^2 \; . \qquad (2.17)
$$

2.1.5 One-Body Potential

Within the formalism of QHD-II, the Dirac equation for the baryons in the asymmetric nuclear matter can be written in the most general form as,

$$\begin{aligned} i\hbar\frac{\partial\psi}{\partial t} &= \vec{\alpha}\left[c\vec{p} - g_{\rm v}\vec{V} - \frac{1}{2}g_\rho\tau_3\vec{b_3} - \frac{e}{2}(1+\tau_3)\vec{A}\right]\psi \\ &+ \left[g_{\rm v}V_0 + \beta(Mc^2 - g_s\phi) + \frac{1}{2}g_\rho\tau_3 b_{3,0} + \frac{e}{2}(1+\tau_3)A_0\right]\psi \end{aligned} \tag{2.18}$$

where the momentum is defined as $\vec{p} = -i\hbar\vec{\nabla}$ and we have used the expressions $\vec{\alpha} = \begin{pmatrix} 0 & \vec{\sigma} \\ \vec{\sigma} & 0 \end{pmatrix}$ and $\beta = \gamma^0 = \begin{pmatrix} 1 & 0 \\ 0 & -1 \end{pmatrix}$.

The mass of the nucleons is reduced due to the interaction with the scalar meson, while the momentum is reduced as a consequence of the vector meson interactions. The effective reduced mass and the reduced momentum are defined as,

$$c\vec{p}^* = c\vec{p} - g_{\rm v}\vec{V} - \frac{1}{2}g_\rho\tau_3\vec{b_3} - \frac{e}{2}(1+\tau_3)\vec{A} \tag{2.19}$$

$$M^*c^2 = Mc^2 - g_s\phi \tag{2.20}$$

and the Dirac equation can be written in terms of these quantities,

$$i\hbar\frac{\partial\psi}{\partial t} = \left[\vec{\alpha}c\vec{p}^* + g_{\rm v}V_0 + \beta M^*c^2 + \frac{1}{2}g_\rho\tau_3 b_{3,0} + \frac{e}{2}(1+\tau_3)A_0\right]\psi\ . \tag{2.21}$$

Therefore, the one body Hamiltonian of the system can be found from the Dirac equation as;

$$h = \sqrt{(c\vec{p}^*)^2 + (M^*c^2)^2} + g_{\rm v}V_0 + \frac{1}{2}g_\rho\tau_3 b_{3,0} + \frac{e}{2}(1+\tau_3)A_0\ . \tag{2.22}$$

In the isospin space the 2x2 Pauli isospin matrix, τ_3, is defined to be $\tau_3 = \begin{pmatrix} 1 & 0 \\ 0 & -1 \end{pmatrix}$ and the nucleon is an isospin doublet, $\psi = \begin{pmatrix} \psi_p \\ \psi_n \end{pmatrix}$. Inserting these definitions in the Dirac equation allows us to find the proton and neutron one-body potentials seperately;

$$\begin{aligned} h_p = U_p &= \sqrt{(c\vec{p} - g_{\rm v}\vec{V} - \frac{1}{2}g_\rho\vec{b_3} - e\vec{A})^2 + (Mc^2 - g_s\phi)^2} + g_{\rm v}V_0 + \frac{1}{2}g_\rho b_{3,0} + eA_0 \\ h_n = U_n &= \sqrt{(c\vec{p} - g_{\rm v}\vec{V} + \frac{1}{2}g_\rho\vec{b_3})^2 + (Mc^2 - g_s\phi)^2} + g_{\rm v}V_0 - \frac{1}{2}g_\rho b_{3,0}\ . \end{aligned} \tag{2.23}$$

The first terms are the free particle hamiltonians for protons and neutrons with mass M^* and momentum p_p^* and p_n^* repectively. All the other terms arise from the interaction of baryons via the exchange of mesons. From the equations, it can be observed that only the proton one body potential has an interaction term with the electromagnetic field.

Given in Eq. (2.20), the reduced mass should be calculated self consistently with the scalar field from the argument that at zero temperature and at equilibrium, the system will minimize its energy with respect to ϕ_0 [4]

$$\left(\frac{\partial E}{\partial \phi_0}\right) = 0 \,. \tag{2.24}$$

Hence, using the self consistency condition yields;

$$M_0^* c^2 = Mc^2 - \frac{g_s^2}{\mu_s^2}(\rho_{s,p}^0 + \rho_{s,n}^0) - \left[-\frac{\kappa}{2}\frac{1}{g_s\mu_s^2}(Mc^2 - M_0^* c^2)^2 + \frac{\lambda}{6}\frac{1}{g_s^2\mu_s^2}(Mc^2 - M_0^* c^2)^3\right] \,. \tag{2.25}$$

2.2 Asymmetric Nuclear Matter Equation of State at Finite Temperature

Equation of state is simply a connection between the temperature, pressure and density of the system. In nuclear physics, equation of state is directly related to the structure of the nuclear interactions and hence, it is important in revealing the qualitative behaviour of the system. Also, studies on the equation of state for asymmetric nuclear matter lead us to explore the isovector part and the symmetry energy dependence, which are additional outcomes to understand the neutron rich matter. The effects of the symmetry energy term in the equation of state becomes more important as isospin asymmetry grows in the system [7]. Furthermore, revealing the asymmetric nuclear matter equation of state makes important contributions to the studies in the structure of unstable finite nuclei as well as to understand some critical topics in astrophysics such as supernova and neutron star physics [6]. Also the nucleosynthesis process and the cooling of neutron stars are better explained due to the increasing knowledge in the isospin dependence of the nuclear matter [3].

In this section, the temperature dependent equation of state for isospin asymmetric nuclear matter will be derived in the frame of relativistic mean field theory.

In order to define the properties of a system with single particle modes $\{n_{\vec{k}\lambda}\} = \{n_1, n_2, n_3, ..., n_\infty\}$ at finite temperature, the standard expressions of statistical thermodynamics should be intro-

duced. The grand partition function Z_g for N number of particles with j number of energy states is defined as [1]

$$Z_G = \sum_N \sum_j \langle Nj|e^{-\beta(E_j-\mu N)}|Nj\rangle = Tr\left(e^{-\beta(\widehat{H}-\mu\widehat{N})}\right) \tag{2.26}$$

where μ denotes the chemical potential of the system, the temperature is given by the relation $\beta \equiv 1/k_B T$ and k_B is the Boltzmann constant. $\widehat{H}$ and $\widehat{B}$ are the Hamiltonian and the baryon number operators of the mean field theory which can be given for an interacting system of fermions as,

$$\begin{aligned} H_{MFT} &= V\left[-\frac{1}{2}(\mu_{\rm v})^2 V_0^2 + \frac{1}{2}(\mu_s)^2\phi_0^2 - \frac{1}{2}(\mu_\rho)^2 b_{3,0}^2\right] \\ &+ (g_{\rm v}V_0 + \frac{1}{2}g_\rho\tau_3 b_{3,0} + \sqrt{(c\vec{p}^*)^2 + (M^*c^2)^2})\widehat{B} \\ \widehat{B} &= \sum_{k\lambda} A_{k\lambda}^+ A_{k\lambda} \end{aligned} \tag{2.27}$$

where $A_{k\lambda}^+$ and $A_{k\lambda}^-$ are the creation and the destruction operators respectively [4]. After employing the mean field operators, the grand partition function becomes

$$\begin{aligned} Z_G &= \sum_{n_1...n_\infty} \langle n_1...n_\infty|e^{-\beta(\widehat{H}-\mu\widehat{B})}|n_1...n_\infty\rangle \\ &= \exp\left\{-\beta V\left[-\frac{1}{2}(\mu_{\rm v})^2 V_0^2 + \frac{1}{2}(\mu_s)^2\phi_0^2 + \frac{\kappa}{6}\phi_0^3 + \frac{\lambda}{24}\phi_0^4 - \frac{1}{2}\mu_\rho^2 b_{3,0}^2\right]\right\} \\ &\cdot \prod_{i=1}^{\infty}\sum_{n=0}^{1}\left[e^{-\beta(E_i^*+g_{\rm v}V_0+\frac{1}{2}g_\rho b_{3,0}-\mu)}\right] . \end{aligned} \tag{2.28}$$

$\mu^* = g_{\rm v}V_0 - \frac{1}{2}g_\rho b_{3,0} - \mu$ is the reduced chemical potential and $E_i^* = \sqrt{(c\vec{p}^*)^2 + (M^*c^2)^2}$ is the reduced single particle energy. Partition function is a useful quantity to connect the microscopic properties of the system to the macroscopic dynamics. Consequently, the thermodynamical potential $\Omega(T, V, \mu)$ can be defined in terms of Z_G to describe the macroscopic properties of the system such as the energy and pressure densities [1].

$$\begin{aligned} \Omega(T,V,\mu) &= -k_B T \ln Z_G \\ &= V\left[-\frac{1}{2}\left(\frac{g_{\rm v}}{\mu_{\rm v}}\right)^2\rho_B^2 + \frac{1}{2}\left(\frac{\mu_s}{g_s}\right)^2\left(Mc^2 - M^*c^2\right)^2\right. \\ &+ \left.\frac{\kappa}{6}\frac{\left(Mc^2-M^*c^2\right)^3}{g_s^3} + \frac{\lambda}{24}\frac{\left(Mc^2-M^*c^2\right)^4}{g_s^4} - \frac{1}{8}\left(\frac{g_\rho}{\mu_\rho}\right)^2\left(\rho_3^0\right)^2\right] \\ &- \frac{1}{\beta}\sum_i \ln\left[1 + e^{-\beta(E_i^*-\mu^*)}\right] . \end{aligned} \tag{2.29}$$

Then the baryon density is written in the following relation as the derivative of $\Omega(T, V, \mu)$ with respect to the chemical potential;

$$\rho_B = -\left(\frac{\partial \Omega}{\partial \mu}\right)_{T,V} = \frac{\gamma}{(2\pi\hbar)^3} \int_0^{p_f} d^3p \frac{1}{1 + e^{\beta(E_i^* - \mu^*)}} \ . \tag{2.30}$$

Here, γ is the spin-isospin factor which is equal to 2 for asymmetric nuclear matter.

Furthermore, the scalar density is defined as,

$$\rho_s = \frac{\gamma}{(2\pi\hbar)^3} \int_0^{p_f} d^3p \frac{M^* c^2}{\sqrt{\vec{p}^2 c^2 + (M^* c^2)^2}} \frac{1}{1 + e^{\beta(E_i^* - \mu^*)}} \ . \tag{2.31}$$

From the thermodynamical relation $\varepsilon = \frac{1}{V}\frac{\partial(\beta\Omega)}{\partial\beta} + \mu\rho_B$, the energy density for the system of baryons with isospin degrees of freedom can be obtained with the use of the above expressions for ρ_B and ρ_s.

$$\begin{aligned}
\varepsilon &= \frac{1}{2}\left(\frac{g_\mathrm{v}}{\mu_\mathrm{v}}\right)^2 (\rho_B)^2 + \frac{1}{2}\left(\frac{\mu_s}{g_s}\right)^2 \left(Mc^2 - M^* c^2\right)^2 + \frac{\kappa}{6g_s^3}\left(Mc^2 - M^* c^2\right)^3 \\
&+ \frac{\lambda}{24 g_s^4}\left(Mc^2 - M^* c^2\right)^4 + \frac{1}{8}\left(\frac{g_\rho}{\mu_\rho}\right)^2 \left(\rho_3^0\right)^2 \\
&+ \frac{\gamma}{(2\pi\hbar)^3} \int_0^{p_f} d^3p \sqrt{p^2 c^2 + (M^* c^2)^2} \frac{1}{1 + e^{\beta(E_i^* - \mu^*)}} \ .
\end{aligned} \tag{2.32}$$

Another thermodynamical relation is used for the pressure density of the system $P = \rho_B \frac{\partial E}{\partial \rho_B} - E(\rho_B)$ that results in

$$\begin{aligned}
p &= \frac{1}{2}\left(\frac{g_\mathrm{v}}{\mu_\mathrm{v}}\right)^2 (\rho_B)^2 - \frac{1}{2}\left(\frac{\mu_s}{g_s}\right)^2 \left(Mc^2 - M^* c^2\right)^2 - \frac{\kappa}{6g_s^3}\left(Mc^2 - M^* c^2\right)^3 \\
&- \frac{\lambda}{24 g_s^4}\left(Mc^2 - M^* c^2\right)^4 + \frac{1}{8}\left(\frac{g_\rho}{\mu_\rho}\right)^2 \left(\rho_{B,p}^0 - \rho_{B,n}^0\right) \\
&+ \frac{1}{3}\frac{\gamma}{(2\pi\hbar)^3} \int_0^{p_f} d^3p \frac{(c\vec{p})^2}{\sqrt{(c\vec{p})^2 + (M^* c^2)^2}} \frac{1}{1 + e^{\beta(E_i^* - \mu^*)}} \ .
\end{aligned} \tag{2.33}$$

Furthermore, by importing the temperature dependent scalar density expression, the reduced mass can be written as a function of temperature.

$$\begin{aligned}
M^* c^2 &= Mc^2 - \left(\frac{g_s}{\mu_s}\right)^2 \frac{\gamma}{(2\pi\hbar)^3} \int_0^{p_f} d^3p \frac{M^* c^2}{\sqrt{\vec{p}^2 c^2 + (M^* c^2)^2}} \frac{1}{1 + e^{\beta(E_i^* - \mu^*)}} \\
&+ \left(\frac{g_s}{\mu_s}\right)^2 \left[\frac{\kappa}{2g_s^3}\left(Mc^2 - M^* c^2\right)^2 + \frac{\lambda}{6g_s^4}\left(Mc^2 - M^* c^2\right)^3\right] \ .
\end{aligned} \tag{2.34}$$

This equation can be solved self consistently and the resulting curve for the change in the effective mass with respect to the baryon density is given in Fig. 2.1. The calculations are implemented for different values of asymmetry parameter ($I = 0.0,\ 0.2,\ 0.5$ and 0.8) at a fixed temperature $T = 5\ MeV$. The same trend is observed for all asymmetry values. As a consequence of the large scalar field, the effective mass decreases with increasing baryon density and the ratio M^*/M is less than unity at even ordinary densities [1]. Below and around the saturation density $\rho_0 = 0.15\ fm^{-3}$ the effective mass does not show any significant variance for different asymmetries. Also at such low energies, the effective mass does not change with increasing temperature and therefore it is not demonstrated here.

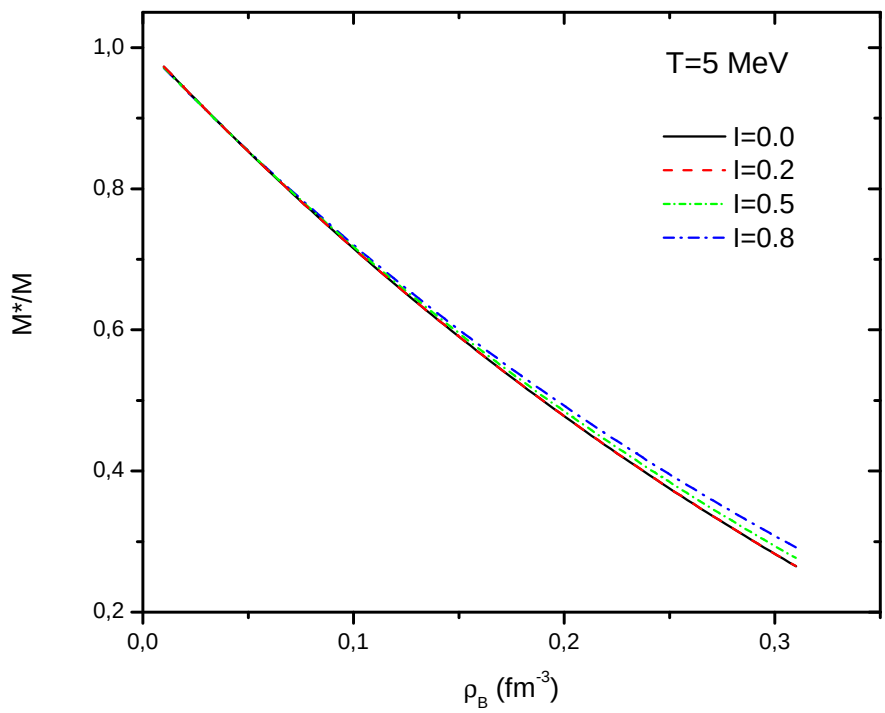

Figure 2.1: Effective mass of asymmetric nuclear matter as a function of baryon density ρ_B, for different values of asymmetry parameter, $I = 0.0,\ 0.2,\ 0.5$ and 0.8.

2.2.1 Spinodal Instabilities

It has been observed that in the heavy-ion collisions at energies around Fermi energy per particle, the heated and compressed nuclear matter that is produced during the collision breaks

up and leads to the formation of several fragments [25]. This multifragmentation process is a signal of liquid-gas phase transition within the nuclear matter [26]. The liquid gas phase transitions take place in the systems with short range repulsive and longer-range attractive forces as in the case of van der Waals type forces and the nuclear system is also expected to go under such phase transitions [9]. The dynamics of the phase transition and the corresponding fragmentation can be described by the spinodal decomposition mechanism. While the hot and compressed nuclear matter expands and cools after the collision, the system goes into an unstable zone called the spinodal region, where the amplitudes of density fluctuations grow exponentially with time, leading to the formation of unstable modes and fragments [26]. At heavy ion collisions with low and intermediate center of mass energies, the hadronic states are expected to go under van der Waals type liquid-gas phase transitions, while at higher energies the formation of quark gluon plasma is expected [3].

The spinodal region and the phase coexistence of the nuclear matter can be examined through the equation of state, from which the boundaries of the spinodal region, the critical temperature or the isospin asymmetry dependence of the system can be obtained.

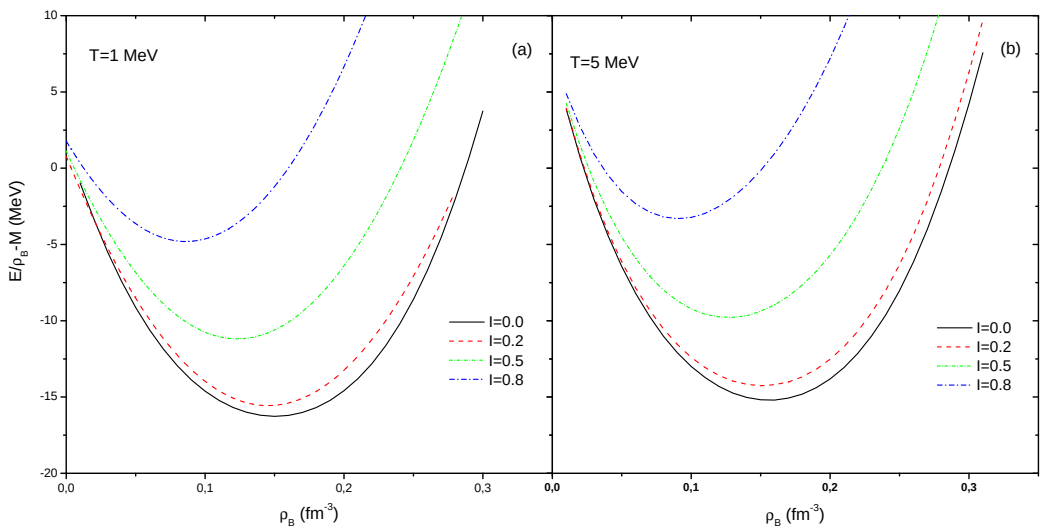

Figure 2.2: Energy per nucleon as a function of the baryon density ρ_B, for different values of asymmetry parameter at fixed temperatures $T = 1\ MeV$ in panel (a) and $T = 5\ MeV$ in panel (b).

Fig. 2.2 shows the energy per nucleon as a function of density for different values of asymmetry parameter, at temperatures $T = 1\ MeV$ for panel (a) and $T = 5\ MeV$ for panel (b).

It is observed that as the densities move further from the ordinary nuclear density, the system becomes less bound. The isospin dependence of the system can be observed from the graph where the upper-most curve with $I = 0.8$ indicates the neutron rich matter and the curve at the bottom denotes the symmetric nuclear matter. The remarkable difference between the two curves arises from the contribution of the symmetry energy term in the asymmetric nuclear matter equation of state. The system gets less bound as the asymmetry parameter increases. At intermediate densities near ρ_0, the system saturates, where the attractive scalar interaction dominates. It can be observed that the system reaches the saturation point at higher values of binding energy and smaller values of baryon density as the system becomes richer in neutrons.

Furthermore, the temperature dependence of the saturation curve is demonstrated in Fig. 2.3 for asymmetries $I = 0.0$, $I = 0.5$ and $I = 0.8$ in (a), (b) and (c) respectively. As the temperature increases, the system becomes less bound for all values of I and no bound states exist above $T = 18\ MeV$ for $I = 0.5$ and $T = 10\ MeV$ for $I = 0.8$. Also, the system saturates at higher values of baryon density with increasing temperature.

By using Eq. (2.33), the baryon density variation of pressure can be observed in Fig. 2.4 for different temperatures up to 20 MeV and fixed asymmetries. The isotherms resemble the behaviour of the classical van der Waals curves which adresses the liquid-gas phase transition in the system. The dashed lines are constructed by connecting the inflection points where the pressure is minimum and its first order derivative is zero. Below this boundary, the derivative of the pressure is negative and the system is mechanically unstable. It can be observed that this unstable region, which is called the spinodal instability region, is only present up to critical temperature T_C [24, 27]. Above this temperature $\partial P/\partial \rho$ is always positive, pressure becomes an increasing function of density and the system can only be in the gas phase [28]. As the temperature and baryon density decrease, the system tends to enter the spinodal region where the density fluctuations grow rapidly, leading to multifragmentation process.

For subcritical temperatures, the two phases of nuclear matter can coexist inside the spinodal region where the liquid nuclear matter is in equilibrium with the gas phase. In the phase coexistence region, two different values for the baryon density are found for a given pressure and temperature associated with the two different phases [11]. The pressures and the chemical potentials of two phases coincide in the liquid-gas mixture [29]. At the critical point, the liquid and gas densities become equal and the coexistence region disappears into a uniform nuclear

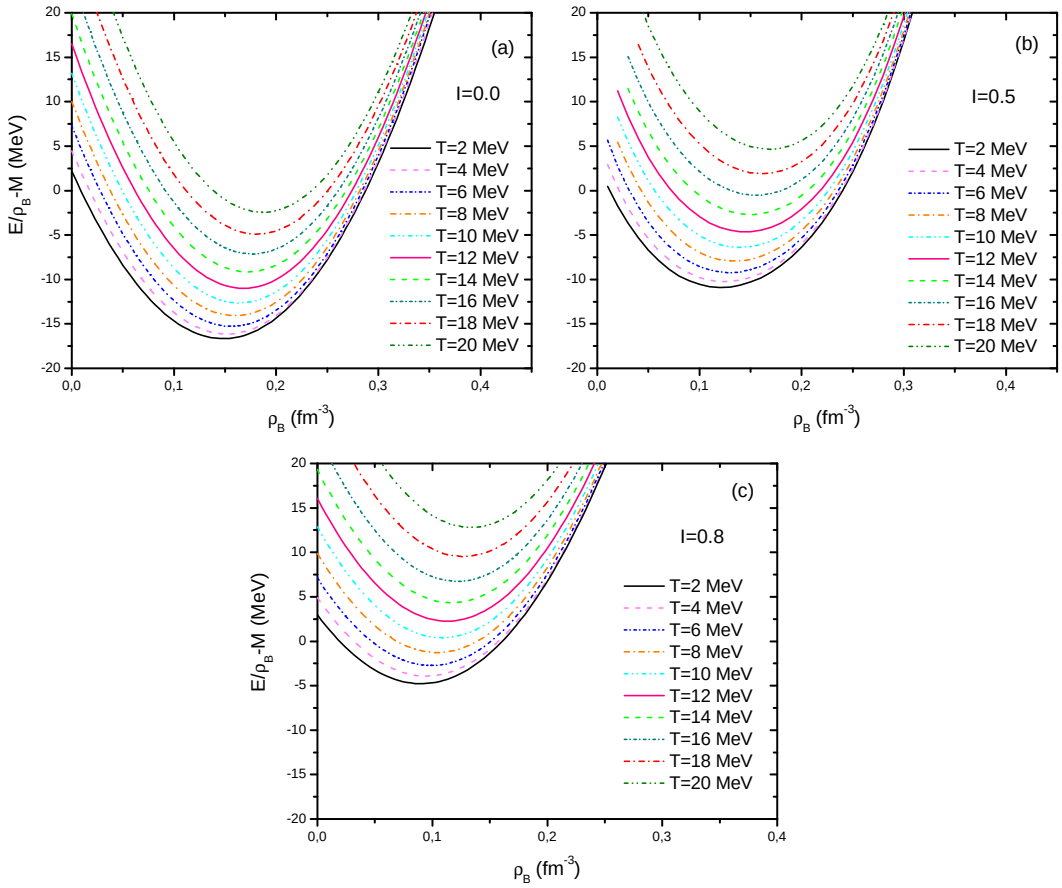

Figure 2.3: Energy per nucleon as a function of the baryon density ρ_B, for fixed asymmetry values $I = 0.0$ in panel (a), $I = 0.5$ in panel (b) and $I = 0.8$ in panel (c), at various temperatures.

matter at gas state in above temperatures.

In this work, we determined the critical temperature to be around $T_c = 14\ MeV$ for $I = 0.0$, corresponding to a critical density around $\rho_B = 0.4\rho_0$. When the asymmetry is changed to $I = 0.2$, the critical temperature is found as approximately $T_c = 14\ MeV$ and $T_c = 12\ MeV$ when $I = 0.5$.

The isospin dependence of the equation of state is presented in Fig. 2.5 at fixed temperatures $T = 5\ MeV$ and $T = 1\ MeV$. From the graph, we can conclude that the equation of state of hot asymmetric nuclear matter has a strong dependence on isospin at low energy scales. It can be observed that the minimum pressure value of the system increases with

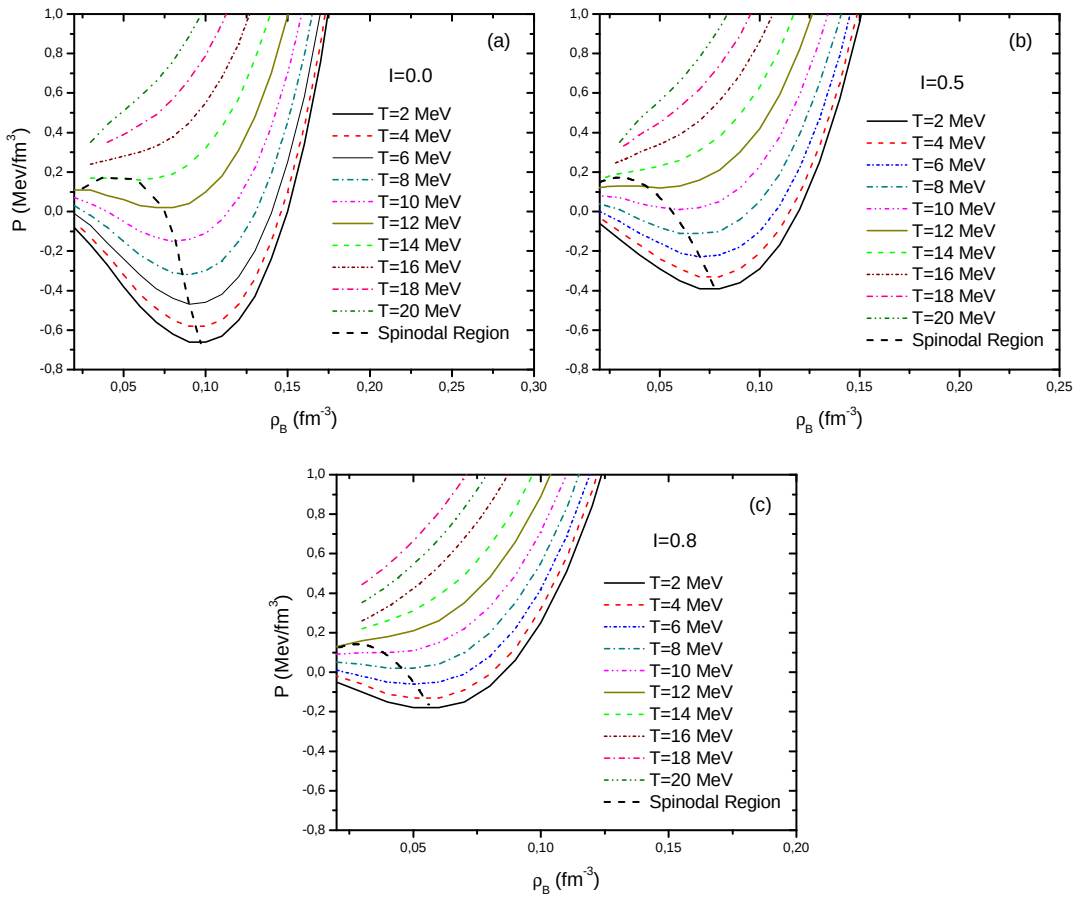

Figure 2.4: Pressure as a function of the baryon density ρ_B, for fixed asymmetry values $I = 0.0$ in panel (a), $I = 0.2$ in panel (b) and $I = 0.5$ in panel (c), at various temperatures.

increasing asymmmetry. The behaviour of the curves indicates that the neutron rich nuclear matter reaches T_c at lower temperatures and densities than the symmetric nuclear matter, therefore the spinodal region is smaller.

2.2.2 Chemical Potential

Within the picture of standard thermodynamics, the neutron and proton chemical potentials can be defined as the baryon density derivatives of the single particle energies, $\mu_q = \left(\frac{\partial U_q}{\partial \rho_q}\right)$, where q denotes the neutron or proton [30]. Physically, the chemical potential can be understood as the incerase in the energy when the number of particles in the system is raised by unity. It should be noted that, since the nuclear matter is a closed system with no exchange of particles with the surroundings, μ_p and μ_n refer to the local values of the chemical potentials

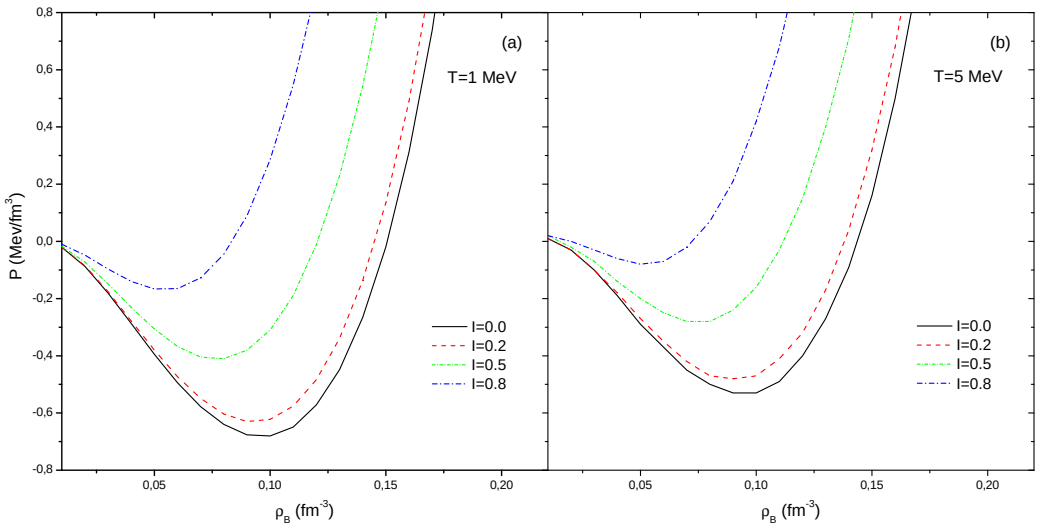

Figure 2.5: Pressure as a function of the baryon density ρ_B, for different values asymmetry parameter at fixed temperatures $T = 1\ MeV$ in panel (a) and $T = 5\ MeV$ in panel (b).

for neutron and proton [15].

As stated in Ref. 30, in the presence of the ρ meson interaction, the chemical potential is a quantity that depends on both the third component of the isospin operator, τ_3 and the ρ meson effective coupling, g_ρ. Therefore, the isospin dynamics of the system can be investigated with the analysis of the density dependence of μ_p and μ_n.

If the chemical potentials of the liquid and gas phases are equal, the system is said to be in chemical equilibrium and the phase coexistence region is specified with the Gibbs conditions;

$$\begin{aligned} \mu_q^L(T, \rho_q^L) &= \mu_q^G(T, \rho_q^G) \\ p_q^L(T, \rho_q^L) &= p_q^G(T, \rho_q^G) \end{aligned} \tag{2.35}$$

where p_q is the pressure and the liquid and gas phases are denoted by L and G respectively. In non-equilibrium cases, the local mass flow in the system occurs from the regions with higher values of chemical potential to the lower ones until the equilibrium is established [15].

Furthermore, the stability conditions for the liquid gas mixture can be defined as [30],

$$\begin{aligned} &\rho_B \left(\frac{\partial p}{\partial \rho_B}\right)_{T,I} > 0 \\ &\left(\frac{\partial \mu_p}{\partial I}\right)_{T,p} < 0 \quad or \quad \left(\frac{\partial \mu_n}{\partial I}\right)_{T,p} > 0\,. \end{aligned} \tag{2.36}$$

For the asymmetric nuclear matter at zero temperature, the chemical potential is given for proton and neutron in terms of the baryon densities and the asymmetry parameter as,

$$\mu_p = \sqrt{\left(\frac{3\pi^2}{2}\rho_{B,p}\right)^{2/3}(1-I)^{2/3}(\hbar c)^2 + (M^* c^2)^2} \tag{2.37}$$

$$\mu_n = \sqrt{\left(\frac{3\pi^2}{2}\rho_{B,n}\right)^{2/3}(1+I)^{2/3}(\hbar c)^2 + (M^* c^2)^2}\ . \tag{2.38}$$

$\rho_{B,p}$ and $\rho_{B,n}$ can be written in terms of the Fermi momentum as below,

$$\rho_{B,q} = \frac{1}{3\pi^2}k_{F,q}^3 \tag{2.39}$$

where the Fermi momentum is defined as $k_{F,p} = k_F(1-I)^{1/3}$ for proton and $k_{F,n} = k_F(1+I)^{1/3}$ for neutron. It can be observed that if the nuclear system is symmetric, the asymmetry parameter is zero and $\mu_p = \mu_n$.

For a nuclear system consists of protons and neutrons, the chemical potential is also reduced such as the mass and momentum of baryons, due to the interaction. The reduced chemical potential of proton is

$$\begin{aligned} \mu_p^* &= \mu - \left[g_{\mathrm{v}}V_0 + \frac{1}{2}g_\rho b_{3,0} + eA_0\right] \\ &= \mu - \rho_B\left(\frac{g_{\mathrm{v}}^2}{\mu_{\mathrm{v}}^2} - \frac{1}{4}\frac{g_\rho^2}{\mu_\rho^2}I\right)\ . \end{aligned} \tag{2.40}$$

For neutron, it is

$$\begin{aligned} \mu_n^* &= \mu - \left[g_{\mathrm{v}}V_0 - \frac{1}{2}g_\rho b_{3,0}\right] \\ &= \mu - \rho_B\left(\frac{g_{\mathrm{v}}^2}{\mu_{\mathrm{v}}^2} + \frac{1}{4}\frac{g_\rho^2}{\mu_\rho^2}I\right)\ . \end{aligned} \tag{2.41}$$

The isospin dynamics of the asymmetric nuclear matter can also be studied by demonstrating the baryon density variations of the proton and neutron chemical potentials, as shown in Fig. 2.6. The solid lines represent μ_p while the dashed lines stand for μ_n, both are given at different values of asymmetry at $T = 5\ MeV$. For $I = 0.0$ case, the chemical potentials of neutron and proton coincide.

The variations of μ_p and μ_n as a fuction of asymmetry parameter are also shown in Fig. 2.7 at $T = 5\ MeV$. We can observe that μ_p is a decreasing function of asymmetry while μ_n increases as I is increased. Also, as the initial baryon density of the system is changed from

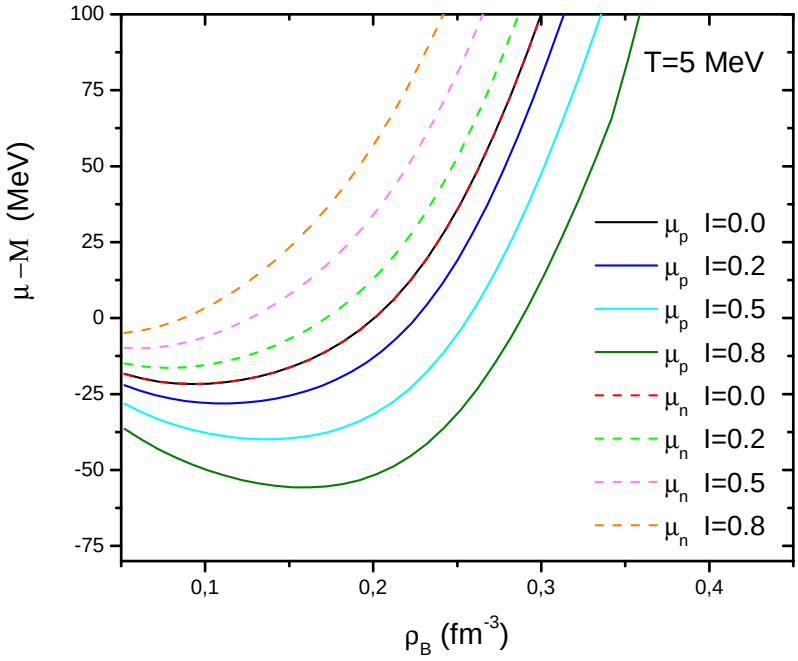

Figure 2.6: Proton and neutron chemical potentials as a function of the baryon density ρ_B, for different values of asymmetry parameter at fixed temperature $T = 5\ MeV$.

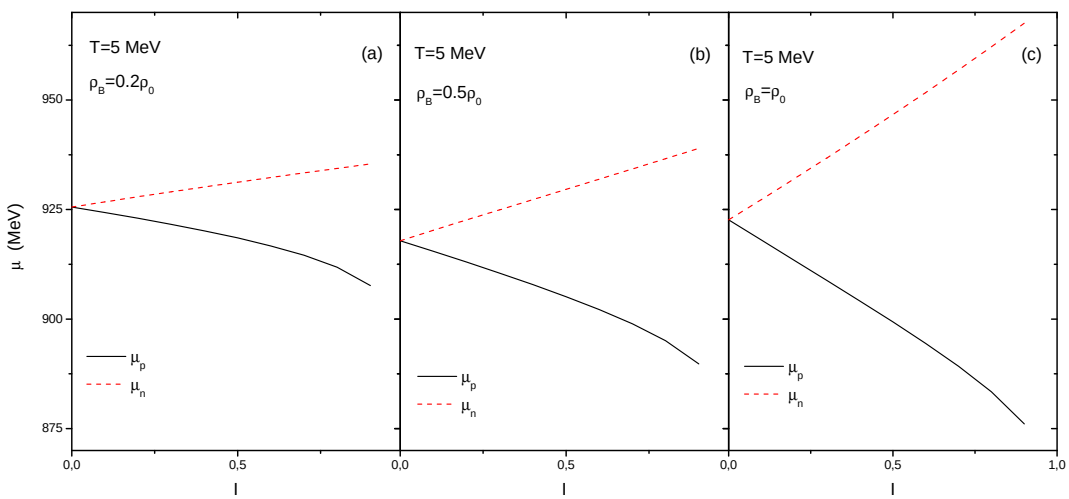

Figure 2.7: Proton and neutron chemical potentials as a function of the asymmetry parameter I, for fixed values of initial baryon densities $\rho_B = 0.0\rho_0$ in panel (a), $\rho_B = 0.5\rho_0$ in panel (b) and $\rho_B = 0.8\rho_0$ in panel (a), at fixed temperature $T = 5\ MeV$.

$\rho_B = 0.2\rho_0$ to $\rho_B = \rho_0$, the gap between the proton and neutron chemical potentials are also increased.

Fig. 2.8 demonstrates the density dependence of the reduced chemical potentials given in Eqs. (2.40) and (2.41). Again, the dashed lines show the reduced chemical potential for neutron and solid lines represent the proton. For all values of asymmetry parameter, the same descending trend is observed with increasing baryon density.

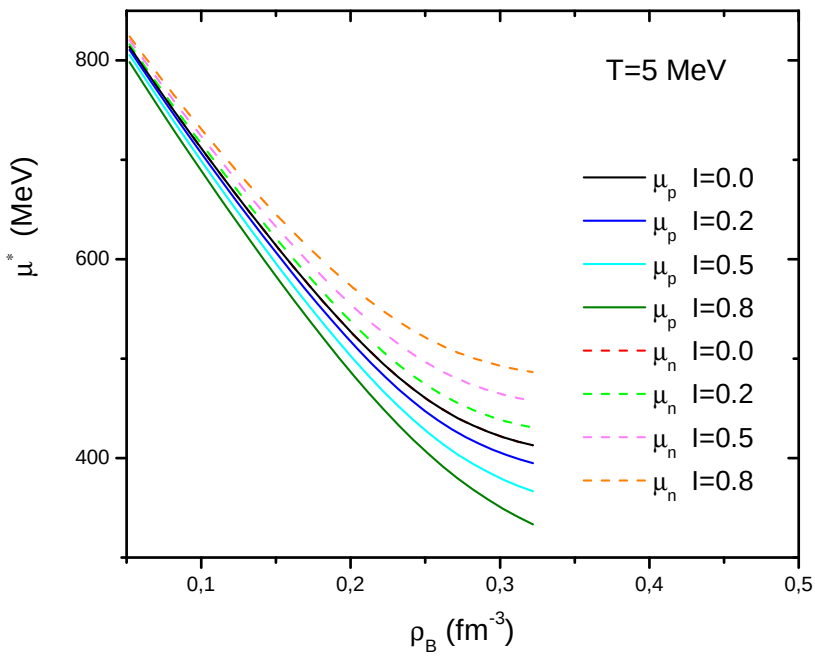

Figure 2.8: Reduced proton and neutron chemical potentials as a function of the baryon density ρ_B, for different values of asymmetry parameter at fixed temperature $T = 5\ MeV$

CHAPTER 3

STOCHASTIC MEAN FIELD APPROACH

3.1 The Stochastic Extention of the Mean-Field Theory

The relativistic mean field theory is a good approximation concerning the evolution of the average collective motion at low energies. At this energy scales, the collisional fluctuations that result from two body collisions are not important and only the one body dissipation mechanism is sufficient to describe the dynamics of the system [17]. However, this approach have limitations in describing the fluctuation mechanism and can not be used to investigate the dynamics of the spinodal region. The stochastic extension of the mean field theory is therefore proposed to describe the density fluctuations at low energies (around $10\ MeV$/nucleon) in a microscopic level [31].

If we consider a nuclear many body system that consists of protons and neutrons, in the standard mean field approximation the initial state of the system will be well defined and this will provide a deterministic evolution in time. For such a system, the time dependent wave function is a Slater determinant that consists of a number of single particle wave functions, $\phi_j(\vec{r}, t)$, and the time evolution is investigated with the Time-Dependent Hartree-Fock (TDHF) equation [18],

$$i\hbar\frac{\partial}{\partial t}\rho_q(t) = [h_\alpha(\rho), \rho_q(t)] \tag{3.1}$$

where q denotes the neutron or proton, $h(\rho)$ is the self-consistent mean field Hamiltonian and $\rho(t)$ is the single particle density matrix defined as $\rho(\vec{r}, \vec{r}^{\,\prime}, t) = \sum_j \phi_j^*(\vec{r}, t) n_j \phi_j(\vec{r}^{\,\prime}, t)$. Here, n_j denotes the occupation factor and it is equal to 1 for occupied states and 0 for unoccupied ones.

The stochastic approach offers a probabilistic description that can simulate the mean field fluctuations by retaining only initial correlations. In this manner, a superposition of determinantal wave functions are used instead of a single Slater determinant to describe the initial conditions [32]. Being different from the standard TDHF, the time dependent single particle wave functions for proton and neutron evolve under the effect of the mean field potential of the corresponding event and the time evolution of each member of the single particle density matrix $\rho_q^\lambda(t)$, is given by the transport equation,

$$i\hbar\frac{\partial}{\partial t}\rho_q^\lambda(t) = \Big[h_q(\rho_q^\lambda), \rho_q^\lambda(t)\Big] \tag{3.2}$$

It should be noted that, $\rho_q(t)$ is a four by four matrix in the spinor space whose elements are Gaussian random numbers [20].

By imposing the random initial conditions in the ensemble of the density matrices, the initial density fluctuations and the one-body dissipation mechanism is generated within a stochastic manner in the mean field theory of the collision dynamics.

3.2 Vlasov Equation

Since we are studying the semi-classical limit of the relativistic mean field theory, the TDHF equation can be reduced to the Vlasov equation and can be derived by starting from the non-linear Walecka Model for the asymmetric nuclear matter. This relativistic differential equation provides the time evolution of the phase space distribution function and therefore will be used to describe the fluctuation dynamics of the system at low energies [33].

By using the QHD-II Lagrangian density, the Dirac equation for the nucleon field is obtained in Eq. (2.6) within the relativistic mean field approximation,

$$i\hbar\partial_t\psi = \{\vec{\alpha}c\vec{p^*} + \beta M^* c^2 + g_{\rm v}V_0 + \frac{1}{2}\tau_3 b_{3,0} + \frac{1}{2}e(1+\tau_3)A_0\}\psi \tag{3.3}$$

where the reduced momentum $\vec{p}^*$ is given as $c\vec{p^*} = c\vec{p} - g_{\rm v}\vec{V} - \frac{1}{2}g_\rho\tau_a\vec{b_a} - \frac{1}{2}e(1+\tau_3)\vec{A}$ and the reduced mass is $M^* = Mc^2 - g_s\phi$.

The nucleon field can be expressed in terms of the large (ψ_L) and small (ψ_S) components as $\psi = \begin{pmatrix}\psi_L\\ \psi_S\end{pmatrix}$. Furthermore, following the use of the definitions $\vec{\alpha} = \begin{pmatrix}0 & \vec{\sigma}\\ \vec{\sigma} & 0\end{pmatrix}$ and $\beta = \gamma^0 =$

$\begin{pmatrix} 1 & 0 \\ 0 & -1 \end{pmatrix}$, the Dirac equation can be splitted into two coupled equations;

$$i\hbar\partial_t\psi_L = \vec{\sigma}c\vec{p^*}\psi_S + M^*c^2\psi_L + \left(g_{\rm v}V_0 + \frac{1}{2}\tau_3 b_{3,0} + \frac{1}{2}e(1+\tau_3)A_0\right)\psi_L$$
$$i\hbar\partial_t\psi_S = \vec{\sigma}c\vec{p^*}\psi_L - M^*c^2\psi_S + \left(g_{\rm v}V_0 + \frac{1}{2}\tau_3 b_{3,0} + \frac{1}{2}e(1+\tau_3)A_0\right)\psi_S \ . \tag{3.4}$$

In the relativistic mean field approximation, the nucleons can be treated as free particles moving in the classical fields that are created by mesons. So, the plane wave solutions for free nucleons in a uniform system can be introduced as $\Psi = \psi(\vec{p},\lambda)e^{i(\vec{p}\cdot\vec{x}-\varepsilon(k)t)}$, where $\psi(\vec{p},\lambda)$ is a four component Dirac spinor with spin index λ. With this free particle solution, the Dirac equation becomes,

$$\varepsilon\psi(\vec{p},\lambda) - \vec{\alpha}c\vec{p^*}\psi(\vec{p},\lambda) - \left(g_{\rm v}V_0 + \frac{1}{2}g_\rho\tau_3 b_{3,0} + \frac{1}{2}e(1+\tau_3)A_0\right)\psi(\vec{p},\lambda)$$
$$- \quad \beta M^*c^2\psi(\vec{p},\lambda) = 0 \ . \tag{3.5}$$

Solving this equation for the Dirac spinor provides us the relations between the large and small components of the nucleon field and consequently, the two coupled equations reduce to a single one;

$$\psi_L = \frac{\vec{\sigma}\cdot c\vec{p^*}}{\varepsilon^* - M^*c^2}\psi_S \quad \text{and} \quad \psi_S = \frac{\vec{\sigma}\cdot c\vec{p^*}}{\varepsilon^* + M^*c^2}\psi_L, \tag{3.6}$$

$$\varepsilon\psi(\vec{p},\lambda) = \left(\varepsilon^* + g_{\rm v}V_0 + \frac{1}{2}g_\rho\tau_3 b_{3,0} + \frac{1}{2}g_\rho e(1+\tau_3)A_0\right)\psi(\vec{p},\lambda) \tag{3.7}$$

where the energy operator is $\varepsilon^* = \sqrt{(c\vec{p^*})^2 + (M^*c^2)^2}$. More generally, the operator form of this equation can be used,

$$i\hbar\partial_t\psi(\vec{x},t) = \left[\sqrt{(c\vec{p^*})^2 + (M^*c^2)^2} + g_{\rm v}V_0 + \frac{1}{2}g_\rho\tau_3 b_{3,0} + \frac{1}{2}e(1+\tau_3)A_0\right]\psi(\vec{x},t) \tag{3.8}$$

in which we can define the effective one body Hamiltonian as $h = E^* + g_{\rm v}V_0 + \frac{1}{2}g_\rho\tau_3 b_{3,0} + \frac{1}{2}g_\rho e(1+\tau_3)A_0$ and E^* is the operator form of ε^*.

The simplest form of Eq. (3.8), $i\hbar\partial_t\psi(\vec{x},t) = h\psi(\vec{x},t)$, can be used to investigate the time evolution of the single particle baryon density matrix $\rho(\vec{r_1},\vec{r_2},t) = \psi^\dagger(\vec{r_1},t)\psi(\vec{r_2},t)$ between two space positions $\vec{r_1}$ and $\vec{r_2}$,

$$i\hbar\partial_t\rho(\vec{r_1},\vec{r_2},t) = h(\vec{r_1})\rho(\vec{r_1},\vec{r_2},t) - h(\vec{r_2})\rho(\vec{r_1},\vec{r_2},t) \ . \tag{3.9}$$

This result is analogous to the non-relativistic TDHF equation.

The phase space distribution function can be defined as the Wigner transform of the baryon density matrix;

$$f(\vec{p},\vec{r},t) = \int \frac{d^3s}{(2\pi\hbar c)^3} e^{-i\vec{p}\cdot\vec{s}/\hbar} \rho(\vec{r}+\frac{\vec{s}}{2},\vec{r}-\frac{\vec{s}}{2},t) \tag{3.10}$$

where $\vec{r} = (\vec{r}_1 + \vec{r}_2)/2$ and $\vec{s} = \vec{r}_1 - \vec{r}_2$ are used in the transformation. In this expression, $\rho(\vec{r}+\frac{\vec{s}}{2},\vec{r}-\frac{\vec{s}}{2},t) = \langle \vec{r}+\frac{\vec{s}}{2}|\rho(t)|\vec{r}-\frac{\vec{s}}{2}\rangle$ is the expectation value of the single particle density operator.

Also, applying another Wigner transformation to $h(\rho)$ allows us to obtain the one-body Hamiltonian in terms of $\vec{r}$, $\vec{p}$ and t as,

$$h(\vec{r},\vec{p},t) = \int \frac{d^3s}{(2\pi\hbar c)^3} e^{-i\vec{p}\cdot\vec{s}/\hbar} h(\vec{r}+\frac{\vec{s}}{2},\vec{r}-\frac{\vec{s}}{2},t) \tag{3.11}$$

with the definition $h(\vec{r}+\frac{\vec{s}}{2},\vec{r}-\frac{\vec{s}}{2},t) = \langle \vec{r}+\frac{\vec{s}}{2}|h[\rho]|\vec{r}-\frac{\vec{s}}{2}\rangle$.

Since the Hamiltonian and the single particle density operator are Hermitian, the Wigner transformation of the TDHF equation yields,

$$\begin{aligned} i\hbar\frac{\partial}{\partial t} f(\vec{r},\vec{p},t) &= (h[\rho]\rho(t))_W - (\rho(t)h[\rho])_W \\ &= h(\vec{r},\vec{p})\left(e^{(i\hbar/2)\overleftrightarrow{\wedge}} - e^{(-i\hbar/2)\overleftrightarrow{\wedge}}\right) f(\vec{r},\vec{p},t) \\ &= 2ih(\vec{r},\vec{p})\sin\left(\frac{\hbar}{2}\overleftrightarrow{\wedge}\right) f(\vec{r},\vec{p},t) \end{aligned} \tag{3.12}$$

where the operator $\overleftrightarrow{\wedge}$ is given as $\overleftarrow{\nabla}_r\overrightarrow{\nabla}_p - \overleftarrow{\nabla}_p\overrightarrow{\nabla}_r$. It should be noted that the gradient operators act in the direction of the arrows. Furthermore, the Taylor expansion for $\sin\left(\frac{\hbar}{2}\overleftrightarrow{\wedge}\right)$ can be introduced as,

$$\frac{\partial}{\partial t} f(\vec{r},\vec{p},t) = 2h(\vec{r},\vec{p},t)\left[\frac{1}{2}\overleftrightarrow{\wedge} + \frac{\hbar^2}{3!}\left(\frac{1}{2}\overleftrightarrow{\wedge}\right)^3 + ...\right] f(\vec{r},\vec{p},t). \tag{3.13}$$

In the semi-classical limit $\hbar \to 0$, then only the first term of the expansion is non-zero. Hence,

$$\begin{aligned} \frac{\partial}{\partial t} f(\vec{r},\vec{p},t) &= 2h(\vec{r},\vec{p},t)\left[\frac{1}{2}\overleftrightarrow{\wedge}\right] f(\vec{r},\vec{p},t) \\ &= h(\vec{r},\vec{p},t)\left[\overleftarrow{\nabla}_r\overrightarrow{\nabla}_p - \overleftarrow{\nabla}_p\overrightarrow{\nabla}_r\right] f(\vec{r},\vec{p},t)\,. \end{aligned} \tag{3.14}$$

This is actually called as the relativistic Vlasov equation,

$$\frac{\partial}{\partial t} f(\vec{r},\vec{p},t) + \vec{\nabla}_p h(\vec{r},\vec{p},t)\cdot\vec{\nabla}_r f(\vec{r},\vec{p},t) - \vec{\nabla}_r h(\vec{r},\vec{p},t)\cdot\vec{\nabla}_p f(\vec{r},\vec{p},t) = 0 \tag{3.15}$$

which describes the time evolution of the phase space distribution function in the semi-classical limit. In an asymmetric system of protons and neutrons, the phase space distribution function should be introduced seperately for the components. As a result, two coupled Vlasov equations are found for such a system;

$$\frac{\partial}{\partial t} f_p(\vec{r},\vec{p},t) + \vec{\nabla}_p h_p(\vec{r},\vec{p},t) \cdot \vec{\nabla}_r f_p(\vec{r},\vec{p},t) - \vec{\nabla}_r h_p(\vec{r},\vec{p},t) \cdot \vec{\nabla}_p f_p(\vec{r},\vec{p},t) = 0 \ , \tag{3.16}$$

$$\frac{\partial}{\partial t} f_n(\vec{r},\vec{p},t) + \vec{\nabla}_p h_n(\vec{r},\vec{p},t) \cdot \vec{\nabla}_r f_n(\vec{r},\vec{p},t) - \vec{\nabla}_r h_n(\vec{r},\vec{p},t) \cdot \vec{\nabla}_p f_n(\vec{r},\vec{p},t) = 0 \tag{3.17}$$

where $h_p(\vec{r},\vec{p},t)$ and $h_n(\vec{r},\vec{p},t)$ are the one body potentials seperately for proton and neutron.

Furthermore, in the semi-classical limit of the stochastic approach, we need to generate an ensemble of phase space distribution functions $f_q^{\lambda}(\vec{r},\vec{p},t)$, where λ shows the event label. Since we are dealing with the asymmetric nuclear matter, the phase space distribution function should be specified for neutron and proton seperately, denoted by $q = (p,n)$. In the semi-classical limit, the main assumption of this approach is that, each initial phase space distribution function $f^{\lambda}(\vec{r},\vec{p},0)$ is a Gaussian random number with a mean field value $\overline{f(\vec{r},\vec{p},0)} = f_0(\vec{r},\vec{p})$, where the overline denotes the averaging over the ensemble. A second moment is defined for $f^{\lambda}(\vec{r},\vec{p},0)$ as

$$\overline{\delta f(\vec{r},\vec{p},0)\delta f(\vec{r}',\vec{p}',0)} = (2\pi\hbar^3)\delta(\vec{r}-\vec{r}')\delta(\vec{p}-\vec{p}')f_0(\vec{r},\vec{p})[1-f_0(\vec{r},\vec{p})] \ . \tag{3.18}$$

In the homogeneous initial state, where the system is at equilibrium, the initial phase space distribution function only depends on the momentum and can be denoted by a Fermi-Dirac distribution function $f_0(\vec{p}) = 1/[e^{\beta(\varepsilon_0^*-\mu_0^*)}+1]$, where $\beta = 1/k_BT$ [32].

3.3 Linearization of the Field Equations

In the spinodal region, the early amplitudes of the density fluctuations are small and therefore, the dynamical evolution of the system can be investigated by linearizing the density

expressions as follows,

$$\begin{aligned}
\rho_{B,q} &\to \rho^0_{B,q} + \delta\rho_{B,q}(\vec{r},t) \\
\rho_{s,q} &\to \rho^0_{s,q} + \delta\rho_{s,q}(\vec{r},t) \\
\vec{\rho}_{\mathrm{v},q} &\to \vec{\rho}^0_{\mathrm{v},q} + \delta\vec{\rho}_{\mathrm{v},q}(\vec{r},t)
\end{aligned} \tag{3.19}$$

where the higher order terms are ignored. Then in the linear regime, the linearized meson field expressions become

$$\begin{aligned}
\phi &\to \phi_0 + \delta\phi(\vec{r},t) \\
V^\mu &\to V^\mu_0 + \delta V^\mu(\vec{r},t) \\
b^\mu &\to b^\mu_0 + \delta b^\mu(\vec{r},t) \\
A^\mu &\to A^\mu_0 + \delta A^\mu(\vec{r},t)\ .
\end{aligned} \tag{3.20}$$

Here, the time and space components of the vector fields should be linearized seperately and despite the fact that the vector components of the fields $\vec{V}$, $\vec{b}$, $\vec{A}$ are zero in the equilibrium state, the corresponding fluctuations $\delta\vec{V}$, $\delta\vec{b}$, $\delta\vec{A}$ are non-zero.

The linearized field equation for the scalar field is found as,

$$\left(\partial_\mu\partial^\mu + \mu_{\mathrm{s}}^2 + \kappa\phi_0(\vec{r},t) + \frac{\lambda}{2}\phi_0^2(\vec{r},t)\right)\delta\phi(\vec{r},t) = g_{\mathrm{s}}\delta\rho_{\mathrm{s}}(\vec{r},t) \tag{3.21}$$

and will be solved self consistently with the reduced mass in order to obtain $\delta\phi(\vec{r},t)$. Furthermore, two seperate linearized field equations are obtained for each of the space and time components of the neutral vector meson, the charged vector meson and the photon field, given respectively as

$$\begin{aligned}
\left(\partial_\mu\partial^\mu + \mu_{\mathrm{v}}^2\right)\delta V_0(\vec{r},t) &= g_{\mathrm{v}}\delta\rho_B(\vec{r},t) \\
\left(\partial_\mu\partial^\mu + \mu_{\mathrm{v}}^2\right)\delta\vec{V}(\vec{r},t) &= g_{\mathrm{v}}\delta\vec{\rho}_{\mathrm{v}}(\vec{r},t)
\end{aligned} \tag{3.22}$$

$$\begin{aligned}
\left(\partial_\mu\partial^\mu + \mu_\rho^2\right)\delta b_0(\vec{r},t) &= \frac{1}{2}g_\rho\left(\delta\rho_{B,p}(\vec{r},t) - \delta\rho_{B,n}(\vec{r},t)\right) \\
\left(\partial_\mu\partial^\mu + \mu_\rho^2\right)\delta\vec{b}(\vec{r},t) &= \frac{1}{2}g_\rho\left(\delta\vec{\rho}_{\mathrm{v},p}(\vec{r},t) - \delta\vec{\rho}_{\mathrm{v},n}(\vec{r},t)\right)
\end{aligned} \tag{3.23}$$

$$\begin{aligned}
\partial_\mu\partial^\mu\delta A_0(\vec{r},t) &= \delta\rho_p(\vec{r},t) \\
\partial_\mu\partial^\mu\delta\vec{A}(\vec{r},t) &= \delta\vec{\rho}_p(\vec{r},t)\ .
\end{aligned} \tag{3.24}$$

3.4 Linearization of the Vlasov Equation

In order to obtain information about the fluctuations in the phase space distribution function, the Vlasov equation can be linearized around the equilibrium value, $f_0(\vec{p})$. Hence, considering the linear response treatment, the small amplitude fluctuations in the phase space distribution function and the one-body Hamiltonian U_0 are given as $f_q(\vec{r},\vec{p},t) = f_0(\vec{p}) + \delta f_q(\vec{r},\vec{p},t)$ and $U_q(\vec{r},\vec{p},t) = U_{q,0}(\vec{p}) + \delta U_q(\vec{r},\vec{p},t)$ where $q = (p,n)$. For a reminder, the phase space distribution function of an average, homogeneous initial state is given in the form of a Fermi-Dirac distribution $f_0(\vec{p}) = 1/\left[e^{\beta(\epsilon_0^* - \mu_0^*)} + 1\right]$. Since the system is initially in a homogeneous equilibrium state, the time and space derivatives of $f_0(\vec{p})$ and $U_0(\vec{p})$ vanishes however, the momentum derivatives are not zero and $\vec{\nabla}_p U_q(\vec{p})$ corresponds to the velocities of the single particles in the mean-field potential.

Imposing the linear expansions, the Vlasov equation becomes

$$\frac{\partial}{\partial t}\delta f_p(\vec{r},\vec{p},t) + \vec{\mathrm{v}}_{0,p}\cdot\vec{\nabla}_r\delta f_p(\vec{r},\vec{p},t) - \vec{\nabla}_p f_{0,p}(\vec{p})\cdot\vec{\nabla}_r\delta U_p(\vec{r},\vec{p},t) = 0 \tag{3.25}$$

for proton, and

$$\frac{\partial}{\partial t}\delta f_n(\vec{r},\vec{p},t) + \vec{\mathrm{v}}_{0,n}\cdot\vec{\nabla}_r\delta f_n(\vec{r},\vec{p},t) - \vec{\nabla}_p f_{0,n}(\vec{p})\cdot\vec{\nabla}_r\delta U_n(\vec{r},\vec{p},t) = 0 \tag{3.26}$$

for neutron.

The phase space distribution functions for proton and neutron should be specified uniquely at time t as $f_p(\vec{r},\vec{p},t) = \frac{1}{e^{\beta(\varepsilon_p^* - \mu_p^*)}+1}$ and $f_n(\vec{r},\vec{p},t) = \frac{1}{e^{\beta(\varepsilon_n^* - \mu_n^*)}+1}$. Also, the fluctuations in U_p and U_n can also be written linearly in terms of the small amplitude fluctuations in the meson fields as follows,

$$\begin{aligned}\delta U_q &= \left(\frac{\partial U_q}{\partial V_i}\right)_0 \delta V_i + \left(\frac{\partial U_q}{\partial V_0}\right)_0 \delta V_0 + \left(\frac{\partial U_q}{\partial \phi}\right)_0 \delta\phi + \left(\frac{\partial U_q}{\partial b_{3,i}}\right)_0 \delta b_{3,i} \\ &+ \left(\frac{\partial U_q}{\partial b_{3,0}}\right)_0 \delta b_0 + \left(\frac{\partial U_q}{\partial A_i}\right)_0 \delta A_i + \left(\frac{\partial U_q}{\partial A_0}\right)_0 \delta A_0 \end{aligned} \tag{3.27}$$

where the sub index zero indicates the equilibrium state.

The derivatives can simply be evaluated following Eq. (2.23), then δU_q and δU_n can be found as,

$$\begin{aligned}\delta U_p &= -g_{\mathrm{v}}\frac{c\vec{p}}{\varepsilon_0^*}\delta V_i(\vec{r},t) + g_{\mathrm{v}}\delta V_0(\vec{r},t) - g_s\frac{M_0^* c^2}{\varepsilon_0^*}\delta\phi(\vec{r},t) - \frac{1}{2}g_\rho\frac{c\vec{p}}{\varepsilon_0^*}\delta b_{3,i}(\vec{r},t) \\ &+ \frac{1}{2}g_\rho\delta b_0(\vec{r},t) - e\frac{c\vec{p}}{\varepsilon_0^*}\delta A_i(\vec{r},t) + e\delta A_0(\vec{r},t) \end{aligned} \tag{3.28}$$

$$\delta U_p = -g_{\rm v}\frac{c\vec{p}}{\varepsilon_0^*}\delta V_i(\vec{r},t) + g_{\rm v}\delta V_0(\vec{r},t) - g_s\frac{M_0^* c^2}{\varepsilon_0^*}\delta\phi(\vec{r},t) + \frac{1}{2}g_\rho\frac{c\vec{p}}{\varepsilon_0^*}\delta b_{3,i}(\vec{r},t) + \frac{1}{2}g_\rho\delta b_0(\vec{r},t) \tag{3.29}$$

By definition, the baryon, scalar and vector densities can be given as the Fourier transforms of the phase space distribution function, seperately for neutron and proton;

$$\rho_{B,q}(\vec{r},t) = \gamma\int\frac{d^3p}{(2\pi\hbar)^3}f_q(\vec{r},\vec{p},t) \tag{3.30}$$

$$\rho_{{\rm s},q}(\vec{r},t) = \gamma\int\frac{d^3p}{(2\pi\hbar)^3}\frac{M^*c^2}{\varepsilon_q^*}f_q(\vec{r},\vec{p},t) \tag{3.31}$$

$$\vec{\rho}_{{\rm v},q}(\vec{r},t) = \gamma\int\frac{d^3p}{(2\pi\hbar)^3}\frac{c\vec{p}_q^*}{\varepsilon_q^*}f_q(\vec{r},\vec{p},t)\ . \tag{3.32}$$

Here, γ denotes the spin-isospin character of the system, which is equal to 2 in our case, for the asymmetric nuclear matter. Relating the densities to the phase space distribution function allows us to find the small amplitude fluctuations in the densities following the fact that $\delta f_q(\vec{r},\vec{p},t)$ satisfies the linearized Vlasov equation.

Previously, we have introduced the small fluctuations in the phase space distribution function $\delta f_q(\vec{r},\vec{p},t)$ and the densities $\delta\rho_B(\vec{r},t)$, $\delta\rho_s(\vec{r},t)$, $\delta\vec{\rho}_\nu(\vec{r},t)$ in terms of space, momentum and time. However, the wave number $\vec{k}$ is the quantity that characterizes the collective modes and the growth rates will be investigated depending on the wave number in the following chapter. Therefore, Fourier transformation should be applied in order to obtain these quantities depending on $\vec{k}$, $\vec{p}$ and t in the following manner,

$$\begin{aligned}\delta\tilde{f}_p(\vec{k},\vec{p},t) &= \int_0^\infty\frac{d^3k}{(2\pi)^3}e^{-i\vec{k}\cdot\vec{r}}\delta f_p(\vec{r},\vec{p},t)\\ \delta\tilde{f}_n(\vec{k},\vec{p},t) &= \int_0^\infty\frac{d^3k}{(2\pi)^3}e^{-i\vec{k}\cdot\vec{r}}\delta f_n(\vec{r},\vec{p},t)\ .\end{aligned} \tag{3.33}$$

Hence, the baryon, scalar and vector densities are written as;

$$\begin{aligned}\delta\rho_{B,q}(\vec{k},t) &= \int_0^\infty\frac{d^3k}{(2\pi)^3}e^{-i\vec{k}\cdot\vec{r}}\delta\rho_{B,q}(\vec{r},t)\\ \delta\rho_{s,q}(\vec{k},t) &= \int_0^\infty\frac{d^3k}{(2\pi)^3}e^{-i\vec{k}\cdot\vec{r}}\delta\rho_{s,q}(\vec{r},t)\\ \delta\vec{\rho_{{\rm v},q}}(\vec{k},t) &= \int_0^\infty\frac{d^3k}{(2\pi)^3}e^{-i\vec{k}\cdot\vec{r}}\delta\vec{\rho_{{\rm v},q}}(\vec{r},t)\end{aligned} \tag{3.34}$$

The fluctuations in the meson fields can be expressed in terms of the fluctuations in the densities with the use of these relations.

In order to obtain the frequency ω dependence of the system, another one-sided Fourier transform should be used;

$$\int_0^\infty \frac{\partial}{\partial t}\delta\tilde{f}_q(\vec{k},\vec{p},t)e^{i\omega t}dt = -\delta\tilde{f}_q(\vec{k},\vec{p},0) - i\omega\delta\tilde{f}_q(\vec{k},\vec{p},\omega) \tag{3.35}$$

where $\delta\tilde{f}_q(\vec{k},\vec{p},0)$ represents the Fourier transform of the initial fluctuations in the phase space distribution function. Furthermore, the one-sided Fourier transforms of density fluctuations can be found as,

$$\begin{aligned}
\delta\rho_{B,q}(\vec{k},\omega) &= \int_0^\infty dt e^{i\omega t}\delta\rho_{B,q}(\vec{k},t) && (3.36)\\
\delta\rho_{s,q}(\vec{k},\omega) &= \int_0^\infty dt e^{i\omega t}\delta\rho_{s,q}(\vec{k},t) && (3.37)\\
\delta\rho_{\vec{\mathrm{v}},q}(\vec{k},\omega) &= \int_0^\infty dt e^{i\omega t}\delta\rho_{\vec{\mathrm{v}},q}(\vec{k},t)\ . && (3.38)
\end{aligned}$$

Furthermore, for a free particle, the solution of the Klein-Gordon equation is assumed to be a plane wave function with the form $\phi(x^\mu) = e^{i(\vec{k}\cdot\vec{x}-wt)} = e^{i(k_\mu x^\mu)}$. Consequently, from the covarient field equations, the independent fluctuations in the fields can be found as,

$$\begin{aligned}
\delta\phi(\vec{k},\omega) &= \left[\frac{g_s}{-(\omega/c)^2 + k^2 + {\mu_s}^2 + \kappa\phi_0 + \frac{\lambda}{2}\phi_0^2}\right]\delta\rho_s(\vec{k},\omega)\\
\delta V_0(\vec{k},\omega) &= \frac{g_{\mathrm{v}}}{-(\omega/c)^2 + k^2 + {\mu_{\mathrm{v}}}^2}\delta\rho_B(\vec{k},\omega)\\
\delta\vec{V}(\vec{k},\omega) &= \frac{g_{\mathrm{v}}}{-(\omega/c)^2 + k^2 + {\mu_{\mathrm{v}}}^2}\delta\vec{\rho}_{\mathrm{v}}(\vec{k},\omega)\\
\delta b_0(\vec{k},\omega) &= \frac{g_\rho}{-(\omega/c)^2 + k^2 + {\mu_\rho}^2}\frac{1}{2}\delta\rho_3(\vec{k},\omega)\\
\delta\vec{b}(\vec{k},\omega) &= \frac{g_\rho}{-(\omega/c)^2 + k^2 + {\mu_\rho}^2}\frac{1}{2}\delta\vec{\rho}_3(\vec{k},\omega)\\
\delta A_0(\vec{k},\omega) &= \frac{e}{-(\omega/c)^2 + k^2}\delta\rho_{B,p}(\vec{k},\omega)\\
\delta\vec{A}(\vec{k},\omega) &= \frac{e}{-(\omega/c)^2 + k^2}\delta\vec{\rho}_{B,p}(\vec{k},\omega) && (3.39)
\end{aligned}$$

where we have used the expressions that is found earlier, $\mu_s^2\phi_0 + \frac{\kappa}{2}\phi_0^2 + \frac{\lambda}{6}\phi_0^3 = g_s{\rho_s}^0$, $V_0^0 = \frac{g_{\mathrm{v}}}{\mu_{\mathrm{v}}^2}\rho_B^0$, $b_0^0 = \frac{g_\rho}{2\mu_\rho^2}\rho_3^0$ and $A_0^0 = 0$. In the expressions, the source terms can be defined in terms of the associated proton and neutron densities as

$$\begin{aligned}
\delta\rho_s &= \delta\rho_{s,p}(\vec{k},\omega) + \delta\rho_{s,n}(\vec{k},\omega)\\
\delta\rho_B &= \delta\rho_{B,p}(\vec{k},\omega) + \delta\rho_{B,n}(\vec{k},\omega)\\
\delta\vec{\rho}_{\mathrm{v}} &= \delta\vec{\rho}_{\mathrm{v},p}(\vec{k},\omega) + \delta\vec{\rho}_{\mathrm{v},n}(\vec{k},\omega)\\
\delta\rho_3 &= \delta\rho_{B,p}(\vec{k},\omega) - \delta\rho_{B,n}(\vec{k},\omega)\ . && (3.40)
\end{aligned}$$

One important point to emphasize is that the fluctuations depend on $(\vec{k},\omega)$ while the meson fields are constants in equilibrium that are independent of space and time. Then the expressions for U_p and U_n can be rewritten as a function of frequency as,

$$\begin{aligned}\delta U_p &= -\left(G_\omega^2+G_\rho^2+G_\gamma^2\right)\frac{c\vec{p}}{\varepsilon_0^*}\cdot\delta\vec{\rho}_{\mathrm{v},p}-\left(G_\omega^2-G_\rho^2\right)\frac{c\vec{p}}{\varepsilon_0^*}\cdot\delta\vec{\rho}_{\mathrm{v},n}\\ &+ \left(G_\omega^2+G_\rho^2+G_\gamma^2\right)\delta\rho_{B,p}+\left(G_\omega^2-G_\rho^2\right)\delta\rho_{B,n}-\frac{M_0^*c^2}{\varepsilon_0^*}G_\sigma^2\delta\rho_{\mathrm{s}} \qquad (3.41)\end{aligned}$$

$$\begin{aligned}\delta U_n &= -\left(G_\omega^2-G_\rho^2\right)\frac{c\vec{p}}{\varepsilon_0^*}\cdot\delta\vec{\rho}_{\mathrm{v},p}-\left(G_\omega^2+G_\rho^2\right)\frac{c\vec{p}}{\varepsilon_0^*}\cdot\delta\vec{\rho}_{\mathrm{v},n}\\ &+ \left(G_\omega^2-G_\rho^2\right)\delta\rho_{B,p}+\left(G_\omega^2+G_\rho^2\right)\delta\rho_{B,n}-\frac{M_0^*c^2}{\varepsilon_0^*}G_\sigma^2\left(\delta\rho_{\mathrm{s},p}+\delta\rho_{\mathrm{s},n}\right) \qquad (3.42)\end{aligned}$$

where we have defined the quantities G_ω^2, G_σ^2, G_ρ^2 and G_γ^2 in terms of the point couplings,

$$\begin{aligned}G_\omega^2 &= \frac{g_{\mathrm{v}}^2}{-(\omega/c)^2+k^2+\mu_{\mathrm{v}}{}^2} \quad , \quad G_\sigma^2=\frac{g_s^2}{-(\omega/c)^2+k^2+\mu_s{}^2+\kappa\phi_0+\frac{\lambda}{2}\phi_0^2}\ ,\\ G_\rho^2 &= \frac{1}{4}\frac{g_\rho^2}{-(\omega/c)^2+k^2+\mu_\rho{}^2} \quad , \quad G_\gamma^2=\frac{e^2}{-(\omega/c)^2+k^2}\ . \qquad (3.43)\end{aligned}$$

Using this relations and the Eqs. (3.33-3.34), the linearized coupled Vlasov equations can be obtained for neutron and proton respectively as,

$$\begin{aligned}&\frac{\partial}{\partial_t}\int_0^\infty f_n(\vec{k},\vec{p},t)+i\vec{v}_0\cdot\vec{k}\delta f_n(\vec{k},\vec{p},t)-\left[i\vec{\nabla}_p f_n^0\cdot\vec{k}\right]\{-\left(G_\omega^2-G_\rho^2\right)\frac{c\vec{p}}{\varepsilon_0^*}\cdot\delta\vec{\rho_{\mathrm{v},p}}(\vec{k},t)\\ -&\left(G_\omega^2+G_\rho^2\right)\frac{c\vec{p}}{\varepsilon_0^*}\cdot\delta\vec{\rho_{\mathrm{v},n}}(\vec{k},t)+\left(G_\omega^2-G_\rho^2\right)\delta\rho_{B,p}(\vec{k},t)+\left(G_\omega^2+G_\rho^2\right)\delta\rho_{B,n}(\vec{k},t)\\ -&G_\sigma^2\frac{M_0^*c^2}{\varepsilon_0^*}\delta\rho_{s,p}(\vec{k},t)-G_\sigma^2\frac{M_0^*c^2}{\varepsilon_0^*}\delta\rho_{s,n}(\vec{k},t)\}=0 \qquad (3.44)\end{aligned}$$

$$\begin{aligned}&\frac{\partial}{\partial_t}\int_0^\infty f_p(\vec{k},\vec{p},t)+i\vec{v}_0\cdot\vec{k}\delta f_p(\vec{k},\vec{p},t)-\left[i\vec{\nabla}_p f_p^0\cdot\vec{k}\right]\{-\left(G_\omega^2+G_\rho^2+G_\gamma^2\right)\frac{c\vec{p}}{\varepsilon_0^*}\cdot\delta\vec{\rho_{\mathrm{v},p}}(\vec{k},\omega)\\ -&\left(G_\omega^2-G_\rho^2\right)\frac{c\vec{p}}{\varepsilon_0^*}\cdot\delta\vec{\rho_{\mathrm{v},n}}(\vec{k},\omega)+\left(G_\omega^2+G_\rho^2+G_\rho^2\right)\delta\rho_{B,p}(\vec{k},\omega)\\ +&\left(G_\omega^2-G_\rho^2\right)\delta\rho_{B,n}(\vec{k},\omega)-G_\sigma^2\frac{M_0^*c^2}{\varepsilon_0^*}\delta\rho_{s,p}(\vec{k},\omega)-G_\sigma^2\frac{M_0^*c^2}{\varepsilon_0^*}\delta\rho_{s,n}(\vec{k},\omega)\}=0\ . \qquad (3.45)\end{aligned}$$

Consequently, the expressions for $\delta f_n(\vec{k},\vec{p},\omega)$ and $\delta f_p(\vec{k},\vec{p},\omega)$ are obtained as follows,

$$\begin{aligned}\delta f_n(\vec{k},\vec{p},\omega) &= -\frac{\vec{\nabla}_p f_n^0\cdot\vec{k}}{\omega-\vec{v_0}\cdot\vec{k}}\{-\left(G_\omega^2-G_\rho^2\right)\frac{c\vec{p}}{\varepsilon_0^*}\cdot\delta\vec{\rho_{\mathrm{v},p}}(\vec{k},\omega)\\ &- \left(G_\omega^2+G_\rho^2\right)\frac{c\vec{p}}{\varepsilon_0^*}\cdot\delta\vec{\rho_{\mathrm{v},n}}(\vec{k},\omega)+\left(G_\omega^2-G_\rho^2\right)\delta\rho_{B,p}(\vec{k},\omega)+\left(G_\omega^2+G_\rho^2\right)\delta\rho_{B,n}(\vec{k},\omega)\\ &- G_\sigma^2\frac{M_0^*c^2}{\varepsilon_0^*}\delta\rho_{s,p}(\vec{k},\omega)-G_\sigma^2\frac{M_0^*c^2}{\varepsilon_0^*}\delta\rho_{s,n}(\vec{k},\omega)\}+\frac{i\delta f_n(\vec{k},\vec{p},0)}{\omega-\vec{v_0}\cdot\vec{k}} \qquad (3.46)\end{aligned}$$

$$
\begin{aligned}
\delta f_p(\vec{k},\vec{p},\omega) &= -\frac{\vec{\nabla}_p f_p^0\cdot\vec{k}}{\omega-\vec{v_0}\cdot\vec{k}}\{-\left(G_\omega^2+G_\rho^2+G_\gamma^2\right)\frac{c\vec{p}}{\varepsilon_0^*}\cdot\delta\vec{\rho_{\mathrm{v},p}}(\vec{k},\omega)\\
&- \left(G_\omega^2-G_\rho^2\right)\frac{c\vec{p}}{\varepsilon_0^*}\cdot\delta\vec{\rho_{\mathrm{v},n}}(\vec{k},\omega)+\left(G_\omega^2+G_\rho^2+G_\rho^2\right)\delta\rho_{B,p}(\vec{k},\omega)\\
&+ \left(G_\omega^2-G_\rho^2\right)\delta\rho_{B,n}(\vec{k},\omega)-G_\sigma^2\frac{M_0^*c^2}{\varepsilon_0^*}\delta\rho_s(\vec{k},\omega)\}+\frac{i\delta f_n(\vec{k},\vec{p},0)}{\omega-\vec{v_0}\cdot\vec{k}}\ .
\end{aligned}
\tag{3.47}
$$

While obtaining these relations, the only contribution to the initial fluctuation terms are considered to belong to the phase space distribution functions and the initial fluctuations of the meson fields are ignored.

3.5 Density Fluctuations

Integrating Eq. (3.44) and using the definition of the neutron baryon density fluctuation $\delta\tilde{\rho}_{\mathrm{B},n}(\vec{k},\omega)=\gamma\int\frac{d^3p}{(2\pi\hbar)^3}\delta\tilde{f}_n(\vec{k},\vec{p},\omega)$ allows us to find a relation between the density fluctuations as follows,

$$
\begin{aligned}
&\delta\rho_{B,n}(\vec{k},\omega)\{1+\gamma\int_0^\infty\frac{d^3p}{(2\pi\hbar)^3}\frac{\vec{\nabla}_p f_n^0\cdot\vec{k}}{\omega-\vec{v_0}\cdot\vec{k}}\left(G_\omega^2+G_\rho^2\right)\}\\
=\ & -\gamma\int_0^\infty\frac{d^3p}{(2\pi\hbar)^3}\frac{\vec{\nabla}_p f_n^0\cdot\vec{k}}{\omega-\vec{v_0}\cdot\vec{k}}\{-\left(G_\omega^2+G_\rho^2\right)\frac{c\vec{p}}{\varepsilon_0^*}\cdot\delta\vec{\rho_{\mathrm{v},p}}(\vec{k},\omega)\\
-\ & \left(G_\omega^2+G_\rho^2\right)\frac{c\vec{p}}{\varepsilon_0^*}\cdot\delta\vec{\rho_{\mathrm{v},n}}(\vec{k},\omega)+\left(G_\omega^2-G_\rho^2\right)\delta\rho_{B,p}(\vec{k},\omega)\\
-\ & G_\sigma^2\frac{M_0^*c^2}{\varepsilon_0^*}(\delta\rho_{s,p}(\vec{k},\omega)-\delta\rho_{s,n}(\vec{k},\omega))\}+\gamma\int_0^\infty\frac{d^3p}{(2\pi\hbar)^3}\frac{i\delta f_n(\vec{k},\vec{p},0)}{\omega-\vec{v_0}\cdot\vec{k}}\ .
\end{aligned}
\tag{3.48}
$$

Furthermore, defining the proton baryon density fluctuation as

$\delta\tilde{\rho}_{\mathrm{B},p}(\vec{k},\omega)=\gamma\int\frac{d^3p}{(2\pi\hbar)^3}\delta\tilde{f}_p(\vec{k},\vec{p},\omega)$ and integrating Eq. (3.45) yields to another equation,

$$
\begin{aligned}
&\delta\rho_{B,p}(\vec{k},\omega)\{1+\gamma\int_0^\infty\frac{d^3p}{(2\pi\hbar)^3}\frac{\vec{\nabla}_p f_p^0\cdot\vec{k}}{\omega-\vec{v_0}\cdot\vec{k}}\left(G_\omega^2+G_\rho^2+G_\gamma^2\right)\}\\
=\ & -\gamma\int_0^\infty\frac{d^3p}{(2\pi\hbar)^3}\frac{\vec{\nabla}_p f_p^0\cdot\vec{k}}{\omega-\vec{v_0}\cdot\vec{k}}\{-\left(G_\omega^2+G_\rho^2+G_\gamma^2\right)\frac{c\vec{p}}{\varepsilon_0^*}\cdot\delta\vec{\rho_{\mathrm{v},p}}(\vec{k},\omega)\\
-\ & \left(G_\omega^2-G_\rho^2\right)\frac{c\vec{p}}{\varepsilon_0^*}\cdot\delta\vec{\rho_{\mathrm{v},n}}(\vec{k},\omega)+\left(G_\omega^2-G_\rho^2\right)\delta\rho_{B,n}(\vec{k},\omega)\\
-\ & G_\sigma^2\frac{M_0^*c^2}{\varepsilon_0^*}(\delta\rho_{s,p}(\vec{k},\omega)+\delta\rho_{s,n}(\vec{k},\omega))\}+\gamma\int_0^\infty\frac{d^3p}{(2\pi\hbar)^3}+\frac{i\delta f_p(\vec{k},\vec{p},0)}{\omega-\vec{v_0}\cdot\vec{k}}\ .
\end{aligned}
\tag{3.49}
$$

From Eq. (3.31), the scalar density fluctuation is defined as

$$\delta\rho_{s,q}(\vec{k},\omega) = \gamma \int_0^\infty \frac{d^3p}{(2\pi\hbar)^3} \delta\left[\left(\frac{M^*c^2}{\varepsilon_0^*}\right) f_q(\vec{k},\vec{p},\omega)\right] \tag{3.50}$$

and another relation between the density fluctuations can be found by employing the expressions for $\delta\rho_{s,p}$ and $\delta\rho_{s,n}$ into the corresponding Vlasov equation. In order to simplify the calculations, we define the quantities $f_n^{'} = \left(\frac{M^*c^2}{\varepsilon_n^*}\right) f_n(\vec{k},\vec{p},\omega)$ and $f_p^{'} = \left(\frac{M^*c^2}{\varepsilon_p^*}\right) f_p(\vec{k},\vec{p},\omega)$. Then, the fluctuations in $f_n^{'}(\vec{k},\vec{p},\omega)$ and $f_p^{'}(\vec{k},\vec{p},\omega)$ should be calculated first.

In order to linearize $f_q^{'}(\vec{k},\vec{p},\omega)$ around an equilibrium point, the terms $\left(\frac{M^*c^2}{\varepsilon_q^*}\right)$ and $f_q(\vec{k},\vec{p},\omega)$ should be linearized seperately as

$\delta f_q^{'}(\vec{k},\vec{p},\omega) = \left[\left(\frac{M^*c^2}{\varepsilon_q^*}\right)_0 + \delta\left(\frac{M^*c^2}{\varepsilon_q^*}\right)\right]\left[f_q^0(\vec{k},\vec{p},\omega) + \delta f_q^0(\vec{k},\vec{p},\omega)\right]$, where q stands for the neutron or proton.

Since we are considering the linear response treatment of dynamical evolution, the second order terms in δ vanish and the equation become $\delta f_q^{'}(\vec{k},\vec{p},\omega) = \left(\frac{M^*c^2}{\varepsilon_q^*}\right)\delta f_q(\vec{k},\vec{p},\omega) + f_q^0(\vec{k},\vec{p},\omega)\delta\left(\frac{M^*c^2}{\varepsilon_q^*}\right)$.

Previously $\delta f_n(\vec{k},\vec{p},\omega)$ and $\delta f_p(\vec{k},\vec{p},\omega)$ are obtained in Eqs. (3.46) and (3.47) so the only unknown terms in the above expressions are the fluctuations in $\left(\frac{M^*c^2}{\varepsilon_q^*}\right)$. It can be observed that $\left(\frac{M^*c^2}{\varepsilon_n^*}\right)$ depends on the meson fields ϕ, V_i and $b_{3,i}$ and $\left(\frac{M^*c^2}{\varepsilon_p^*}\right)$ depends on the same with an additional term A_i, the photon field. Hence, the corresponding fluctuations can be written as

$$\begin{aligned}
\delta\left(\frac{M^*c^2}{\varepsilon_n^*}\right) &= \left[\frac{\partial}{\partial\phi}\frac{M^*c^2}{\varepsilon_n^*}\right]_0 \delta\phi + \left[\frac{\partial}{\partial V_i}\frac{M^*c^2}{\varepsilon_n^*}\right]_0 \delta V_i + \left[\frac{\partial}{\partial b_{3,i}}\frac{M^*c^2}{\varepsilon_n^*}\right]_0 \delta b_{3,i} \\
\delta\left(\frac{M^*c^2}{\varepsilon_p^*}\right) &= \left[\frac{\partial}{\partial\phi}\frac{M^*c^2}{\varepsilon_p^*}\right]_0 \delta\phi + \left[\frac{\partial}{\partial V_i}\frac{M^*c^2}{\varepsilon_p^*}\right]_0 \delta V_i + \left[\frac{\partial}{\partial b_{3,i}}\frac{M^*c^2}{\varepsilon_p^*}\right]_0 \delta b_{3,i} \\
&+ \left[\frac{\partial}{\partial A_i}\frac{M^*c^2}{\varepsilon_p^*}\right]_0 \delta A_i
\end{aligned} \tag{3.51}$$

where $i = 0, 1, 2, 3$ represents the time and spatial coordinates.

The derivatives can be evaluated and $f_n^{'}(\vec{k},\vec{p},\omega)$ and $f_p^{'}(\vec{k},\vec{p},\omega)$ can be obtained in this manner. Then two more equations that relate the density fluctuations are revealed through the

Vlasov equations;

$$
\begin{aligned}
& \gamma \int_0^\infty \frac{d^3p}{(2\pi\hbar)^3} \left(\frac{M_0^* c^2}{\varepsilon_0^*}\right) \frac{i\delta f_n(\vec{k},\vec{p},0)}{\omega - \vec{v_0}\cdot\vec{k}} \\
= \; & \delta\rho_{\vec{\mathrm{v}},p}\gamma \int_0^\infty \frac{d^3p}{(2\pi\hbar)^3} \left\{ \frac{c\vec{p}}{\varepsilon_0^*} \left(\frac{M_0^* c^2}{\varepsilon_0^*}\right) \frac{\vec{\nabla}_p f_n^0 \cdot \vec{k}}{\omega - \vec{v_0}\cdot\vec{k}} \left[-\left(G_\omega^2 - G_\rho^2\right)\right] - f_n^0 \left(G_\omega^2 - G_\rho^2\right) \left(\frac{M_0^* c^2}{\varepsilon_0^{*3}}\right) c\vec{p} \right\} \\
+ \; & \delta\rho_{\vec{\mathrm{v}},n}\gamma \int_0^\infty \frac{d^3p}{(2\pi\hbar)^3} \left\{ \frac{c\vec{p}}{\varepsilon_0^*} \left(\frac{M_0^* c^2}{\varepsilon_0^*}\right) \frac{\vec{\nabla}_p f_n^0 \cdot \vec{k}}{\omega - \vec{v_0}\cdot\vec{k}} \left[-\left(G_\omega^2 + G_\rho^2\right)\right] - f_n^0 \left(G_\omega^2 + G_\rho^2\right) \left(\frac{M_0^* c^2}{\varepsilon_0^{*3}}\right) c\vec{p} \right\} \\
+ \; & \delta\rho_{s,p}\gamma \int_0^\infty \frac{d^3p}{(2\pi\hbar)^3} \left\{ -G_\sigma^2 \left(\frac{M_0^* c^2}{\varepsilon_0^*}\right)^2 \frac{\vec{\nabla}_p f_n^0 \cdot \vec{k}}{\omega - \vec{v_0}\cdot\vec{k}} - f_n^0 G_\rho^2 \left(\frac{-c^2p^2}{\varepsilon_0^{*3}}\right) \right\} \\
+ \; & \delta\rho_{s,n} \left[1 - \gamma \int_0^\infty \frac{d^3p}{(2\pi\hbar)^3} \left\{ G_\sigma^2 \left(\frac{M_0^* c^2}{\varepsilon_0^*}\right)^2 \frac{\vec{\nabla}_p f_n^0 \cdot \vec{k}}{\omega - \vec{v_0}\cdot\vec{k}} + f_n^0 G_\rho^2 \left(\frac{-c^2p^2}{\varepsilon_0^{*3}}\right) \right\} \right] \\
+ \; & \delta\rho_{B,p}\gamma \int_0^\infty \frac{d^3p}{(2\pi\hbar)^3} \left(\frac{M_0^* c^2}{\varepsilon_0^*}\right) \frac{\vec{\nabla}_p f_n^0 \cdot \vec{k}}{\omega - \vec{v_0}\cdot\vec{k}} \left(G_\omega^2 - G_\rho^2\right) \\
+ \; & \delta\rho_{B,n}\gamma \int_0^\infty \frac{d^3p}{(2\pi\hbar)^3} \left(\frac{M_0^* c^2}{\varepsilon_0^*}\right) \frac{\vec{\nabla}_p f_n^0 \cdot \vec{k}}{\omega - \vec{v_0}\cdot\vec{k}} \left(G_\omega^2 + G_\rho^2\right)
\end{aligned}
\tag{3.52}
$$

and

$$
\begin{aligned}
& \gamma \int_0^\infty \frac{d^3p}{(2\pi\hbar)^3} \left(\frac{M_0^* c^2}{\varepsilon_0^*}\right) \frac{i\delta f_p(\vec{k},\vec{p},0)}{\omega - \vec{v_0}\cdot\vec{k}} \\
= \; & \delta\rho_{\vec{\mathrm{v}},p}\gamma \int_0^\infty \frac{d^3p}{(2\pi\hbar)^3} \left\{ \frac{c\vec{p}}{\varepsilon_0^*} \frac{M_0^* c^2}{\varepsilon_0^*} \left(G_\omega^2 + G_\rho^2 + G_\gamma^2\right) \left(-\frac{\vec{\nabla}_p f_n^0 \cdot \vec{k}}{\omega - \vec{v_0}\cdot\vec{k}} + \frac{1}{\varepsilon_0^*} \right) \right\} \\
+ \; & \delta\rho_{\vec{\mathrm{v}},n}\gamma \int_0^\infty \frac{d^3p}{(2\pi\hbar)^3} \left\{ -\frac{c\vec{p}}{\varepsilon_0^*} \frac{M_0^* c^2}{\varepsilon_0^*} \left(G_\omega^2 - G_\rho^2\right) \left(\frac{\vec{\nabla}_p f_n^0 \cdot \vec{k}}{\omega - \vec{v_0}\cdot\vec{k}} + \frac{1}{\varepsilon_0^*} \right) \right\} \\
+ \; & \delta\rho_{s,p} \left[1 - \gamma \int_0^\infty \frac{d^3p}{(2\pi\hbar)^3} G_\sigma^2 \left\{ \left(\frac{M_0^* c^2}{\varepsilon_0^*}\right)^2 \frac{\vec{\nabla}_p f_n^0 \cdot \vec{k}}{\omega - \vec{v_0}\cdot\vec{k}} + f_p^0 \left(\frac{-c^2p^2}{\varepsilon_0^{*3}}\right) \right\} \right] \\
- \; & \delta\rho_{s,n}\gamma \int_0^\infty \frac{d^3p}{(2\pi\hbar)^3} G_\sigma^2 \left\{ \left(\frac{M_0^* c^2}{\varepsilon_0^*}\right)^2 \frac{\vec{\nabla}_p f_n^0 \cdot \vec{k}}{\omega - \vec{v_0}\cdot\vec{k}} + f_p^0 \left(\frac{-c^2p^2}{\varepsilon_0^{*3}}\right) \right\} \\
+ \; & \delta\rho_{B,p}\gamma \int_0^\infty \frac{d^3p}{(2\pi\hbar)^3} \left(\frac{M_0^* c^2}{\varepsilon_0^*}\right) \frac{\vec{\nabla}_p f_n^0 \cdot \vec{k}}{\omega - \vec{v_0}\cdot\vec{k}} \left(G_\omega^2 + G_\rho^2 + G_\gamma^2\right) \\
+ \; & \delta\rho_{B,n}\gamma \int_0^\infty \frac{d^3p}{(2\pi\hbar)^3} \left(\frac{M_0^* c^2}{\varepsilon_0^*}\right) \frac{\vec{\nabla}_p f_n^0 \cdot \vec{k}}{\omega - \vec{v_0}\cdot\vec{k}} \left(G_\omega^2 - G_\rho^2\right) \; .
\end{aligned}
\tag{3.53}
$$

Finally, the last two relations between the density fluctuations can be obtained starting from the definiton of the current density $\vec{\rho}_{\mathrm{v},q}(\vec{k},\omega) = \gamma \int_0^\infty \frac{d^3p}{(2\pi\hbar)^3} \left(\frac{c\vec{p}^*}{\varepsilon_q^*}\right) f_q(\vec{k},\vec{p},\omega)$ and can be

evaluated in a similar procedure presented above. As a result, we have found

$$
\begin{aligned}
& \gamma \int_0^\infty \frac{d^3p}{(2\pi\hbar)^3} \frac{c\vec{p}}{\varepsilon_0^*} \frac{i\delta f_p(\vec{k},\vec{p},0)}{\omega - \vec{v_0}\cdot\vec{k}} \\
= \; & \delta\rho_{\vec{\mathrm{v}},p} \left[1 - \gamma \int_0^\infty \frac{d^3p}{(2\pi\hbar)^3} \left(G_\omega^2 + G_\rho^2 + G_\gamma^2\right) \left\{ f_p^0 \left(\frac{c^2\vec{p}^2}{\varepsilon_0^{*3}} - \frac{1}{\varepsilon_0^{*3}} \right) + \left(\frac{c\vec{p}}{\varepsilon_0^*} \right)^2 \frac{\vec{\nabla}_p f_p^0 \cdot \vec{k}}{\omega - \vec{v_0}\cdot\vec{k}} \right\} \right] \\
- \; & \delta\rho_{\vec{\mathrm{v}},n} \gamma \int_0^\infty \frac{d^3p}{(2\pi\hbar)^3} \left(G_\omega^2 - G_\rho^2\right) \left\{ f_p^0 \left(\frac{c^2\vec{p}^2}{\varepsilon_0^{*3}} - \frac{1}{\varepsilon_0^{*3}} \right) + \left(\frac{c\vec{p}}{\varepsilon_0^{*2}} \right) \frac{\vec{\nabla}_p f_p^0 \cdot \vec{k}}{\omega - \vec{v_0}\cdot\vec{k}} \right\} \\
- \; & \delta\rho_{s,p} \gamma \int_0^\infty \frac{d^3p}{(2\pi\hbar)^3} G_\sigma^2 \left(\frac{M_0^* c^2}{\varepsilon_0^*} \right) \frac{c\vec{p}}{\varepsilon_0^*} \left(\frac{f_p^0}{\varepsilon_0^*} + \frac{\vec{\nabla}_p f_n^0 \cdot \vec{k}}{\omega - \vec{v_0}\cdot\vec{k}} \right) \\
- \; & \delta\rho_{s,n} \gamma \int_0^\infty \frac{d^3p}{(2\pi\hbar)^3} G_\sigma^2 \left(\frac{M_0^* c^2}{\varepsilon_0^*} \right) \frac{c\vec{p}}{\varepsilon_0^*} \left(\frac{f_p^0}{\varepsilon_0^*} + \frac{\vec{\nabla}_p f_n^0 \cdot \vec{k}}{\omega - \vec{v_0}\cdot\vec{k}} \right) \\
+ \; & \delta\rho_{B,p} \gamma \int_0^\infty \frac{d^3p}{(2\pi\hbar)^3} \frac{c\vec{p}}{\varepsilon_0^*} \frac{\vec{\nabla}_p f_n^0 \cdot \vec{k}}{\omega - \vec{v_0}\cdot\vec{k}} \left(G_\omega^2 + G_\rho^2 + G_\gamma^2\right) \\
- \; & \delta\rho_{B,n} \gamma \int_0^\infty \frac{d^3p}{(2\pi\hbar)^3} \frac{c\vec{p}}{\varepsilon_0^*} \frac{\vec{\nabla}_p f_n^0 \cdot \vec{k}}{\omega - \vec{v_0}\cdot\vec{k}} \left(G_\omega^2 - G_\rho^2\right)
\end{aligned}
\tag{3.54}
$$

and

$$
\begin{aligned}
& \gamma \int_0^\infty \frac{d^3p}{(2\pi\hbar)^3} \frac{c\vec{p}}{\varepsilon_0^*} \frac{i\delta f_n(\vec{k},\vec{p},0)}{\omega - \vec{v_0}\cdot\vec{k}} \\
= \; & \delta\vec{\rho}_{\nu,n} \left[1 - \gamma \int_0^\infty \frac{d^3p}{(2\pi\hbar)^3} \left(G_\omega^2 + G_\rho^2\right) \left\{ f_n^0 \left(\frac{c^2\vec{p}^2}{\varepsilon_0^*} - \frac{1}{\varepsilon_0^*} \right) + \left(\frac{c\vec{p}}{\varepsilon_0^*} \right)^2 \frac{\vec{\nabla}_p f_p^0 \cdot \vec{k}}{\omega - \vec{v_0}\cdot\vec{k}} \right\} \right] \\
- \; & \delta\vec{\rho}_{\nu,p} \gamma \int_0^\infty \frac{d^3p}{(2\pi\hbar)^3} \left(G_\omega^2 - G_\rho^2\right) \left\{ f_n^0 \left(\frac{c^2\vec{p}^2}{\varepsilon_0^{*3}} - \frac{1}{\varepsilon_0^*} \right) + \left(\frac{c\vec{p}}{\varepsilon_0^*} \right)^2 \frac{\vec{\nabla}_p f_n^0 \cdot \vec{k}}{\omega - \vec{v_0}\cdot\vec{k}} \right\} \\
+ \; & \delta\rho_{B,p} \gamma \int_0^\infty \frac{d^3p}{(2\pi\hbar)^3} \frac{c\vec{p}}{\varepsilon_0^*} \frac{\vec{\nabla}_p f_n^0 \cdot \vec{k}}{\omega - \vec{v_0}\cdot\vec{k}} \left(G_\omega^2 - G_\rho^2\right) \\
+ \; & \delta\rho_{B,n} \gamma \int_0^\infty \frac{d^3p}{(2\pi\hbar)^3} \frac{c\vec{p}}{\varepsilon_0^*} \frac{\vec{\nabla}_p f_n^0 \cdot \vec{k}}{\omega - \vec{v_0}\cdot\vec{k}} \left(G_\omega^2 + G_\rho^2\right) \\
- \; & \delta\rho_{s,p} \gamma \int_0^\infty \frac{d^3p}{(2\pi\hbar)^3} G_\sigma^2 \left(\frac{M_0^* c^2}{\varepsilon_0^*} \right) \frac{c\vec{p}}{\varepsilon_0^*} \left(\frac{f_p^0}{\varepsilon_0^*} + \frac{\vec{\nabla}_p f_n^0 \cdot \vec{k}}{\omega - \vec{v_0}\cdot\vec{k}} \right) \\
- \; & \delta\rho_{s,n} \gamma \int_0^\infty \frac{d^3p}{(2\pi\hbar)^3} G_\sigma^2 \left(\frac{M_0^* c^2}{\varepsilon_0^*} \right) \frac{c\vec{p}}{\varepsilon_0^*} \left(\frac{f_p^0}{\varepsilon_0^*} + \frac{\vec{\nabla}_p f_n^0 \cdot \vec{k}}{\omega - \vec{v_0}\cdot\vec{k}} \right) .
\end{aligned}
\tag{3.55}
$$

Six coupled equations are found above containing the relations between the Fourier transforms of the small amplitude fluctuations of baryon, scalar and vector densities for proton and neutron seperately.

In nuclear matter, the spinodal instabilities can be treated as sound waves with imaginary

velocities in the spinodal region [5]. Since the sound waves move longitudinally, we consider only the unstable collective longitudinal modes along the propagation direction, $\delta\vec{\rho}_\nu = \delta\rho_\nu\vec{k}$. Hence, this yields to the conditions $\vec{\nabla}_p f_0 \cdot \vec{k} = (\nabla_p f_0)k\cos\theta$ and $\vec{v}_0 \cdot \vec{k} = v_0 k\cos\theta$.

The following definitions are for the stochastic source terms that contain the information about the initial conditions of the system and will be used in the rest of the chapter;

$$\begin{pmatrix} \tilde{S}_{\rm v}(\vec{k},\omega) \\ \tilde{S}_{\rm s}(\vec{k},\omega) \\ \tilde{S}_B(\vec{k},\omega) \end{pmatrix} = \gamma \int \frac{d^3p}{(2\pi\hbar)^3} \begin{pmatrix} c\vec{p}\cdot\vec{k}/\varepsilon_0^* \\ M_0^* c^2/\varepsilon_0^* \\ 1 \end{pmatrix} \frac{\delta\tilde{f}(\vec{k},\vec{p},0)}{\omega - \vec{\rm v}_0\cdot\vec{k}} \ . \tag{3.56}$$

Also, the Linhard functions in the long wavelength limit for the vector, scalar and baryon densities are given by

$$\begin{pmatrix} \chi_{\rm v}(\vec{k},\omega) \\ \chi_{\rm s}(\vec{k},\omega) \\ \chi_B(\vec{k},\omega) \end{pmatrix} = \gamma \int \frac{d^3p}{(2\pi\hbar)^3} \begin{pmatrix} c\vec{p}\cdot\hat{k}/\varepsilon_0^* \\ M_0^* c^2/\varepsilon_0^* \\ 1 \end{pmatrix} \frac{\vec{k}\cdot\vec{\nabla}_p f_0(\vec{p})}{\omega - \vec{\rm v}_0\cdot\vec{k}} \tag{3.57}$$

and

$$\tilde{\chi}_{\rm s}(\vec{k},\omega) = \gamma \int \frac{d^3p}{(2\pi\hbar)^3} \left[\frac{(cp)^2}{\varepsilon_0^{*3}} f_0(\vec{p}) - \left(\frac{M_0^* c^2}{\varepsilon_0^*}\right)^2 \frac{\vec{k}\cdot\vec{\nabla}_p f_0(\vec{p})}{\omega - \vec{\rm v}_0\cdot\vec{k}} \right] , \tag{3.58}$$

$$\tilde{\chi}_{\rm v}(\vec{k},\omega) = \gamma \int \frac{d^3p}{(2\pi\hbar)^3} c\vec{p}\cdot\hat{k} \left[\frac{M_0^* c^2}{\varepsilon_0^{*2}} \frac{\vec{k}\cdot\vec{\nabla}_p f_0(\vec{p})}{\omega - \vec{\rm v}_0\cdot\vec{k}} \right] , \tag{3.59}$$

$$\tilde{\chi}_B(\vec{k},\omega) = \gamma \int \frac{d^3p}{(2\pi\hbar)^3} \left[\frac{\varepsilon_0^{*2} - (c\vec{p}\cdot\hat{k})^2}{\varepsilon_0^{*3}} f_0(\vec{p}) - \frac{(c\vec{p}\cdot\hat{k})^2}{\varepsilon_0^{*2}} \frac{\vec{k}\cdot\vec{\nabla}_p f_0(\vec{p})}{\omega - \vec{\rm v}_0\cdot\vec{k}} \right] . \tag{3.60}$$

By using these definitions in the mean field limit, the six coupled equations can be written in the form of a matrix equation;

$$\begin{pmatrix} A_1^p & A_2^p & A_3^p & A_1^n & A_2^n & A_3^n \\ B_1^p & B_2^p & B_3^p & B_1^n & B_2^n & B_3^n \\ C_1^p & C_2^p & C_3^p & C_1^n & C_2^n & C_3^n \\ D_1^p & D_2^p & D_3^p & D_1^n & D_2^n & D_3^n \\ E_1^p & E_2^p & E_3^p & E_1^n & E_2^n & E_3^n \\ F_1^p & F_2^p & F_3^p & F_1^n & F_2^n & F_3^n \end{pmatrix} \begin{pmatrix} \delta\tilde{\rho_{{\rm v},p}}(\vec{k},\omega) \\ \delta\tilde{\rho_{s,p}}(\vec{k},\omega) \\ \delta\tilde{\rho}_{B,p}(\vec{k},\omega) \\ \delta\tilde{\rho}_{{\rm v},n}(\vec{k},\omega) \\ \delta\tilde{\rho}_{s,n}(\vec{k},\omega) \\ \delta\tilde{\rho}_{B,n}(\vec{k},\omega) \end{pmatrix} = i \begin{pmatrix} \tilde{S}_B^p(\vec{k},\omega) \\ \tilde{S}_s^p(\vec{k},\omega) \\ \tilde{S}_{\rm v}^p(\vec{k},\omega) \\ \tilde{S}_B^n(\vec{k},\omega) \\ \tilde{S}_s^n(\vec{k},\omega) \\ \tilde{S}_{\rm v}^n(\vec{k},\omega) \end{pmatrix} \tag{3.61}$$

where the elements of the six by six coefficient matrix can be written in terms of the Linhard functions as

$$\begin{pmatrix} A_1^p \\ B_1^p \\ C_1^p \\ D_1^p \\ E_1^p \\ F_1^p \end{pmatrix} = \begin{pmatrix} -\left(G_\omega^2+G_\rho^2+G_\gamma^2\right)\chi_p^{\mathrm{v}} \\ -\left(G_\omega^2+G_\rho^2+G_\gamma^2\right)\tilde{\chi}_p^{\mathrm{v}} \\ 1-\left(G_\omega^2+G_\rho^2+G_\gamma^2\right)\tilde{\chi}_p^{b} \\ -\left(G_\omega^2-G_\rho^2\right)\chi_n^{\mathrm{v}} \\ -\left(G_\omega^2-G_\rho^2\right)\tilde{\chi}_n^{\mathrm{v}} \\ -\left(G_\omega^2-G_\rho^2\right)\tilde{\chi}_n^{b} \end{pmatrix} \qquad \begin{pmatrix} A_2^p \\ B_2^p \\ C_2^p \\ D_2^p \\ E_2^p \\ F_2^p \end{pmatrix} = \begin{pmatrix} -G_\sigma^2\chi_p^{\mathrm{s}} \\ 1-G_\sigma^2\tilde{\chi}_p^{\mathrm{s}} \\ -G_\sigma^2\tilde{\chi}_p^{\mathrm{v}} \\ -G_\sigma^2\chi_n^{\mathrm{s}} \\ -G_\sigma^2\tilde{\chi}_n^{\mathrm{s}} \\ -G_\sigma^2\tilde{\chi}_n^{\mathrm{v}} \end{pmatrix}$$

$$\begin{pmatrix} A_3^p \\ B_3^p \\ C_3^p \\ D_3^p \\ E_3^p \\ F_3^p \end{pmatrix} = \begin{pmatrix} 1+\left(G_\omega^2+G_\rho^2+G_\gamma^2\right)\chi_p^{b} \\ \left(G_\omega^2+G_\rho^2+G_\gamma^2\right)\chi_p^{\mathrm{s}} \\ \left(G_\omega^2+G_\rho^2+G_\gamma^2\right)\chi_p^{\mathrm{v}} \\ \left(G_\omega^2-G_\rho^2\right)\chi_n^{\mathrm{b}} \\ \left(G_\omega^2-G_\rho^2\right)\chi_n^{\mathrm{s}} \\ \left(G_\omega^2-G_\rho^2\right)\chi_n^{\mathrm{v}} \end{pmatrix} \qquad \begin{pmatrix} A_1^n \\ B_1^n \\ C_1^n \\ D_1^n \\ E_1^n \\ F_1^n \end{pmatrix} = \begin{pmatrix} -\left(G_\omega^2-G_\rho^2\right)\chi_p^{\mathrm{v}} \\ -\left(G_\omega^2-G_\rho^2\right)\tilde{\chi}_p^{\mathrm{v}} \\ -\left(G_\omega^2-G_\rho^2\right)\tilde{\chi}_p^{b} \\ -\left(G_\omega^2+G_\rho^2\right)\chi_n^{\mathrm{v}} \\ -\left(G_\omega^2+G_\rho^2\right)\tilde{\chi}_p^{\mathrm{v}} \\ 1-\left(G_\omega^2+G_\rho^2\right)\tilde{\chi}_n^{b} \end{pmatrix}$$

$$\begin{pmatrix} A_2^n \\ B_2^n \\ C_2^n \\ D_2^n \\ E_2^n \\ F_2^n \end{pmatrix} = \begin{pmatrix} -G_\sigma^2\chi_p^{\mathrm{s}} \\ -G_\sigma^2\tilde{\chi}_p^{\mathrm{s}} \\ -G_\sigma^2\tilde{\chi}_p^{\mathrm{v}} \\ -G_\sigma^2\chi_n^{\mathrm{s}} \\ 1-G_\sigma^2\tilde{\chi}_n^{\mathrm{s}} \\ -G_\sigma^2\tilde{\chi}_n^{\mathrm{v}} \end{pmatrix} \qquad \begin{pmatrix} A_3^n \\ B_3^n \\ C_3^n \\ D_3^n \\ E_3^n \\ F_3^n \end{pmatrix} = \begin{pmatrix} \left(G_\omega^2-G_\rho^2\right)\chi_p^{b} \\ \left(G_\omega^2-G_\rho^2\right)\chi_p^{s} \\ \left(G_\omega^2-G_\rho^2\right)\chi_p^{\mathrm{v}} \\ 1+\left(G_\omega^2+G_\rho^2\right)\chi_n^{b} \\ \left(G_\omega^2+G_\rho^2\right)\tilde{\chi}_n^{s} \\ \left(G_\omega^2+G_\rho^2\right)\tilde{\chi}_n^{\mathrm{v}} \end{pmatrix}. \tag{3.62}$$

These components of the coefficient matrix are related to G_ω^2, G_ρ^2, G_γ^2 and G_σ^2 in such a way that the coupling of the photon field (G_γ^2) can be oserved easily and the effect of the Coulomb interaction in the system can be investigated.

The determinant of the coefficient matrix is defined to be the susceptibility as follows,

$$\varepsilon(\vec{k},\omega) = \begin{vmatrix} A_1^p & A_2^p & A_3^p & A_1^n & A_2^n & A_3^n \\ B_1^p & B_2^p & B_3^p & B_1^n & B_2^n & B_3^n \\ C_1^p & C_2^p & C_3^p & C_1^n & C_2^n & C_3^n \\ D_1^p & D_2^p & D_3^p & D_1^n & D_2^n & D_3^n \\ E_1^p & E_2^p & E_3^p & E_1^n & E_2^n & E_3^n \\ F_1^p & F_2^p & F_3^p & F_1^n & F_2^n & F_3^n \end{vmatrix}. \tag{3.63}$$

The condition

$$\varepsilon(\vec{k},\omega) = 0 \tag{3.64}$$

denotes the dispersion relation. In the spinodal region, the imaginary growing and decaying poles of the susceptibility is given as $\omega = i\Gamma$ and $\omega = -i\Gamma$. Here, Γ denotes the growth rate of unstable modes in the spinodal region where $\rho < \rho_{critical}$. However, in the stable region $\rho > \rho_{critical}$, the frequencies are real and unstable modes are not produced. The growth rates in the spinodal region will be investigated as a function of the wave number in the following chapter. Also, the expressions of the Linhard functions and consequently the matrix elements in the spinodal region in terms of the growing and decaying poles are given in Appendix A.

3.6 Density Correlations

Density correlation functions provide useful information about the time evolution of the unstable modes starting from the initial conditions in the spinodal region. In this thesis, only the equal time baryon density correlations will be evaluated [32].

The proton density fluctuation $\delta\tilde{\rho}_{B,p}$ can be found by expanding the determinant of the six by six matrix according to the Kramer's Rule;

$$\delta\tilde{\rho}_{B,p} = \frac{1}{\varepsilon(\vec{k},\omega)} \begin{vmatrix} A_1^p & A_2^p & i\hbar\tilde{S}_{B,p} & A_1^n & A_2^n & A_3^n \\ B_1^p & B_2^p & i\hbar\tilde{S}_{s,p} & B_1^n & B_2^n & B_3^n \\ C_1^p & C_2^p & i\hbar\tilde{S}_{\mathrm{v},p} & C_1^n & C_2^n & C_3^n \\ D_1^p & D_2^p & i\hbar\tilde{S}_{B,n} & D_1^n & D_2^n & D_3^n \\ E_1^p & E_2^p & i\hbar\tilde{S}_{s,n} & E_1^n & E_2^n & E_3^n \\ F_1^p & F_2^p & i\hbar\tilde{S}_{\mathrm{v},n} & F_1^n & F_2^n & F_3^n \end{vmatrix} . \tag{3.65}$$

If we choose to expand with respect to the third column, we get

$$
\begin{aligned}
&\delta\tilde{\rho}_{B,p} = \\
&+ \frac{i\hbar\tilde{S}_{\mathrm{v},p}}{\varepsilon(\vec{k},\omega)} \begin{vmatrix} B_1^p & B_2^p & B_1^n & B_2^n & B_3^n \\ C_1^p & C_2^p & C_1^n & C_2^n & C_3^n \\ D_1^p & D_2^p & D_1^n & D_2^n & D_3^n \\ E_1^p & E_2^p & E_1^n & E_2^n & E_3^n \\ F_1^p & F_2^p & F_1^n & F_2^n & F_3^n \end{vmatrix} - \frac{i\hbar\tilde{S}_{s,p}}{\varepsilon(\vec{k},\omega)} \begin{vmatrix} A_1^p & A_2^p & A_1^n & A_2^n & A_3^n \\ C_1^p & C_2^p & C_1^n & C_2^n & C_3^n \\ D_1^p & D_2^p & D_1^n & D_2^n & D_3^n \\ E_1^p & E_2^p & E_1^n & E_2^n & E_3^n \\ F_1^p & F_2^p & F_1^n & F_2^n & F_3^n \end{vmatrix} \\
&+ \frac{i\hbar\tilde{S}_{B,p}}{\varepsilon(\vec{k},\omega)} \begin{vmatrix} A_1^p & A_2^p & A_1^n & A_2^n & A_3^n \\ B_1^p & B_2^p & B_1^n & B_2^n & B_3^n \\ D_1^p & D_2^p & D_1^n & D_2^n & D_3^n \\ E_1^p & E_2^p & E_1^n & E_2^n & E_3^n \\ F_1^p & F_2^p & F_1^n & F_2^n & F_3^n \end{vmatrix} - \frac{i\hbar\tilde{S}_{\mathrm{v},n}}{\varepsilon(\vec{k},\omega)} \begin{vmatrix} A_1^p & A_2^p & A_1^n & A_2^n & A_3^n \\ B_1^p & B_2^p & B_1^n & B_2^n & B_3^n \\ C_1^p & C_2^p & C_1^n & C_2^n & C_3^n \\ E_1^p & E_2^p & E_1^n & E_2^n & E_3^n \\ F_1^p & F_2^p & F_1^n & F_2^n & F_3^n \end{vmatrix} \\
&+ \frac{i\hbar\tilde{S}_{s,n}}{\varepsilon(\vec{k},\omega)} \begin{vmatrix} A_1^p & A_2^p & A_1^n & A_2^n & A_3^n \\ B_1^p & B_2^p & B_1^n & B_2^n & B_3^n \\ C_1^p & C_2^p & C_1^n & C_2^n & C_3^n \\ D_1^p & D_2^p & D_1^n & D_2^n & D_3^n \\ F_1^p & F_2^p & F_1^n & F_2^n & F_3^n \end{vmatrix} - \frac{i\hbar\tilde{S}_{B,n}}{\varepsilon(\vec{k},\omega)} \begin{vmatrix} A_1^p & A_2^p & A_1^n & A_2^n & A_3^n \\ B_1^p & B_2^p & B_1^n & B_2^n & B_3^n \\ C_1^p & C_2^p & C_1^n & C_2^n & C_3^n \\ D_1^p & D_2^p & D_1^n & D_2^n & D_3^n \\ E_1^p & E_2^p & E_1^n & E_2^n & E_3^n \end{vmatrix} .
\end{aligned}
\tag{3.66}
$$

Since the susceptibility depends only on the elements of the coefficient matrix, Eq. (3.66) can be organized in terms of the stochastic source terms;

$$
\delta\tilde{\rho}_{B,p} = \frac{1}{\varepsilon(\vec{k},\omega)} = \frac{i\hbar}{\varepsilon(\vec{k},\omega)} \left[N_1^p i\hbar\tilde{S}_B^p - N_2^p i\hbar\tilde{S}_s^p + N_3^p i\hbar\tilde{S}_{\mathrm{v}}^p - N_4^p i\hbar\tilde{S}_B^n + N_5^p i\hbar\tilde{S}_s^n - N_6^p i\hbar\tilde{S}_{\mathrm{v}}^n \right] .
\tag{3.67}
$$

Here N_i^p with $i = 1, ..., 6$, denotes the five by five matrices in the form,

$$N_1^p = \begin{vmatrix} B_1^p & B_2^p & B_1^n & B_2^n & B_3^n \\ C_1^p & C_2^p & C_1^n & C_2^n & C_3^n \\ D_1^p & D_2^p & D_1^n & D_2^n & D_3^n \\ E_1^p & E_2^p & E_1^n & E_2^n & E_3^n \\ F_1^p & F_2^p & F_1^n & F_2^n & F_3^n \end{vmatrix} \quad N_2^p = \begin{vmatrix} A_1^p & A_2^p & A_1^n & A_2^n & A_3^n \\ C_1^p & C_2^p & C_1^n & C_2^n & C_3^n \\ D_1^p & D_2^p & D_1^n & D_2^n & D_3^n \\ E_1^p & E_2^p & E_1^n & E_2^n & E_3^n \\ F_1^p & F_2^p & F_1^n & F_2^n & F_3^n \end{vmatrix}$$

$$N_3^p = \begin{vmatrix} A_1^p & A_2^p & A_1^n & A_2^n & A_3^n \\ B_1^p & B_2^p & B_1^n & B_2^n & B_3^n \\ D_1^p & D_2^p & D_1^n & D_2^n & D_3^n \\ E_1^p & E_2^p & E_1^n & E_2^n & E_3^n \\ F_1^p & F_2^p & F_1^n & F_2^n & F_3^n \end{vmatrix} \quad N_4^p = \begin{vmatrix} A_1^p & A_2^p & A_1^n & A_2^n & A_3^n \\ B_1^p & B_2^p & B_1^n & B_2^n & B_3^n \\ C_1^p & C_2^p & C_1^n & C_2^n & C_3^n \\ E_1^p & E_2^p & E_1^n & E_2^n & E_3^n \\ F_1^p & F_2^p & F_1^n & F_2^n & F_3^n \end{vmatrix}$$

$$N_5^p = \begin{vmatrix} A_1^p & A_2^p & A_1^n & A_2^n & A_3^n \\ B_1^p & B_2^p & B_1^n & B_2^n & B_3^n \\ C_1^p & C_2^p & C_1^n & C_2^n & C_3^n \\ D_1^p & D_2^p & D_1^n & D_2^n & D_3^n \\ F_1^p & F_2^p & F_1^n & F_2^n & F_3^n \end{vmatrix} \quad N_6^p = \begin{vmatrix} A_1^p & A_2^p & A_1^n & A_2^n & A_3^n \\ B_1^p & B_2^p & B_1^n & B_2^n & B_3^n \\ C_1^p & C_2^p & C_1^n & C_2^n & C_3^n \\ D_1^p & D_2^p & D_1^n & D_2^n & D_3^n \\ E_1^p & E_2^p & E_1^n & E_2^n & E_3^n \end{vmatrix} . \tag{3.68}$$

The evolution of the baryon density fluctuations in time is determined by an inverse Fourier transformation applied to $\delta\tilde{\rho}_{B,p}(\vec{k}, \omega)$ as

$$\delta\tilde{\rho}_{B,p}(\vec{k}, t) = \int \frac{\omega}{2\pi} \delta\tilde{\rho}_{B,p}(\vec{k}, \omega) e^{-i\omega t} . \tag{3.69}$$

In order to evaluate this integral, the Cauchy-Residue Theorem will be used. The non-collective modes of Eq. (3.67) arising from the stochastic source terms are not taken into account since the resulting density fluctuations do not grow in time. So, only the collective poles of susceptibility and the corresponding fluctuations are retained as the dominant contributions.

A counter integral which has a pole at $z = z_0$ that arise from the denominator term, can be considered as $\int_C f(z)dz \equiv \int_C \frac{g(z)}{h(z)} dz$ with the conditions $g(z_0) \neq 0, h(z_0) = 0$ and $h' = \frac{\partial h}{\partial z}|_{z=z_0} \neq 0$. Then, the Cauchy-Residue theorem states that the counter integral can be written as

$$\int_C f(z)dz \equiv \int_C \frac{g(z)}{h(z)} dz = 2\pi i \text{Res}[f(z), z = z_0] = 2\pi i \sum_k \lim_{z \to z_0} \frac{g(z)}{h'(z)} \tag{3.70}$$

where $\lim_{z\to z_0} \frac{g(z)}{h'(z)}$ is the residue of the function.

In Eq. (3.69), there are two poles at $\omega = \pm i\Gamma$ and the integral is evaluated according to the Residue Theorem,

$$\begin{aligned}\delta\tilde{\rho}_{B,p}(\vec{k},t) = & - \hbar \left\{ \frac{\left[N_1^p \tilde{S}_B^p - N_2^p \tilde{S}_s^p + N_3^p \tilde{S}_{\rm v}^p - N_4^p \tilde{S}_B^n + N_5^p \tilde{S}_s^n - N_6^p \tilde{S}_{\rm v}^n\right]}{\partial\varepsilon(\vec{k},\omega)/\partial\omega} |_{\omega=i\Gamma_k} \; e^{\Gamma t} \right. \\ & + \left. \frac{\left[N_1^p \tilde{S}_B^p - N_2^p \tilde{S}_s^p + N_3^p \tilde{S}_{\rm v}^p - N_4^p \tilde{S}_B^n + N_5^p \tilde{S}_s^n - N_6^p \tilde{S}_{\rm v}^n\right]}{\partial\varepsilon(\vec{k},\omega)/\partial\omega} |_{\omega=-i\Gamma_k} \; e^{-\Gamma t} \right\} .\end{aligned} \tag{3.71}$$

Furthermore, the time dependent baryon density fluctuation for proton can be defined in terms of the initial amplitudes of density fluctuations associated with growing and decaying collective poles can be given as follows,

$$\delta\tilde{\rho}_{B,p}(\vec{k},t) = \delta\rho_B^{p+}(\vec{k})e^{+\Gamma_k t} + \delta\rho_B^{p-}(\vec{k})e^{-\Gamma_k t} . \tag{3.72}$$

By comparing the Eqs.(3.71) and (3.72), $\delta\rho_B^{p+}(\vec{k})$ and $\delta\rho_B^{p-}(\vec{k})$ are obtained in terms of the stochastic source terms as

$$\delta\rho_B^{p+}(\vec{k}) = -\hbar \frac{\left[N_1^p \tilde{S}_B^p - N_2^p \tilde{S}_s^p + N_3^p \tilde{S}_{\rm v}^p - N_4^p \tilde{S}_B^n + N_5^p \tilde{S}_s^n - N_6^p \tilde{S}_{\rm v}^n\right]}{\partial\varepsilon(\vec{k},\omega)/\partial\omega} |_{\omega=i\Gamma_k} \tag{3.73}$$

and

$$\delta\rho_B^{p-}(\vec{k}) = -\hbar \frac{\left[N_1^p \tilde{S}_B^p - N_2^p \tilde{S}_s^p + N_3^p \tilde{S}_{\rm v}^p - N_4^p \tilde{S}_B^n + N_5^p \tilde{S}_s^n - N_6^p \tilde{S}_{\rm v}^n\right]}{\partial\varepsilon(\vec{k},\omega)/\partial\omega} |_{\omega=-i\Gamma_k} . \tag{3.74}$$

The same calculations are also valid for obtaining the neutron density fluctuation $\delta\tilde{\rho}_{B,n}(\vec{k},t)$ and the corresponding initial growing and decaying modes. If we expand Eq. (3.61) with

respect to the sixth column by using the Kramer's Rule, we get

$$
\begin{aligned}
\delta\tilde{\rho}_{B,n} &= \frac{1}{\varepsilon(\vec{k},\omega)}\begin{vmatrix} A_1^p & A_2^p & A_3^p & A_1^n & A_2^n & i\hbar\tilde{S}_{B,p} \\ B_1^p & B_2^p & B_3^p & B_1^n & B_2^n & i\hbar\tilde{S}_{s,p} \\ C_1^p & C_2^p & C_3^p & C_1^n & C_2^n & i\hbar\tilde{S}_{\mathrm{v},p} \\ D_1^p & D_2^p & D_3^p & D_1^n & D_2^n & i\hbar\tilde{S}_{B,n} \\ E_1^p & E_2^p & E_3^p & E_1^n & E_2^n & i\hbar\tilde{S}_{s,n} \\ F_1^p & F_2^p & F_3^p & F_1^n & F_2^n & i\hbar\tilde{S}_{\mathrm{v},n} \end{vmatrix} \\
&= -\frac{i\hbar\tilde{S}_{B,p}}{\varepsilon(\vec{k},\omega)}\begin{vmatrix} B_1^p & B_2^p & B_3^p & B_1^n & B_2^n \\ C_1^p & C_2^p & C_3^p & C_2^n & C_2^n \\ D_1^p & D_2^p & D_3^p & D_2^n & D_2^n \\ E_1^p & E_2^p & E_3^p & E_2^n & E_2^n \\ F_1^p & F_2^p & F_3^p & F_2^n & F_2^n \end{vmatrix} + \frac{i\hbar\tilde{S}_{s,p}}{\varepsilon(\vec{k},\omega)}\begin{vmatrix} A_1^p & A_2^p & A_3^p & A_1^n & A_2^n \\ C_1^p & C_2^p & C_3^p & C_1^n & C_2^n \\ D_1^p & D_2^p & D_3^p & D_1^n & D_2^n \\ E_1^p & E_2^p & E_3^p & E_1^n & E_2^n \\ F_1^p & F_2^p & F_3^p & F_1^n & F_2^n \end{vmatrix} \\
&\quad - \frac{i\hbar\tilde{S}_{\mathrm{v},p}}{\varepsilon(\vec{k},\omega)}\begin{vmatrix} A_1^p & A_2^p & A_3^p & A_1^n & A_2^n \\ B_1^p & B_2^p & B_3^p & B_1^n & B_2^n \\ D_1^p & D_2^p & D_3^p & D_1^n & D_2^n \\ E_1^p & E_2^p & E_3^p & E_1^n & E_2^n \\ F_1^p & F_2^p & F_3^p & F_1^n & F_2^n \end{vmatrix} + \frac{i\hbar\tilde{S}_{B,n}}{\varepsilon(\vec{k},\omega)}\begin{vmatrix} A_1^p & A_2^p & A_3^p & A_1^n & A_2^n \\ B_1^p & B_2^p & B_3^p & B_1^n & B_2^n \\ C_1^p & C_2^p & C_3^p & C_1^n & C_2^n \\ E_1^p & E_2^p & E_3^p & E_1^n & E_2^n \\ F_1^p & F_2^p & F_3^p & F_1^n & F_2^n \end{vmatrix} \\
&\quad - \frac{i\hbar\tilde{S}_{s,n}}{\varepsilon(\vec{k},\omega)}\begin{vmatrix} A_1^p & A_2^p & A_3^p & A_1^n & A_2^n \\ B_1^p & B_2^p & B_3^p & B_1^n & B_2^n \\ C_1^p & C_2^p & C_3^p & C_1^n & C_2^n \\ D_1^p & D_2^p & D_3^p & D_1^n & D_2^n \\ F_1^p & F_2^p & F_3^p & F_1^n & F_2^n \end{vmatrix} + \frac{i\hbar\tilde{S}_{\mathrm{v},n}}{\varepsilon(\vec{k},\omega)}\begin{vmatrix} A_1^p & A_2^p & A_3^p & A_1^n & A_2^n \\ B_1^p & B_2^p & B_3^p & B_1^n & B_2^n \\ C_1^p & C_2^p & C_3^p & C_1^n & C_2^n \\ D_1^p & D_2^p & D_3^p & D_1^n & D_2^n \\ E_1^p & E_2^p & E_3^p & E_1^n & E_2^n \end{vmatrix}
\end{aligned}
\tag{3.75}
$$

where the five by five matrices are defined as N_1^n, N_2^n, N_3^n, N_4^n, N_5^n, N_6^n respectively. With this short-hand notations, $\delta\tilde{\rho}_{B,n}(\vec{k},\omega)$ becomes

$$
\delta\tilde{\rho}_{B,n}(\vec{k},\omega) = \frac{i\hbar}{\varepsilon(\vec{k},\omega)}\left[-N_1^n\tilde{S}_B^p + N_2^n\tilde{S}_s^p - N_3^n\tilde{S}_{\mathrm{v}}^p + N_4^n\tilde{S}_B^n - N_5^n\tilde{S}_s^n + N_6^n\tilde{S}_{\mathrm{v}}^n\right] . \tag{3.76}
$$

By applying the Cauchy-Residue Theorem to the inverse Fourier transformation $\delta\tilde{\rho}_{B,n}(\vec{k},t) =$

$\int \frac{\omega}{2\pi}\delta\tilde{\rho}_{B,n}(\vec{k},\omega)e^{-i\omega t}$, the time dependence of the neutron density fluctuation is written as

$$\delta\tilde{\rho}_{B,n}(\vec{k},t) = - \hbar \left\{ \frac{\left[-N_1^n\tilde{S}_B^p + N_2^n\tilde{S}_s^p - N_3^n\tilde{S}_{\rm v}^p + N_4^n\tilde{S}_B^n - N_5^n\tilde{S}_s^n + N_6^n\tilde{S}_{\rm v}^n\right]}{\partial\varepsilon(\vec{k},\omega)/\partial\omega}\Big|_{\omega=i\Gamma_k} e^{\Gamma t} \right.$$
$$\left. + \frac{\left[-N_1^n\tilde{S}_B^p + N_2^n\tilde{S}_s^p - N_3^n\tilde{S}_{\rm v}^p + N_4^n\tilde{S}_B^n - N_5^n\tilde{S}_s^n + N_6^n\tilde{S}_{\rm v}^n\right]}{\partial\varepsilon(\vec{k},\omega)/\partial\omega}\Big|_{\omega=-i\Gamma_k} e^{-\Gamma t} \right\} . \tag{3.77}$$

Likewise the proton baryon density fluctuation, $\delta\tilde{\rho}_{B,n}(\vec{k},t)$ can also be defined in terms of the initial state density fluctuations of the growing and decaying modes with the following definition,

$$\delta\tilde{\rho}_{B,n}(\vec{k},t) = \delta\rho_B^{n+}(\vec{k})e^{+\Gamma_k t} + \delta\rho_B^{n-}(\vec{k})e^{-\Gamma_k t}) . \tag{3.78}$$

Eqs. (3.77) and (3.78) yields to the expressions

$$\delta\rho_B^{n+}(\vec{k}) = -\hbar\frac{\left[-N_1^n\tilde{S}_B^p + N_2^n\tilde{S}_s^p - N_3^n\tilde{S}_{\rm v}^p + N_4^n\tilde{S}_B^n - N_5^n\tilde{S}_s^n + N_6^n\tilde{S}_{\rm v}^n\right]}{\partial\varepsilon(\vec{k},\omega)/\partial\omega}\Big|_{\omega=i\Gamma_k} \tag{3.79}$$

and

$$\delta\rho_B^{n-}(\vec{k}) = -\hbar\frac{\left[-N_1^n\tilde{S}_B^p + N_2^n\tilde{S}_s^p - N_3^n\tilde{S}_{\rm v}^p + N_4^n\tilde{S}_B^n - N_5^n\tilde{S}_s^n + N_6^n\tilde{S}_{\rm v}^n\right]}{\partial\varepsilon(\vec{k},\omega)/\partial\omega}\Big|_{\omega=-i\Gamma_k} . \tag{3.80}$$

The derivative of the susceptibility $\frac{\partial\varepsilon(\vec{k},\omega)}{\partial\omega}$ should be found by taking the derivative of each element of the coefficient matrix with respect to the frequency, ω. The derivatives of the matrix elements are presented in Appendix B.

After the relations for $\delta\tilde{\rho}_{B,p}(\vec{k},t)$ and $\delta\tilde{\rho}_{B,n}(\vec{k},t)$ are obtained in this manner, the correlation function can be defined as

$$\sigma_{ab}(|\vec{r}-\vec{r}'|,t) = \overline{\delta\rho_a^B(\vec{r},t)\delta\rho_b^B(\vec{r}',t)} = \int \frac{d^3k}{(2\pi)^3}e^{i\vec{k}\cdot\vec{x}}\tilde{\sigma}_{ab}(\vec{k},t) \tag{3.81}$$

where a and b represent the neutron or proton. $\vec{r}$ and $\vec{r}'$ denotes the coordinates for two different space points and $|\vec{r}-\vec{r}'|$ is the difference between these locations. The bar represents the average over the ensemble in the stochastic mean field approach.

In the above definition, $\tilde{\sigma}_{ab}(\vec{k},t)$ is the spectral intensity of the baryon density correlations and given by the relation

$$\tilde{\sigma}_{ab}^{BB}(\vec{k},t)(2\pi)^3\delta^3(\vec{k}-\vec{k}') \equiv \overline{\delta\rho_a^B(\vec{k},t)\left(\delta\rho_b^B(\vec{k}',t)\right)^*} . \tag{3.82}$$

Therefore, the total spectral intensity for the baryon correlation function can be written as $\tilde{\sigma}(\vec{k},t) = \tilde{\sigma}_{pp}(\vec{k},t) + \tilde{\sigma}_{np}(\vec{k},t) + \tilde{\sigma}_{pn}(\vec{k},t) + \tilde{\sigma}_{nn}(\vec{k},t)$ where all the contributions are included from proton and neutron. $\tilde{\sigma}^{BB}_{ab}(\vec{k},t)$ can also be written in terms of the initial density fluctuations of the growing and decaying modes as

$$\begin{aligned}\tilde{\sigma}^{BB}_{ab}(\vec{k},t)(2\pi)^3\delta^3(\vec{k}-\vec{k}') &= \overline{\delta\rho^{B+}_a(\vec{k})(\delta\rho^{B+}_b(\vec{k}))^*}e^{2\Gamma_k t} + \overline{\delta\rho^{B-}_a(\vec{k})(\delta\rho^{B-}_b(\vec{k}))^*}e^{-2\Gamma_k t} \\ &+\overline{\delta\rho^{B+}_a(\vec{k})(\delta\rho^{B-}_b(\vec{k}))^*} + \overline{\delta\rho^{B-}_a(\vec{k})(\delta\rho^{B+}_b(\vec{k}))^*}\,. \end{aligned} \tag{3.83}$$

First, let us evaluate the spectral intensity term for $a = b = p$,

$$\begin{aligned}\tilde{\sigma}^{BB}_{pp}(\vec{k},t)(2\pi)^3\delta^3(\vec{k}-\vec{k}') &= \overline{\delta\rho^{B+}_p(\vec{k})(\delta\rho^{B+}_p(\vec{k}))^*}e^{2\Gamma_k t} + \overline{\delta\rho^{B-}_p(\vec{k})(\delta\rho^{B-}_p(\vec{k}))^*}e^{-2\Gamma_k t} \\ &+\overline{\delta\rho^{B+}_p(\vec{k})(\delta\rho^{B-}_p(\vec{k}))^*} + \overline{\delta\rho^{B-}_p(\vec{k})(\delta\rho^{B+}_p(\vec{k}))^*}\,. \end{aligned} \tag{3.84}$$

The terms should be calculated seperately with the use of the short hand notations $d^+_\epsilon = \frac{\partial\varepsilon(\vec{k},\omega)}{\partial\omega}|_{\omega=i\Gamma}$ and $d^-_\epsilon = \frac{\partial\varepsilon(\vec{k},\omega)}{\partial\omega}|_{\omega=-i\Gamma}$ where the $+$ sign denotes the growing mode while $-$ sign is for the decaying mode. The calculations are made in the vision of the main assumption of the Stochastic Mean Field Theory, which stands for the fact that the initial phase-space distribution function $f(\vec{k},\vec{p},0)$ is a Gaussian random number with an average value of $\overline{f(\vec{k},\vec{p},0)} = f_0(\vec{k},\vec{p})$. Its second moment can be given by the relation

$$\overline{\delta\tilde{f}(\vec{k},\vec{p},0)\delta\tilde{f}^*(\vec{k}',\vec{p}',0)} = (2\pi)^3\delta^3(\vec{k}-\vec{k}')(2\pi\hbar)^3\delta^3(\vec{p}-\vec{p}')f_0(\vec{k},\vec{p})[1-f_0(\vec{k},\vec{p}))] \tag{3.85}$$

Furthermore, it can easily be verified that $N^{+*}_i = N^-_i$ and $N^{-*}_i = N^+_i$.

By inserting the Eqs.(3.79) and (3.80), the first and second terms in Eq.(3.84) become

$$\begin{aligned}&\left\{\overline{\left(\delta\rho^B_p(\vec{k})\right)^\pm}\right\}\left\{\overline{\left(\delta\rho^B_p(\vec{k})\right)^\pm}\right\}^* \\ =\ & \frac{\hbar^2}{d^+_\varepsilon d^{+*}_\varepsilon}\Big\{K^{++p}_{BB}|N^+_1|^2 - K^{++p}_{BS}(N^+_1N^-_2 + N^+_2N^-_1) + K^{++p}_{SS}|N^+_2|^2 + K^{++p}_{VV}|N^+_3|^2 \\ +\ & K^{++n}_{BB}|N^+_4|^2 - K^{++n}_{BS}(N^+_4N^-_5 + N^+_5N^-_4) + K^{++n}_{SS}|N^+_5|^2 + K^{++n}_{VV}|N^+_6|^2\Big\}\ . \end{aligned} \tag{3.86}$$

The third and fourth terms can be written as,

$$\begin{aligned}&\left\{\overline{\left(\delta\rho^B_p(\vec{k})\right)^+}\right\}\left\{\overline{\left(\delta\rho^B_p(\vec{k})\right)^-}\right\}^* \\ =\ & \frac{\hbar^2}{d^+_\varepsilon d^{+*}_\varepsilon}\Big\{K^{+-p}_{BB}N^+_1N^+_1 - 2K^{+-p}_{BS}N^+_1N^+_2 + K^{+-p}_{SS}N^+_2N^+_2 + K^{+-p}_{VV}N^+_3N^+_3 \\ +\ & K^{+-n}_{BB}N^+_4N^+_4 - 2K^{+-n}_{BS}N^+_4N^+_5 + K^{+-n}_{SS}N^+_5N^+_5 + K^{+-n}_{VV}N^+_6N^+_6\Big\} \end{aligned} \tag{3.87}$$

and

$$
\begin{aligned}
& \left\{\overline{\left(\delta\rho_p^B(\vec{k})\right)^-}\right\}\left\{\overline{\left(\delta\rho_p^B(\vec{k})\right)^+}\right\}^* \\
= & \frac{\hbar^2}{d_\varepsilon^+ d_\varepsilon^{+*}}\left\{K_{BB}^{+-p}N_1^-N_1^- - 2K_{BS}^{+-p}N_1^-N_2^- + K_{SS}^{+-p}N_2^-N_2^- + K_{VV}^{+-p}N_3^-N_3^-\right. \\
+ & \left. K_{BB}^{+-n}N_4^-N_4^- - 2K_{BS}^{+-n}N_4^-N_5^- + K_{SS}^{+-n}N_5^-N_5^- + K_{VV}^{+-n}N_6^-N_6^-\right\} .
\end{aligned}
\tag{3.88}
$$

The definitions and details of the calculations are given in Appendix C.

Then the final form of the total spectral intensity for proton correlation function is obtained as,

$$
\tilde{\sigma}_{pp}(\vec{k},t) = \hbar^2\frac{E_{pp}^+}{\left(\frac{\partial\varepsilon(k,\omega)}{\partial\omega}\right)_{\omega=i\Gamma_k}}(e^{2\Gamma t}+e^{-2\Gamma t}) + \hbar^2\frac{E_{pp}^{+-}+E_{pp}^{-+}}{\left(\frac{\partial\varepsilon(k,\omega)}{\partial\omega}\right)_{\omega=-i\Gamma_k}} . \tag{3.89}
$$

The short-hand notations are used for

$$
\begin{aligned}
E_{pp}^+ = E_{pp}^- &= K_{BB}^{++p}|N_1^+|^2 - K_{BS}^{++p}(N_1^+N_2^- + N_2^+N_1^-) + K_{SS}^{++p}|N_2^+|^2 + K_{VV}^{++p}|N_3^+|^2 \\
&+ K_{BB}^{++n}|N_4^+|^2 - K_{BS}^{++n}(N_4^+N_5^- + N_5^+N_4^-) + K_{SS}^{++n}|N_5^+|^2 + K_{VV}^{++n}|N_6^+|^2
\end{aligned}
$$

$$
\begin{aligned}
E_{pp}^{+-} &= K_{BB}^{+-p}N_1^+N_1^+ - 2K_{BS}^{+-p}N_1^+N_2^+ + K_{SS}^{+-p}N_2^+N_2^+ + K_{VV}^{+-p}N_3^+N_3^+ \\
&+ K_{BB}^{+-n}N_4^+N_4^+ - 2K_{BS}^{+-n}N_4^+N_5^+ + K_{SS}^{+-n}N_5^+N_5^+ + K_{VV}^{+-n}N_6^+N_6^+
\end{aligned}
$$

$$
\begin{aligned}
E_{pp}^{-+} &= K_{BB}^{+-p}N_1^-N_1^- - 2K_{BS}^{+-p}N_1^-N_2^- + K_{SS}^{+-p}N_2^-N_2^- + K_{VV}^{+-p}N_3^-N_3^- \\
&+ K_{BB}^{+-n}N_4^-N_4^- - 2K_{BS}^{+-n}N_4^-N_5^- + K_{SS}^{+-n}N_5^-N_5^- + K_{VV}^{+-n}N_6^-N_6^- .
\end{aligned}
\tag{3.90}
$$

The spectral intensities $\tilde{\sigma}_{nn}(\vec{k},t)$, $\tilde{\sigma}_{pn}(\vec{k},t)$ and $\tilde{\sigma}_{np}(\vec{k},t)$ can also be calculated by applying the same procedure. For the spectral intensity for neutron correlation function, we can write

$$
\begin{aligned}
\tilde{\sigma}_{nn}^{BB}(\vec{k},t)(2\pi)^3\delta^3(\vec{k}-\vec{k}') &= \overline{\delta\rho_n^{B+}(\vec{k})(\delta\rho_n^{B+}(\vec{k}))^*}e^{2\Gamma_k t} + \overline{\delta\rho_n^{B-}(\vec{k})(\delta\rho_n^{B-}(\vec{k}))^*}e^{-2\Gamma_k t} \\
&+\overline{\delta\rho_n^{B+}(\vec{k})(\delta\rho_n^{B-}(\vec{k}))^*} + \overline{\delta\rho_n^{B-}(\vec{k})(\delta\rho_n^{B+}(\vec{k}))^*} .
\end{aligned}
\tag{3.91}
$$

Using the expressions in Eqs. (3.78-3.79), the terms in this relation can be found as;

$$\begin{aligned}
&\left\{\overline{\left(\delta\rho_n^B(\vec{k})\right)^{\pm}}\right\}\left\{\overline{\left(\delta\rho_n^B(\vec{k})\right)^{\pm}}\right\}^* \\
= \;& \frac{\hbar^2}{d_\varepsilon^+ d_\varepsilon^{+*}}\left\{K_{BB}^{++p}|N_7^+|^2 - K_{BS}^{++p}(N_7^+N_8^- + N_8^+N_7^-) + K_{SS}^{++p}|N_8^+|^2 + K_{VV}^{++p}|N_9^+|^2\right. \\
+ \;& \left. K_{BB}^{++n}|N_{10}^+|^2 - K_{BS}^{++n}(N_{10}^+N_{11}^- + N_{11}^+N_{10}^-) + K_{SS}^{++n}|N_{11}^+|^2 + K_{VV}^{++n}|N_{12}^+|^2\right\}
\end{aligned} \tag{3.92}$$

$$\begin{aligned}
&\left\{\overline{\left(\delta\rho_n^B(\vec{k})\right)^{+}}\right\}\left\{\overline{\left(\delta\rho_n^B(\vec{k})\right)^{-}}\right\}^* \\
= \;& \frac{\hbar^2}{d_\varepsilon^+ d_\varepsilon^{+*}}\left\{K_{BB}^{+-p}N_7^+N_7^+ - 2K_{BS}^{+-p}N_7^+N_8^+ + K_{SS}^{+-p}N_8^+N_8^+ + K_{VV}^{+-p}N_9^+N_9^+\right. \\
+ \;& \left. K_{BB}^{+-n}N_{10}^+N_{10}^+ - 2K_{BS}^{+-n}N_{10}^+N_{11}^+ + K_{SS}^{+-n}N_{11}^+N_{11}^+ + K_{VV}^{+-n}N_{12}^+N_{12}^+\right\}
\end{aligned} \tag{3.93}$$

and

$$\begin{aligned}
&\left\{\overline{\left(\delta\rho_n^B(\vec{k})\right)^{-}}\right\}\left\{\overline{\left(\delta\rho_n^B(\vec{k})\right)^{+}}\right\}^* \\
= \;& \frac{\hbar^2}{d_\varepsilon^+ d_\varepsilon^{+*}}\left\{K_{BB}^{+-p}N_7^-N_7^- - 2K_{BS}^{+-p}N_7^-N_8^- + K_{SS}^{+-p}N_8^-N_8^- + K_{VV}^{+-p}N_9^-N_9^-\right. \\
+ \;& \left. K_{BB}^{+-n}N_{10}^-N_{10}^- - 2K_{BS}^{+-n}N_{10}^-N_{11}^- + K_{SS}^{+-n}N_{11}^-N_{11}^- + K_{VV}^{+-n}N_{12}^-N_{12}^-\right\} \; .
\end{aligned} \tag{3.94}$$

Then $\tilde{\sigma}_{nn}(\vec{k},t)$ becomes

$$\tilde{\sigma}_{nn}(\vec{k},t) = \hbar^2\frac{E_{nn}^+}{\left(\frac{\partial\varepsilon(k,\omega)}{\partial\omega}\right)_{\omega=i\Gamma_k}}(e^{2\Gamma t} + e^{-2\Gamma t}) + \hbar^2\frac{E_{nn}^{+-} + E_{nn}^{-+}}{\left(\frac{\partial\varepsilon(k,\omega)}{\partial\omega}\right)_{\omega=-i\Gamma_k}} \tag{3.95}$$

where

$$\begin{aligned}
E_{nn}^+ = E_{nn}^- \;&=\; K_{BB}^{++p}|N_7^+|^2 - K_{BS}^{++p}(N_7^+N_8^- + N_8^+N_7^-) + K_{SS}^{++p}|N_8^+|^2 + K_{VV}^{++p}|N_9^+|^2 \\
&+\; K_{BB}^{++n}|N_{10}^+|^2 - K_{BS}^{++n}(N_{10}^+N_{11}^- + N_{11}^+N_{10}^-) + K_{SS}^{++n}|N_{11}^+|^2 + K_{VV}^{++n}|N_{12}^+|^2 \\
E_{nn}^{+-} \;&=\; K_{BB}^{+-p}N_7^+N_7^+ - 2K_{BS}^{+-p}N_7^+N_8^+ + K_{SS}^{+-p}N_8^+N_8^+ + K_{VV}^{+-p}N_9^+N_9^+ \\
&+\; K_{BB}^{+-n}N_{10}^+N_{10}^+ - 2K_{BS}^{+-n}N_{10}^+N_{11}^+ + K_{SS}^{+-n}N_{11}^+N_{11}^+ + K_{VV}^{+-n}N_{12}^+N_{12}^+ \\
E_{nn}^{-+} \;&=\; K_{BB}^{+-p}N_7^-N_7^- - 2K_{BS}^{+-p}N_7^-N_8^- + K_{SS}^{+-p}N_8^-N_8^- + K_{VV}^{+-p}N_9^-N_9^- \\
&+\; K_{BB}^{+-n}N_{10}^-N_{10}^- - 2K_{BS}^{+-n}N_{10}^-N_{11}^- + K_{SS}^{+-n}N_{11}^-N_{11}^- + K_{VV}^{+-n}N_{12}^-N_{12}^- \; .
\end{aligned} \tag{3.96}$$

Finally, let us indicate the expressions for $\tilde{\sigma}_{pn}(\vec{k},t) = \tilde{\sigma}_{np}(\vec{k},t)$ as

$$\tilde{\sigma}_{pn}(\vec{k},t) = \tilde{\sigma}_{np}(\vec{k},t) = \hbar^2 \frac{E^{+}_{pn}}{\left(\frac{\partial\varepsilon(k,\omega)}{\partial\omega}\right)_{\omega=i\Gamma_k}} (e^{2\Gamma t} + e^{-2\Gamma t}) + \hbar^2 \frac{2E^{+-}_{pn}}{\left(\frac{\partial\varepsilon(k,\omega)}{\partial\omega}\right)_{\omega=-i\Gamma_k}} \quad (3.97)$$

with using the notations

$$\begin{aligned} E^{+}_{pn} = E^{+}_{np} &= K^{++p}_{BB} N^{+}_{7} N^{-}_{1} - K^{++p}_{BS}(N^{+}_{7} N^{-}_{2} + N^{+}_{8} N^{-}_{1}) + K^{++p}_{SS} N^{+}_{8} N^{-}_{2} + K^{++p}_{VV} N^{+}_{9} N^{-}_{3} \\ &- K^{++n}_{BB} N^{+}_{10} N^{-}_{4} - K^{++n}_{BS}(N^{+}_{10} N^{-}_{5} + N^{+}_{11} N_{4^-}) + K^{++n}_{SS} N^{+}_{11} N^{-}_{5} + K^{++n}_{VV} N^{+}_{12} N^{-}_{6} \end{aligned}$$

$$\begin{aligned} E^{+-}_{pn} = E^{+-}_{np} &= K^{+-p}_{BB} N^{+}_{7} N^{+}_{1} - K^{+-p}_{BS}(N^{+}_{7} N^{+}_{2} + N^{+}_{8} N^{+}_{1}) + K^{+-p}_{SS} N^{+}_{8} N^{+}_{2} + K^{+-p}_{VV} N^{+}_{9} N^{+}_{3} \\ &- K^{+-n}_{BB} N^{+}_{10} N^{+}_{4} - K^{+-n}_{BS}(N^{+}_{10} N^{+}_{5} + N^{+}_{11} N_{4^+}) + K^{+-n}_{SS} N^{+}_{11} N^{+}_{5} + K^{+-n}_{VV} N^{+}_{12} N^{+}_{6} \ . \end{aligned} \quad (3.98)$$

Hence, the total spectral intensity for the baryon correlation function is found in the final form

$$\tilde{\sigma}(\vec{k},t) = \hbar^2 \frac{E^{+}_{pp} + E^{+}_{nn} + 2E^{+}_{pn}}{\left(\frac{\partial\varepsilon(k,\omega)}{\partial\omega}\right)_{\omega=i\Gamma_k}} (e^{2\Gamma t} + e^{-2\Gamma t}) + \hbar^2 \frac{E^{+-}_{pp} + E^{-+}_{pp} + E^{+-}_{nn} + E^{-+}_{nn} + 4E^{+-}_{pn}}{\left(\frac{\partial\varepsilon(k,\omega)}{\partial\omega}\right)_{\omega=-i\Gamma_k}} \ . \quad (3.99)$$

This equation allows us to determine the growth rates of the unstable modes and the shortest growth times. The results are presented in Chapter 4.

As indicated in Eq. (3.81), the equal time correlation function for baryon density can be written in terms of the associated spectral intensity as

$$\begin{aligned} \sigma(|\vec{r} - \vec{r}'|, t) &= \int \frac{d^3k}{(2\pi)^3} e^{i\vec{k}\cdot\vec{x}} \hbar^2 \left\{ \frac{E^{+}_{pp} + E^{+}_{nn} + 2E^{+}_{pn}}{\left(\frac{\partial\varepsilon(k,\omega)}{\partial\omega}\right)_{\omega=i\Gamma_k}} (e^{2\Gamma t} + e^{-2\Gamma t}) \right. \\ &+ \left. \frac{E^{+-}_{pp} + E^{-+}_{pp} + E^{+-}_{nn} + E^{-+}_{nn} + 4E^{+-}_{pn}}{\left(\frac{\partial\varepsilon(k,\omega)}{\partial\omega}\right)_{\omega=-i\Gamma_k}} \right\} \ . \end{aligned} \quad (3.100)$$

The baryon correlation function is a useful quantity in the sense that the relation between the two space points of the nuclear system is obtained and therefore, the size of the fragmentation areas in the spinodal region can be determined.

CHAPTER 4

SPINODAL INSTABILITIES

In this chapter, the growth rates of the most unstable collective modes are examined with the use of the dispersion relation in Eq. (3.64) at different temperatures and the shortest growth times that correspond to the initial growth of density fluctuations are determined. Also, the behaviour of the equal time baryon correlation functions and the corresponding spectral intensities are observed for $T = 1\ MeV$ and $T = 5\ MeV$. In the calculations, the NL3 parameter set is used which includes the coupling constants and masses that are specified in Table 2.1, in the nonlinear Walecka Model.

All of the numerical calculations are implemented for two different initial baryon densities, $\rho_B = 0.2\rho_0$ and $\rho_B = 0.4\rho_0$ in order to simulate the spinodal region for asymmetric nuclear matter. Furthermore, to observe the isospin dependency of the system, the asymmetry parameter is varied as $I = 0.0,\ 0.2,\ 0.5$ and 0.8 from symmetric to neutron rich matter. Additionally, the effects of the Coulomb interaction between the protons are reproduced by incorporating the coupling of the photon field.

4.1 Growth Rates of the Unstable Collective Modes

In Fig. 4.1, the growth rates of the most unstable collective modes are shown as a function of wave number at various temperatures for different values of asymmetry parameter, for initial baryon density $\rho_B = 0.2\rho_0$. In all variations the growth rates show similar trends, increasing until a maximum point and then descending to reach zero at a certain value of wave number. As temperature increases, the wave number associated with the maximum growth rate Γ_{max} shifts approximately from $0.8fm^{-1}$ to $0.4fm^{-1}$ for the system with $I = 0.0$ and it reads

about $0.7fm^{-1}$ to $0.35fm^{-1}$ when the asymmetry parameter increases to $I = 0.8$. Also, the temperature dependence of the system can be observed from the graphs since the growth rates are reduced nearly by 80 percent when the temperature is raised to 10 MeV from 2 MeV for all values of asymmetry.

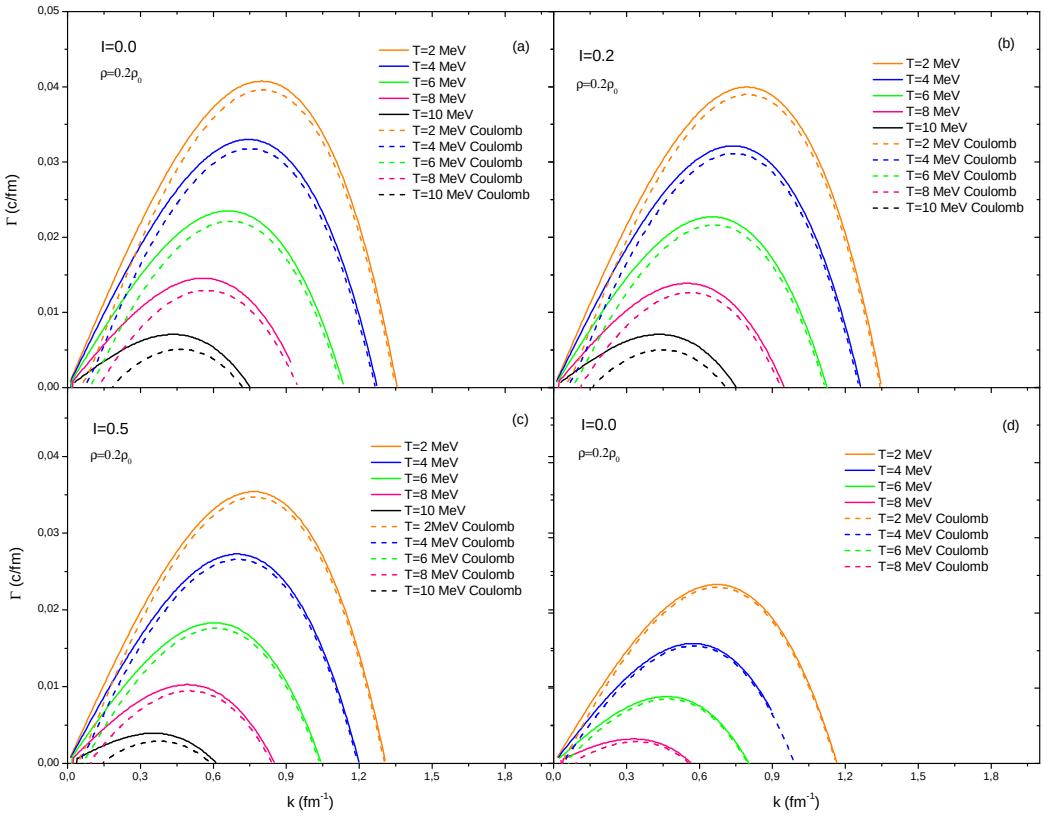

Figure 4.1: Growth rates of the most unstable modes as a function of wave number with an initial baryon density $\rho_B = 0.2\rho_0$ for different values of asymmetry parameters $I = 0.0,\ 0.2,\ 0.5,\ 0.8$ in panels (a), (b), (c) and (d) at various temperatures. The dashed lines indicate the presence of the Coulomb interaction.

The growth rates of unstables modes with initial baryon density $\rho_B = 0.4\rho_0$ is given in Fig. 4.2. For different temperatures, the wave numbers for maximum growth rates are found to be between $0.6fm^{-1}$ to $0.35fm^{-1}$ for symmetric matter and $0.5fm^{-1}$ to $0.2fm^{-1}$ when it comes to the system with $I = 0.8$. It should be noted that the crusts of neutron stars can be described with the conditions $\rho_B = 0.4\rho_0$ and $I = 0.8$ at low temperatures. Also similar to Fig. 4.1, the growth rates are contracted by approximately 90 percent with increasing

temperature.

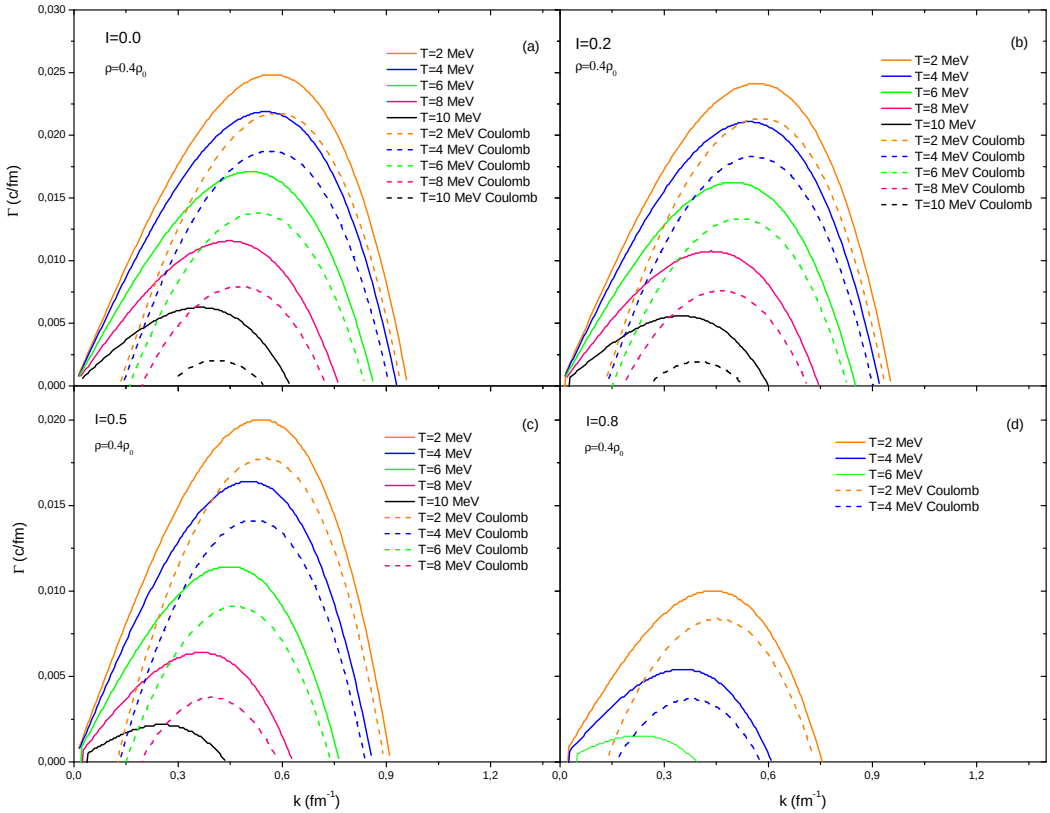

Figure 4.2: Growth rates of the most unstable modes as a function of wave number with an initial baryon density $\rho_B = 0.4\rho_0$ for different values of asymmetry parameters $I = 0.0,\ 0.2,\ 0.5,\ 0.8$ in panels (a), (b), (c) and (d) at various temperatures. The dashed lines indicate the presence of the Coulomb interaction.

In both Fig. 4.1 and 4.2, the effects of the Coulomb interaction are also indicated. The solid lines represent the cases where the electromagnetic interaction does not taken into account while the dashed lines are for the systems that couple to the photon field with $G_\gamma^2 = \frac{e^2}{-(\omega/c)^2+k^2}$. It can be observed that, there occurs a cut-off in the dispersion relations at long wavelengths as a result of the presence of the long-range electromagnetic interaction. By comparing Figs. 4.1 and 4.2, we can conclude that if the system becomes primarily less dense, the rate of the unstable activity is also reduced.

In both graphs, the range of the most unstable modes which is related to the size of the initial condensation region is appeared to decrease with increasing temperature and asymme-

try. Approximately, the most unstable modes are found to occur between the wave numbers $k = (0.3 - 0.7) fm^{-1}$ with corresponding wavelength values $\lambda = (20 - 10)\ fm$.

The growth rates of the unstable modes have a strong isospin dependence and the behaviour of the systems with different asymmetry parameters are given in Figs. 4.3 and 4.4 at temperatures $1\ MeV$ and $5\ MeV$ and with initial densities $\rho_B = 0.4\rho_0$ and $\rho_B = 0.2\rho_0$. We can emphasize that as the system becomes richer in neutrons, the growth rates are reduced by 40 to 60 percent at $T = 1\ MeV$ and 60 to 80 percent at $T = 5\ MeV$ for different initial densities. Also, the range of the unstable modes which characterizes the boundary of the spinodal region becomes narrower with increasing asymmetry, temperature and initial baryon density. In both of the graphs, it can be seen that the effect of the electromagnetic interaction between protons becomes more significant as the initial baryon density is raised from $\rho_B = 0.2\rho_0$ to $\rho_B = 0.4\rho_0$ at constant temperature. The results displays that the systems with higher neutron baryon densities tend to have less unstable behaviour than the symmetric matter at the same temperature.

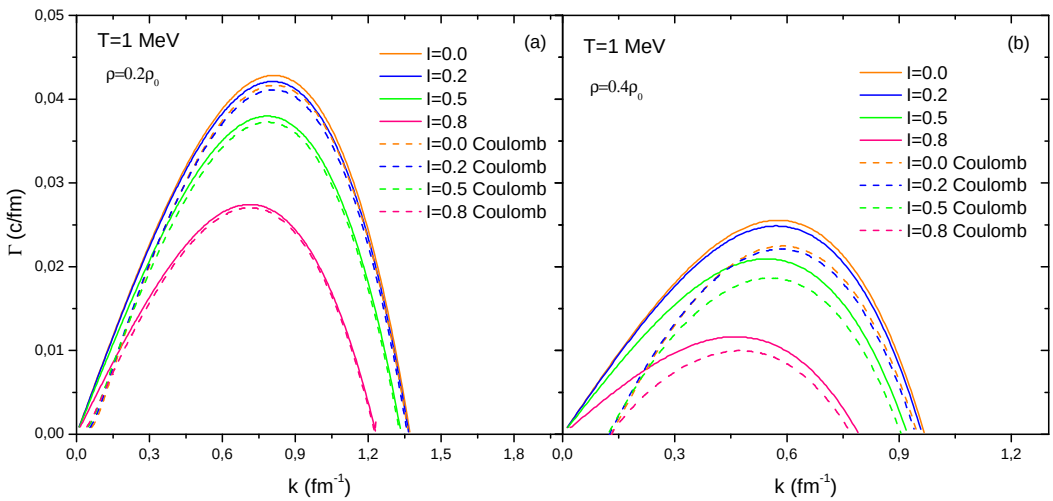

Figure 4.3: Growth rates of the most unstable modes as a function of wave number with an initial baryon densities $\rho_B = 0.2\rho_0$ for panel (a) and $\rho_B = 0.4\rho_0$ for panel (b), for different values of asymmetry parameters $I = 0.0,\ 0.2,\ 0.5,\ 0.8$ at fixed temperature $T = 1\ MeV$. The dashed lines indicate the presence of the Coulomb interaction.

Fig. 4.5 aims to demonstrate the growth rates of the most unstable modes as a function of baryon density for asymmetries $I = 0.0,\ 0.2,\ 0.5$ and $I = 0.8$ at fixed temperatures $T = 1\ MeV$ and $5\ MeV$. The graphs indicate the effect of Coulomb interaction and the

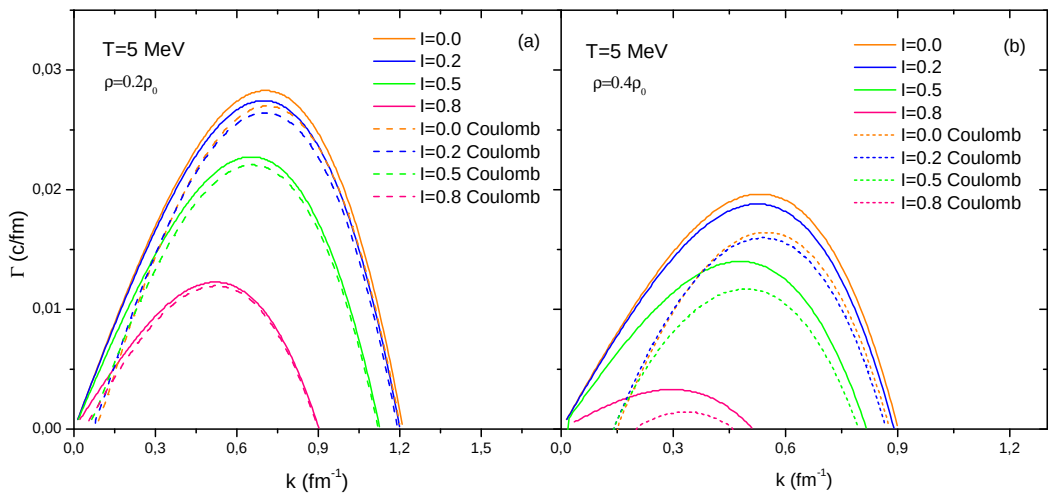

Figure 4.4: Growth rates of the most unstable modes as a function of wave number with an initial baryon densities $\rho_B = 0.2\rho_0$ for panel (a) and $\rho_B = 0.4\rho_0$ for panel (b), for different values of asymmetry parameters $I = 0.0,\ 0.2,\ 0.5,\ 0.8$ at fixed temperature $T = 5\ MeV$. The dashed lines indicate the presence of the Coulomb interaction.

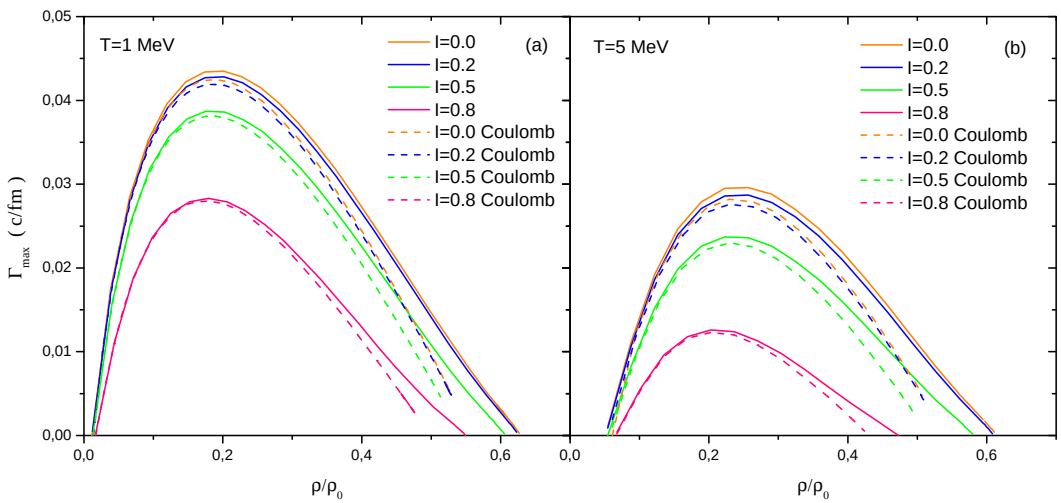

Figure 4.5: Growth rates of the most unstable modes as a function of baryon density ρ_B for different values of asymmetry parameters $I = 0.0,\ \ 0.2,\ 0.5,\ 0.8$, at fixed temperatures $T = 1\ MeV$ for panel (a) and $T = 5\ MeV$ for panel (b). The dashed lines indicate the presence of the Coulomb interaction.

isospin dependence of the nuclear system. The effect of the electromagnetic interaction becomes observable after the system goes beyond the density values at which the most unstable modes stand out approximately between $0.2\rho_0 < \rho_B < 0.3\rho_0$. The density values for

the fastest amplitude modes do not show any significant difference with increasing neutron baryon density, however the corresponding growth rates are decreased by a factor of 35 percent for the case with $T = 1\ MeV$ and 60 percent for $T = 5\ MeV$. Also, we observe that the unstable behaviour shows its peak at slightly higher densities when the temperature is increased. These results verify the observations from Figs. 4.3 and 4.4 and exhibits the isospin dependence of a nuclear system at low densities and low energies.

4.2 The Shortest Growth Time

The shortest growth time of primary baryon density fluctuations is determined by $\tau \equiv 1/\Gamma_k$ and shown in Fig. 4.6 for different values of asymmetry parameter at $T = 1\ MeV$ and $T = 5\ MeV$. For both temperatures, the minimum growth time occurs at the densities that correspond to the dominant unstable modes. It can be said that the unstable behaviour reaches its maximum value more slower as the asymmetry in the system increases. As an illustration, the shortest growth time is 20 fm/c for the symmetric matter at $T = 1\ MeV$ and close to 35 fm/c when $I = 0.8$ at the same temperature.

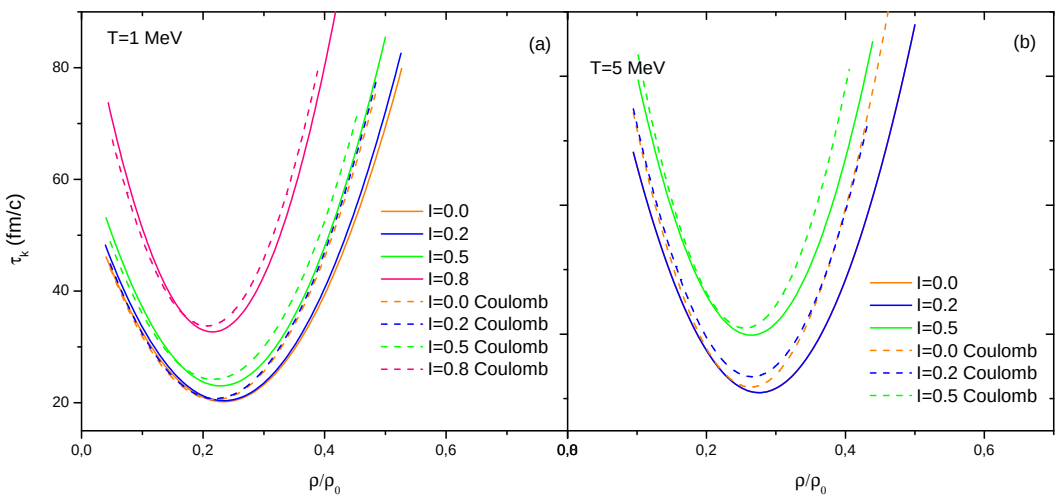

Figure 4.6: Shortest growth times for the most unstable modes as a function of baryon density for different values of asymmetry parameters $I = 0.0,\ 0.2,\ 0.5,\ 0.8$ for panel (a) at $T = 1\ MeV$ and $I = 0.0,\ 0.2,\ 0.5$ for panel (b) at $T = 5\ MeV$. The dashed lines indicate the presence of the Coulomb interaction.

Furthermore, Fig. 4.7 shows the temperature dependence of the shortest growth time for the

asymmetries $I = 0.0,\ 0.2,\ 0.5$ and $I = 0.8$. For symmetric matter, t_k is approximately 20 fm/c at $T = 2\ MeV$ and increases to 60 fm/c at $T = 8\ MeV$. In a system with asymmetry $I = 0.5$, this value can be raised nearly to 90 fm/c as the temperature increases.

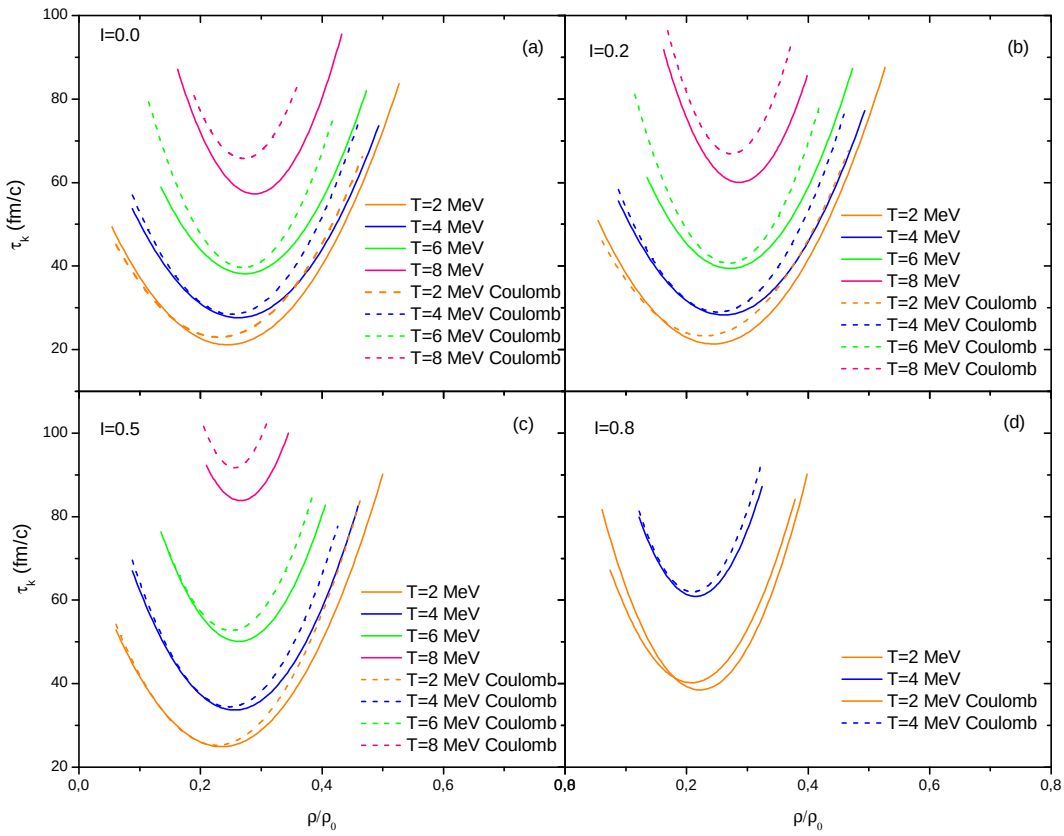

Figure 4.7: Shortest growth times for the most unstable modes as a function of baryon density for various temperatures at fixed values of asymmetry parameters $I = 0.0,\ 0.2,\ 0.5,\ 0.8$ respectively for panels (a), (b), (c) and (d). The dashed lines indicate the presence of the Coulomb interaction.

The multifragmentation of hot nuclear matter at extreme conditions is studied with the heavy-ion collisions in the new generation accelerator facilities. In the low energy regime, the liquid-gas phase transition can be studied in connection with the multifragmentation process, however difficulties arise in making measurements because of the time intervals that the fragments can be observed [31]. The shortest growth times are given in units fm/c which corresponds to the order of 10^{-23} seconds. As a result, proper observables should be found in order to identify and investigate the spinodal region.

4.3 Phase Diagrams

The properties of unstable nuclear matter in the spinodal region can be studied through the phase diagram. The boundary of the spinodal instability region can be determined from the temperature versus baryon density graph as shown in Fig. 4.8. The solid line represents the curve for the unstable mode at wavelength $\lambda = 9\ fm$ while the dashed line is for the case at $\lambda = 12\ fm$. The boundaries of the spinodal region are presented for four different values of asymmetry parameter for comparison. The peaks of the parabola-shaped curves are the critical temperatures above which the system is in equilibrium and can only exist in the gas phase. Oppositely, in the areas under the curves, the system shows unstable behaviour as a mixture of two different states, the liquid phase which is found to have a density value around ρ_0 and the gas phase with a relatively smaller density. In this unstable region, the small ampllitude density fluctuations lead to the formation of fragments in the system. The graphs indicate that the nuclear matter enters the unstable zone at densities smaller than $0.85\ fm^{-3}$, for temperatures below T_C. The value of the critical temperature is increased with increasing wavelength, it is around $10\ MeV$ for $\lambda = 9\ fm$ and close to $12\ MeV$ for $\lambda = 12\ fm$ at the asymmetries up to 0.5.

For asymmetric nuclear matter, one of the parameters that effect the dynamics of the spinodal region is the isospin dependence, therefore the boundaries are given for different asymmetry parameters for the unstable modes of wavelength $\lambda = 9\ fm$ in Fig. 4.9. For all values of I, the parabola-like curves are obtained with their peaks shift towards lower densities for larger values of asymmetry. The maximum density value to observe the multifragmentation is $0.04\ fm^{-3}$ for $I = 0.0$ and $0.03\ fm^{-3}$ for $I = 0.8$, with critical temperatures around $T_c = 11\ MeV$ and $T_C = 7\ MeV$ respectively. The effect of the electromagnetic interaction between the protons via the photon field can also be observed from the graph. The dashed lines show the results of the calculations with Coulomb interaction included. Although the effects are better understood for small asymmetry values, we can observe that the presence of the photon coupling reduces the critical temperature for all I.

In Fig. 4.10, boundary of the spinodal region is presented for neutron rich matter at different wavelength values. It is of importance that the nuclear matter at temperatures near $T = 1\ MeV$ and with asymmetry $I = 0.8$ corresponds to the conditions in the crusts of neutron stars. From the figure, it is observed that for all wavelengths, the system have a possibility to

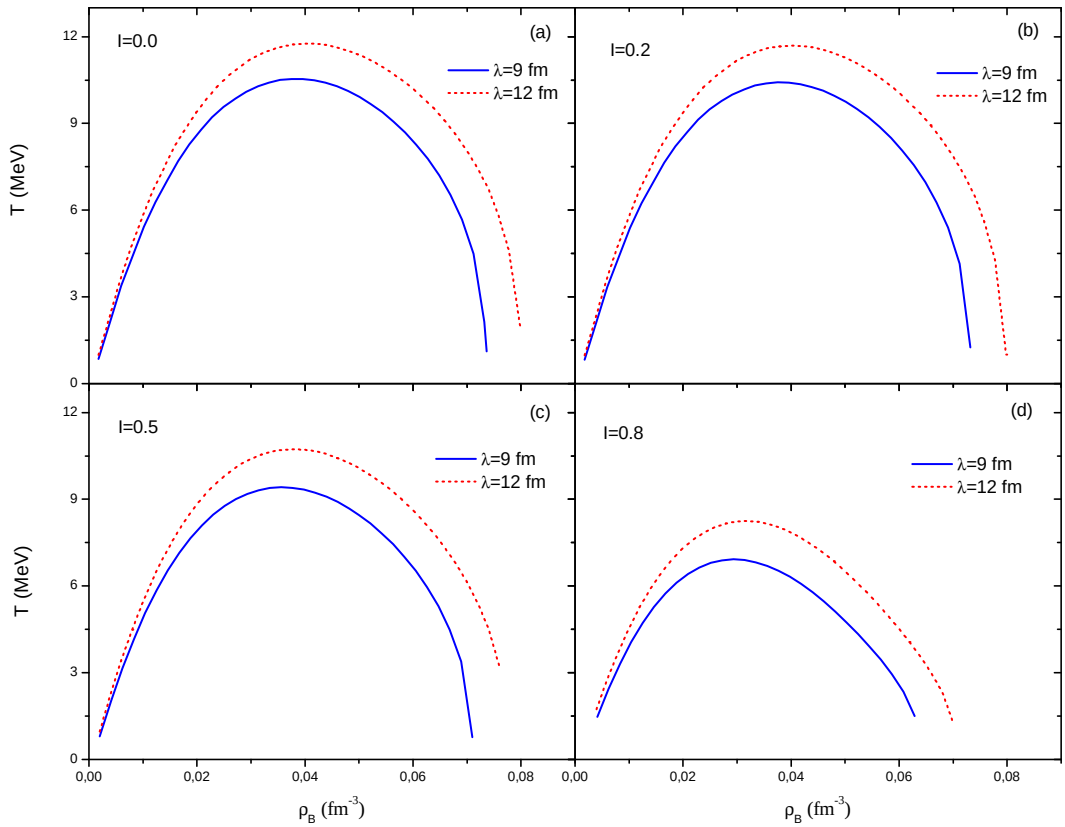

Figure 4.8: Phase Diagrams for asymmetric nuclear matter with asymmetry values $I = 0.0,\ 0.2\ 0.5$ and $I = 0.8$ in panels (a), (b), (c) and (d) respectively. The dashed lines are for the initial wavelength $\lambda = 9\ fm$, while the solid lines represent the initial case with $\lambda = 12\ fm$.

enter the spinodal region up to a baryon density of $\rho_B = 0.5\rho_0$ in average, which is indicated as the saturation point. In these conditions, the spinodal instabilities can not be observed at densities above $\rho_B = 0.5\rho_0$ which is consistent with the results in Ref. 21.

4.4 Spectral Intensities of Baryon Density Correlation Functions

The unstable dynamics can be investigated via the density correlation functions in the spinodal region. According to the derived expression in Eq. (3.98), the spectral intensity of the baryon density correlation function is presented in Fig. 4.11 as a function of wave number for varying asymmetry parameters from $I = 0.0$ to $I = 0.8$ at fixed temperature $T = 1\ MeV$ and with an initial baryon density $\rho_B = 0.4\rho_0$. The calculations are made by assuming six different

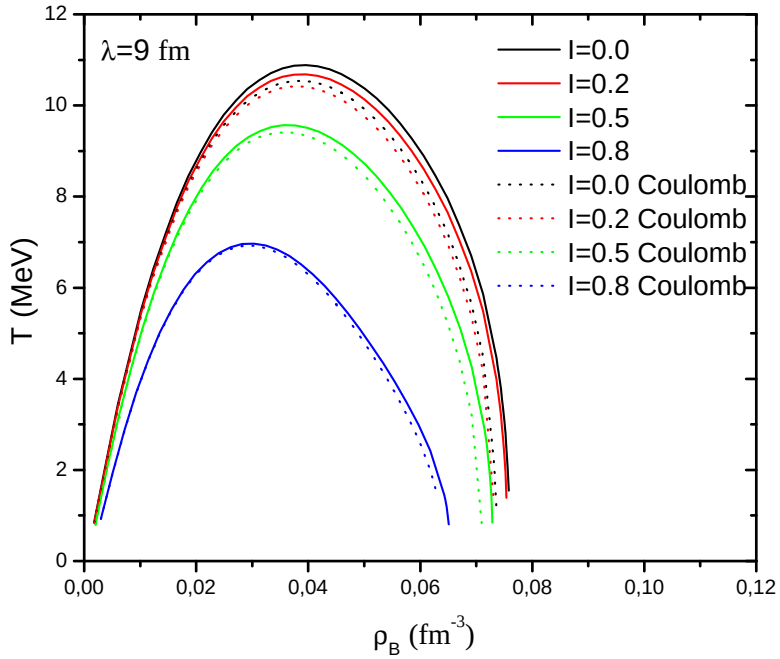

Figure 4.9: Phase Diagram for asymmetric nuclear matter with $\lambda = 9\ fm$, for different asymmetry values $I = 0.0,\ 0.2,\ 0.5$ and $I = 0.8$. The dashed lines indicate the presence of the Coulomb interaction.

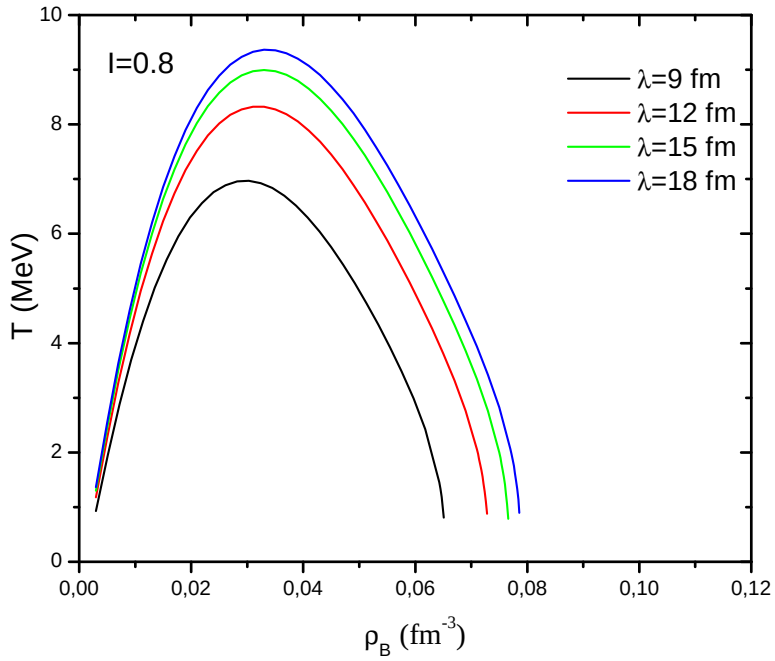

Figure 4.10: Phase Diagram for asymmetric nuclear matter with $I = 0.8$, for different wavelength values $\lambda = 9\ fm,\ 12\ fm,\ 15\ fm$ and $18\ fm$.

initial time values, $t = 0,\ 10,\ 20,\ 30,\ 40$ and $50 fm/c$.

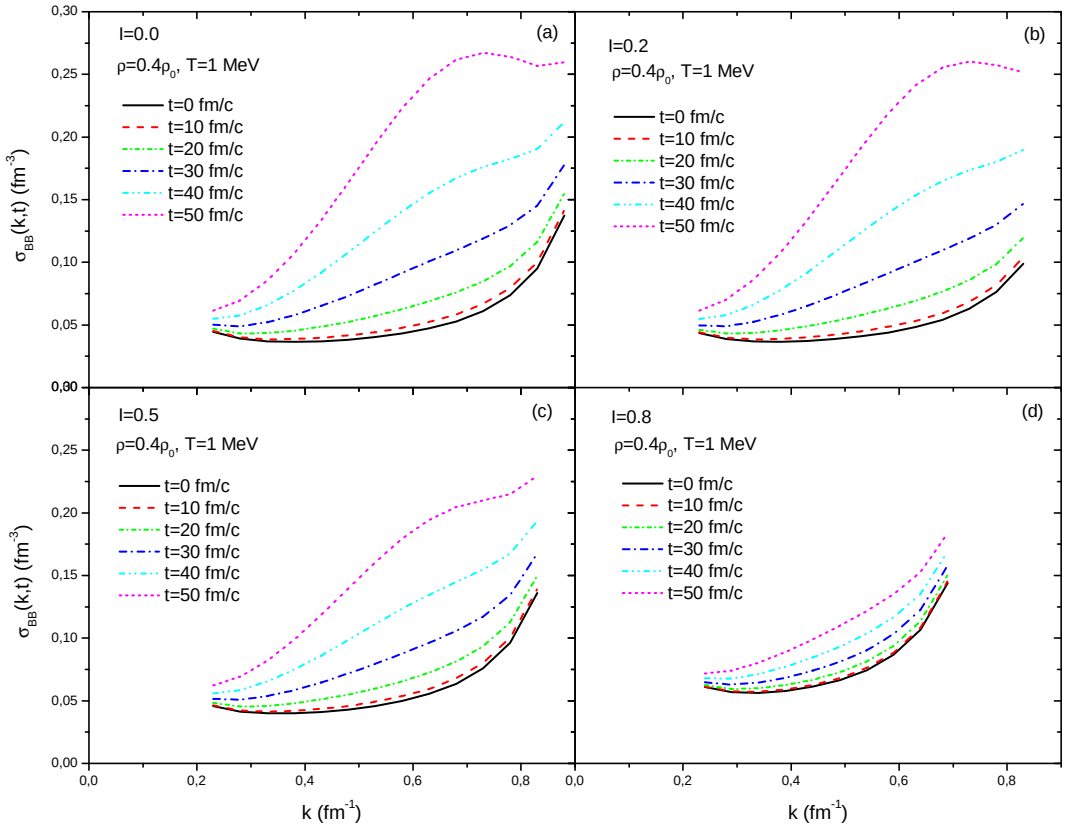

Figure 4.11: Spectral intensity of baryon density correlation function as a function of wave number at $T = 1\ MeV$, initial baryon density $\rho_B = 0.4\rho_0$ and at different asymmetry parameters $I = 0.0,\ 0.2,\ 0.5,\ 0.8$ respectively in panels (a), (b), (c) and (d).

If we consider the curves at $t = 50\ fm/c$, the range of the maximum growth rates match with those obtained in Fig. 4.5 for the most unstable collective modes. For $I = 0.0$ in panel (a), the maximum activity is observed between $k = 0.6 - 0.7\ fm$ where the range of the growth rate reads around $k = 0.6\ fm$ for the dominant unstable mode in Fig. 4.5. As the initial charge asymmetry of the system increases, the growth rates decrease for all initial time values and the curves loose their peaked behaviour.

In Fig. 4.12 the system is given at $T = 5\ MeV$ with all other conditions are the same with Fig. 4.11. $T = 5\ MeV$ is a relatively higher temperature compared to $1\ MeV$ and the neutron rich matter with $I = 0.8$ does not enter the spinodal region at this temperature value. This is an expected result since the equation of state for asymmetric nuclear matter with $I = 0.8$ in

Fig. 2.4 shows that the pressure is monotonically increasing and the mechanically unstable region does not appear at $T = 5\ MeV$. The curves have the same trend in both figures for $T = 1\ MeV$ and $T = 5\ MeV$, however the growth rates are remarkably higher in the case of higher temperature. As an example, the largest growth occurs about $0.25\ fm^{-3}$ in panel (b) of Fig. 4.11 where it reads around $1\ fm^{-3}$ for $T = 5\ MeV$ with the same asymmetry $I = 0.2$.

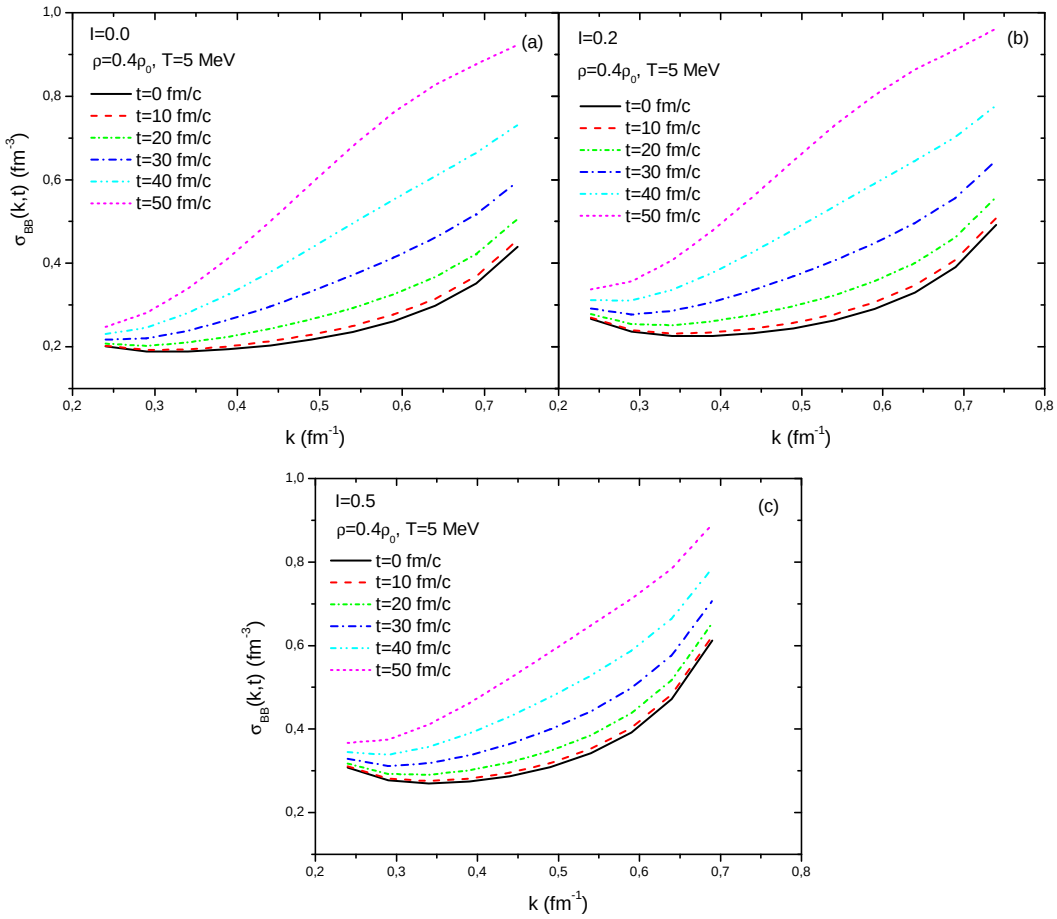

Figure 4.12: Spectral intensity of baryon density correlation function as a function of wave number at $T = 5\ MeV$, initial baryon density $\rho_B = 0.4\rho_0$ and at different asymmetry parameters $I = 0.0,\ 0.2,\ 0.5$ respectively in panels (a), (b) and (c).

We note that as the system have higher dependence on asymmetry, the dominant unstable modes grow less at smaller ranges than the symmetric matter.

Since we have retained only the collective modes, the curves are evaluated up to a cut-off

wave number between the values $k = 0.7 - 0.9\ fm^{-1}$. The non-collective modes do not evolve in time and display their effects at higher wave numbers. Therefore it is sufficient to consider only the long wavelenth regions where the collective unstable modes dominate.

The other parameter that effects the spectral instensity of the baryon correlation function is the initial density value of the system. Fig. 4.13 and 4.14 show the change in the spectral intensity as a function of wave number at $T = 1\ MeV$ and $T = 5\ MeV$, with an initial density $\rho_B = 0.2\rho_0$. By comparing with Figs. 4.11 and 4.12 we observe that when the system is initially less dense, higher peaks occur around the range of the dominant unstable modes. As an example, from the graph with initial conditions $I = 0.0$, $T = 5\ MeV$ and $\rho_B = 0.2\rho_0$, the largest growth rate reads $0.7\ fm^{-3}$ around the wave number $k = 0.9\ fm^{-1}$ while the same result is found as $0.25\ fm^{-3}$ in the system with $\rho_B = 0.4\rho_0$, around $k = 0.7\ fm^{-1}$. Besides the growth rates, the range of the most unstable collective modes are also decreased with increasing density.

4.5 Baryon Density Correlation Functions

The total equal time baryon density correlation function is given in Chapter 3 as a sum of neutron, proton and cross correlation terms. In this chapter, dynamics of the spinodal region, namely the size of the initial condensation regions and the time evolution of the clusters are investigated with the numerical calculations of Eq. (3.99). In all figures except Fig. (4.19), the electromagnetic interaction between the protons are taken into account.

Fig. 4.15 shows the baryon density correlation function in terms of the distance between two locations in space at $T = 1\ MeV$ with an initial baryon density $\rho_B = 0.4\rho_0$. Six different initial time values are assumed in order to observe the time scale of the condensed regions. Besides, the asymmetry dependence of the system is illustrated in the panels (a), (b), (c) and (d) with $I = 0.0,\ 0.2,\ 0.5$ and 0.8 respectively. The time evolution of the density fluctuations is faster when $I = 0.0$ and decreases with increasing asymmetry. In panel (a), $\sigma_{BB}(x = 0,\ t = 50\ fm/c) = 0.026\ fm^{-6}$ while the graph in panel (d) gives $\sigma_{BB}(x = 0,\ \ t = 50\ fm/c) = 0.0007\ fm^{-6}$ for $I = 0.8$. This 75 percent of decrease addresses the effect of isospin dependence of the nuclear matter.

Since the baryon density correlation is a function of the distance between two points $\vec{x} - \vec{x}'$, it

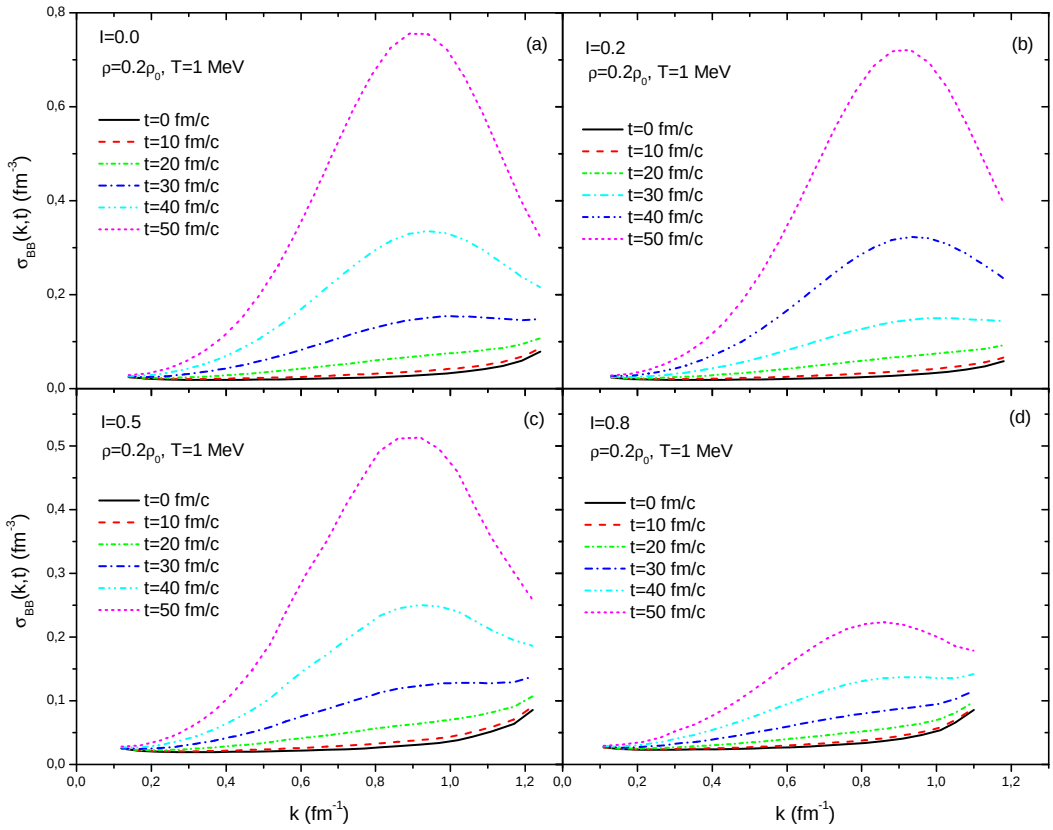

Figure 4.13: Spectral intensity of baryon density correlation function as a function of wave number at $T = 1\ MeV$, initial baryon density $\rho_B = 0.2\rho_0$ and at different asymmetry parameters $I = 0.0,\ 0.2,\ 0.5,\ 0.8$ respectively in panels (a), (b), (c) and (d).

is a physical quantity that is directly related to the size of the initial fragments that is formed during the spinodal decomposition process. For this purpose, the correlation length denoted by x_c, is defined as the width of the correlation at half maximum and it provides an approximate measure of the condensing region in the linear regime. In Fig. 4.15, the correlation length is $2.84\ fm$ for the symmetric matter and $3.6\ fm$ for the neutron rich matter in panel (d). These values correspond to condensing regions of $A = 14$ and $A = 30$ nucleons approximately. It should be noted that, the neutron rich matter with $I = 0.8$ at low temperatures around $T = 1\ MeV$ simulates the conditions in the crusts of neutron stars.

Similar plots in the panels of Fig. 4.16 demonstrate the nuclear matter in the same initial conditions with Fig. 4.15 but at a higher temperature $T = 5\ MeV$. From the phase diagram in Fig. 4.9, it can be recognized that the critical temperature of the asymmetric nuclear matter

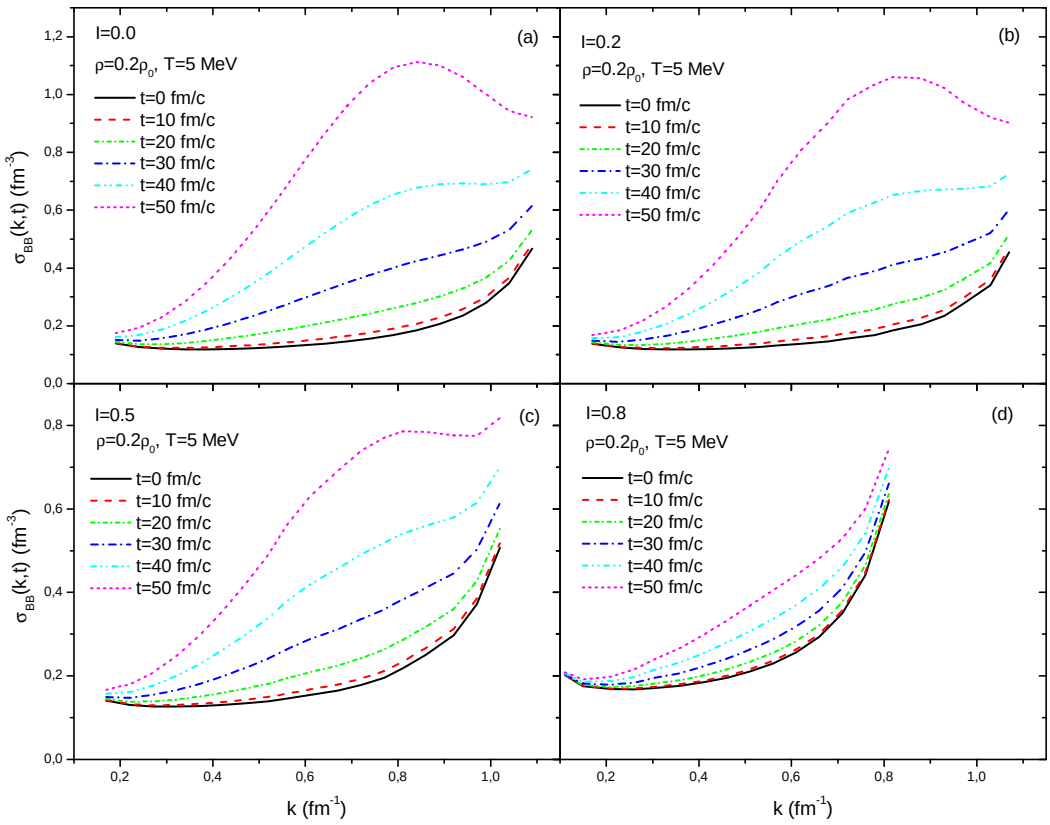

Figure 4.14: Spectral intensity of baryon density correlation function as a function of wave number at $T = 5\ MeV$, initial baryon density $\rho_B = 0.2\rho_0$ and at different asymmetry parameters $I = 0.0,\ 0.2,\ 0.5,\ 0.8$ respectively in panels (a), (b), (c) and (d).

with $I = 0.8$ is around $T_c = 2\ MeV$ at baryon density $\rho_B = 0.4\rho_0$. Therefore at $T = 5\ MeV$, the system is entirely in a stable gas phase and the dynamics of the unstable region is investigated up to $I = 0.5$ at this temperature. For all values of I, the correlation lengths are increased between 15-20 percent and the growth rates are approximately increased by a factor of 2 with increasing temperature.

Furthermore, Fig. 4.17 and 4.18 illustrates the baryon density correlation functions of a system with initial density $\rho_B = 0.2\rho_0$ at $T = 1\ MeV$ and $T = 5\ MeV$ respectively. The qualitative behaviour of the graphs are similar to those of Fig. 4.15 and 4.16. For both temperatures, the growth rates of the density fluctuations are 3 to 7 times greater than the growth rates for initial density $\rho_B = 0.4\rho_0$. Again, the baryon density fluctuations are observed to grow slower with increasing asymmetry. At $T = 1\ MeV$, a decrease about 75 percent is ob-

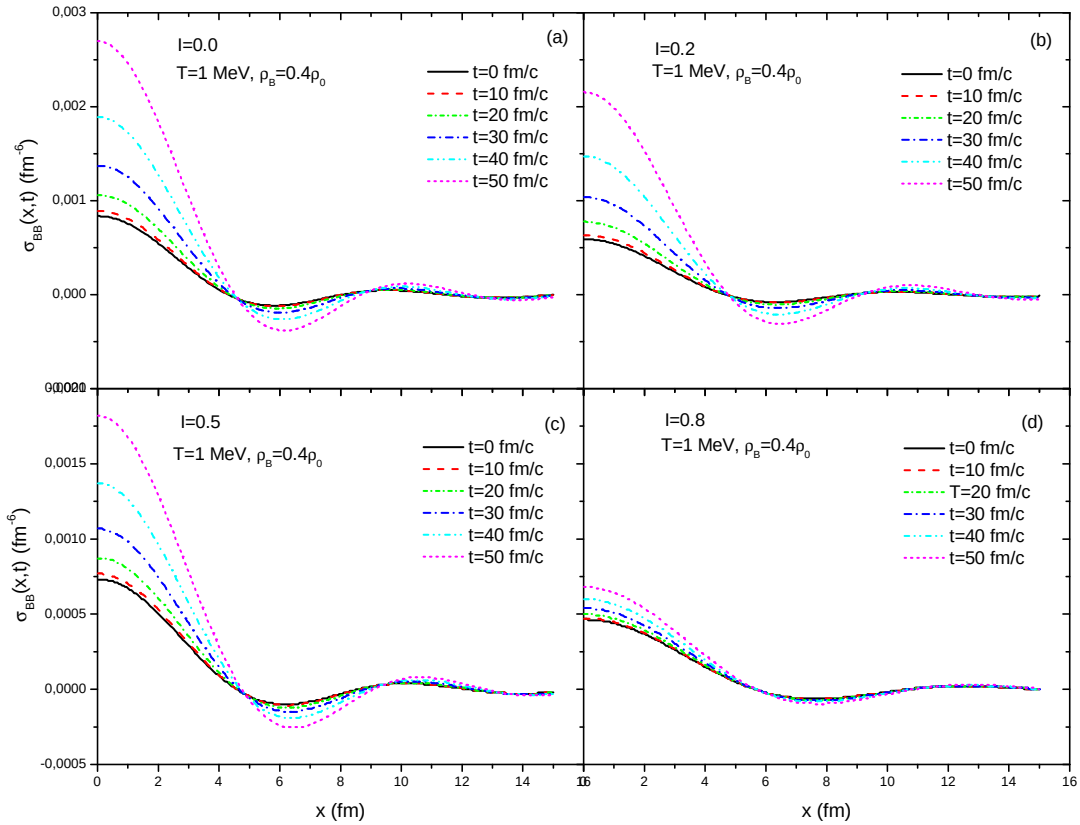

Figure 4.15: Baryon density correlation $\sigma_{BB}(\vec{x},t)$ as a function of distance between two space points at $T = 1\ MeV$, initial baryon density $\rho_B = 0.4\rho_0$ and at different asymmetry parameters $I = 0.0,\ 0.2,\ 0.5,\ 0.8$ respectively in panels (a), (b), (c) and (d).

served between the correlations of panels (a) and (d) of Fig. 4.17. The effect of temperature can be observed also at low densities. For example, for $\rho_B = 0.2\rho_0$, the baryon density correlation for the asymmetric matter with $I = 0.2$ is $\sigma_{BB}(x = 0,\ t = 50\ fm/c) = 0.015\ fm^{-6}$ at temperature $T = 1\ MeV$ and $\sigma_{BB}(x = 0,\ \ t = 50\ fm/c) = 0.019\ fm^{-6}$ at $T = 5\ MeV$. This addresses to an increase around 30 percent.

It is observed that the correlation volume is slightly reduced when the initial baryon density is decreased by half. For the asymmetric matter with $I = 0.5$, the correlation length is found to be around $x_C = 3.6\ fm$ when the initial density is $\rho_B = 0.4\rho_0$ and decreases to $x_C = 2.6\ fm$ when the density is reduced to $\rho_B = 0.2\rho_0$. The associated primary clusters are formed approximately with $A = 30$ and $A = 12$ nucleons. The initial average size of the fragments found from density correlation calculations is consistent with the range of the

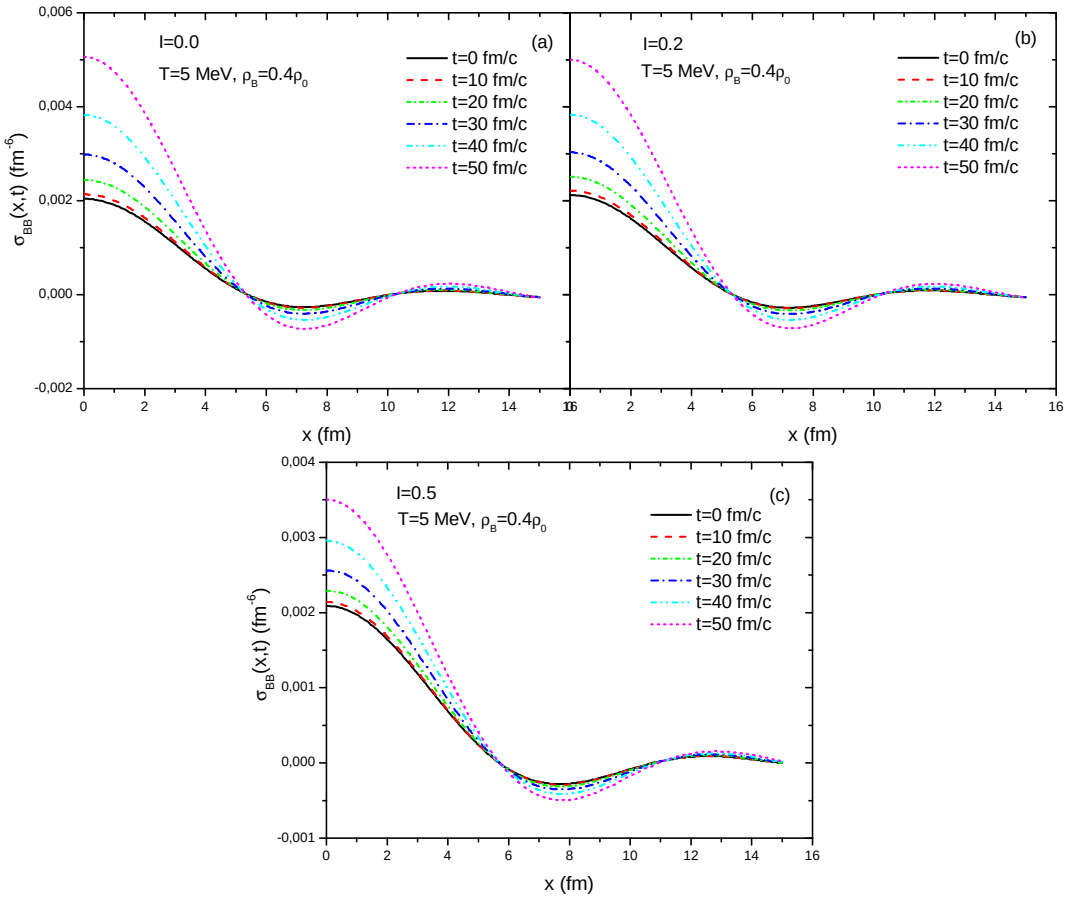

Figure 4.16: Baryon density correlation $\sigma_{BB}(\vec{x},t)$ as a function of distance between two space points at $T = 5\ MeV$, initial baryon density $\rho_B = 0.4\rho_0$ and at different asymmetry parameters $I = 0.0,\ 0.2,\ 0.5,\ 0.8$ respectively in panels (a), (b), (c) and (d).

dominant unstable modes obtained from the dispersion relation.

In order to demonstrate the Coulomb effects in the system, Fig. 4.19 is plotted by implementing zero photon coupling with the same conditions in Fig. 4.16.

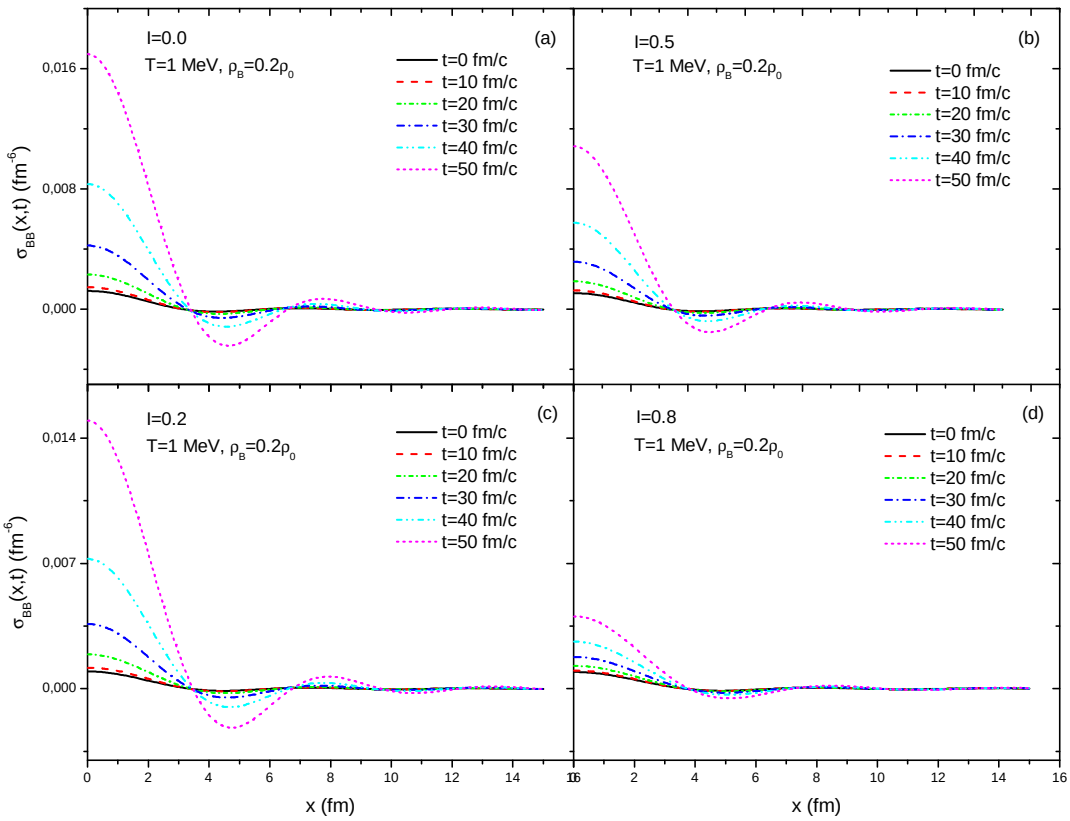

Figure 4.17: Baryon density correlation $\sigma_{BB}(\vec{x},t)$ as a function of distance between two space points at $T = 1\ MeV$, initial baryon density $\rho_B = 0.2\rho_0$ and at different asymmetry parameters $I = 0.0,\ 0.2,\ 0.5,\ 0.8$ respectively in panels (a), (b), (c) and (d).

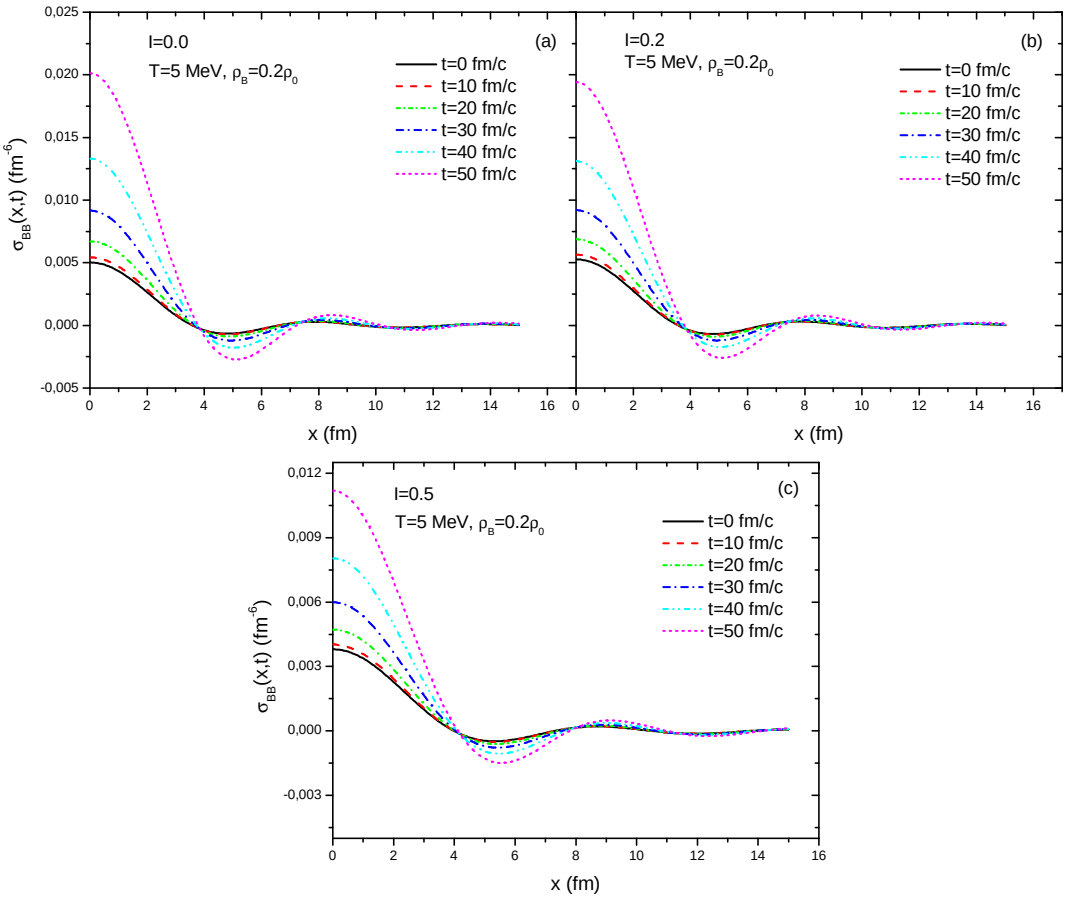

Figure 4.18: Baryon density correlation $\sigma_{BB}(\vec{x},t)$ as a function of distance between two space points at $T = 5\ MeV$, initial baryon density $\rho_B = 0.2\rho_0$ and at different asymmetry parameters $I = 0.0,\ 0.2,\ 0.5$ respectively in panels (a), (b) and (c).

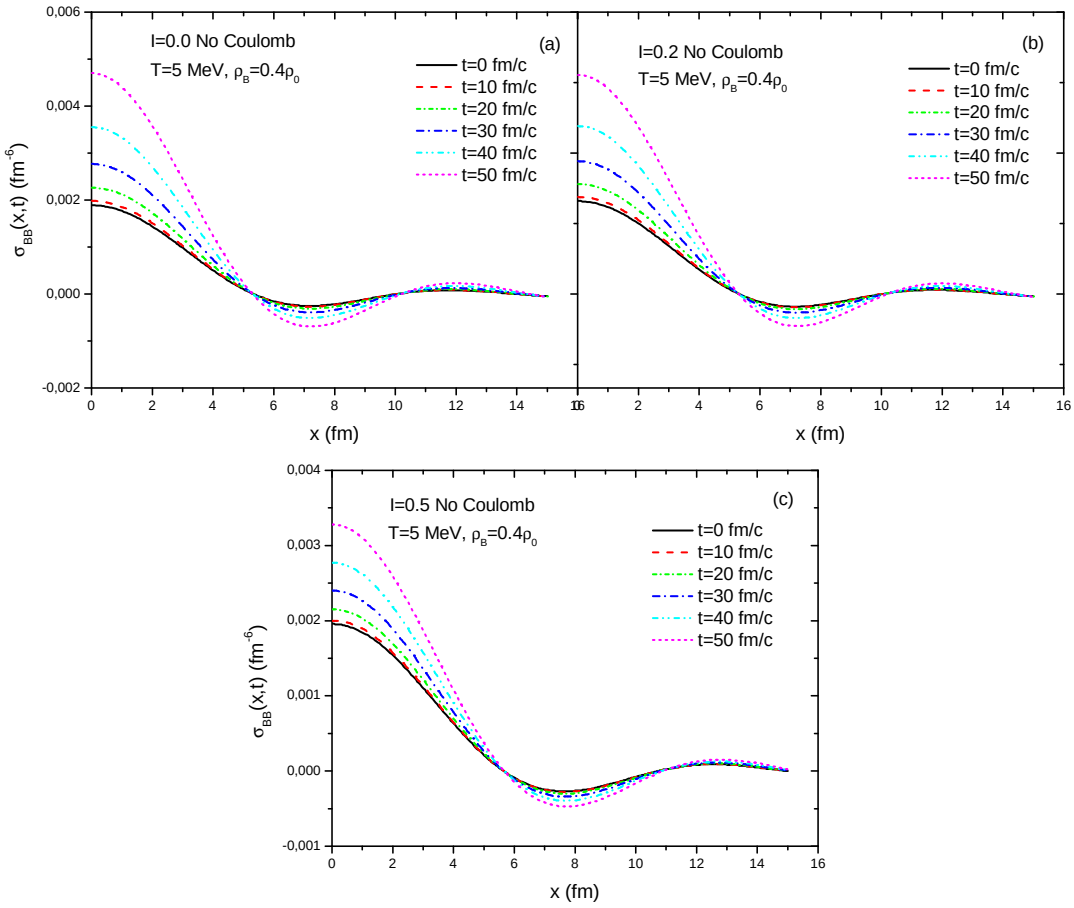

Figure 4.19: Baryon density correlation $\sigma_{BB}(\vec{x},t)$ as a function of distance between two space points at $T = 5\ MeV$, initial baryon density $\rho_B = 0.4\rho_0$ and at different asymmetry parameters $I = 0.0,\ 0.2,\ 0.5$ respectively in panels (a), (b) and (c). The Coulomb interaction is neglected.

CHAPTER 5

CONCLUSION

We investigated the behaviour of the charge asymmetric nuclear matter in the spinodal instability region at low energy regime. In such conditions where the dominant density fluctuations are assumed to arise from the one-body dissipation mechanism, the stochastic mean field theory provides a useful tool to study the dynamics of the density fluctuations [17]. In this thesis, the early growth of spinodal instabilities are examined, therefore it is sufficient to consider the stochastic mean field approach in the linear response treatment.

In the first part, the asymmetric nuclear matter equation of state is obtained for finite temperature within the framework of Walecka-type relativistic mean field theory in the semi-classical limit. The nonlinear extension of the standard Walecka Model is employed with the addition of ρ meson coupling to the nucleon field, which is an isospin doublet. The variance of the effective mass with the baryon density is demonstrated for different values of asymmetry parameter and the saturation curve is examined at various temperatures. From the plots of pressure with respect to the baryon density, the boundary of the spinodal region is determined. We observed that the spinodal region shrinks and the critical temperature decreases from $T = 14\ MeV$ to $T = 12\ MeV$ as the matter gets richer in neutrons. Also, the effects of temperature and isospin asymmetry on the chemical potential of the system is investigated. We have used the NL3 parameter set in the relativistic calculations [22].

The second part of this thesis introduces the stochastic extention to the mean field approximation. In the semi-classical limit, two coupled Vlasov equations are derived and the meson fields are linearized around their equilibrium in order to investigate the early growth of small amplitude density fluctuations. We obtained the dispersion relation with two imaginary poles that characterizes the spinodal region. The growth rates of the dominant unstable modes

are analyzed both as a function of wave number and baryon density. The calculations are implemented for two different values of initial density, $\rho_B = 0.2\rho_0$ and $\rho_B = 0.4\rho_0$, to simulate the conditions of the spinodal region as well as for different initial isospin asymmetries $I = 0.0,\ 0.2,\ 0.5$ and 0.8. Also, the dynamics of the system is investigated at various temperatures.

Since only the effects due to the collective modes are of interest, we studied the evolution of the fluctuations up to certain wave numbers and supressed the effects from the non-collective modes beyond. We have found that the system exhibits more unstable behaviour at densities around $\rho_B = 0.2\rho_0$ and at lower temperatures. As the asymmetry increases, the dominant unstable modes shift towards the longer wavelengths and a narrower region of instability occurs. Also, we have demonstrated that the shortest growth time of the density fluctuations correspond to the maximum activity regions of the most unstable modes.

The boundary of the spinodal region is determined from the density variance curve of temperature which we observed to be between $\rho_B = 0.4\rho_0 - 0.5\rho_0$ for different asymmetries at $T = 1\ MeV$ and $T = 5\ MeV$. We observed that the liquid-gas phase transition takes place until the system reaches the critical temperature T_C and the systems with higher asymmetries tend to gasify at lower temperatures.

The baryon density correlation function is a physical quantity and provides information about the early size of the fragmentation region. The early size of the primary clusters that is extracted from the baryon correlation function is consistent with those found from the dispersion relation. The condensing regions have found to include $A = 15 - 30$ nucleons. In neutron rich matter, larger clusters are formed with more nucleons.

In this thesis, we investigated the properties of asymmetric nuclear matter in the spinodal region where multifragmentation occurs, which is considered as a signal of liquid-gas phase transition. Understanding the isospin dependence of the nuclear dynamics at extreme conditions provide useful information to describe the neutron rich matter that is produced in the intermediate energy heavy ion collisions and in the astrophysical processes.

The stochastic mean field approach is the most suitable framework to investigate the spinodal dynamics in the low energy regime associated with the rapid density fluctuations. The nuclear matter with isospin asymmetry $I = 0.8$ and at temperatures around $T = 1\ MeV$ corresponds

to the conditions in the crusts of the neutron stars. The stochastic approach can be utilized to determine the critical temperature and density for neutron star to enter the spinodal region. Furthermore, with the use of the stochastic extension to the relativistic mean field theory, the analysis of the experiments on deep in-elastic collisions would be possible as well as the investigations of the reactions with neutron rich radioactive beams.

REFERENCES

[1] B. D. Serot, J. D. Walecka, "Advances in Nuclear Physics Vol.16", Plenium Press, New York, 1997; J. D. Walecka, Ann. Phys. **83** (1974) 491.

[2] B. D. Serot, J. D. Walecka, Int. J. Mod. Phys. **E6** (1997) 515.

[3] Sanjeev Kumar, "'Dynamics Of Heavy Ion Collisions At Intermediate Energies", PhD Thesis, Thapar University, 2010.

[4] J.D. Walecka, "Theoretical Nuclear and Subnuclear Physics", Imperial College Press, 2004.

[5] Ph. Chomaz, M. Colonna and J. Randrup, Phys. Rep. **389** (2004) 263.

[6] G. Verde, "The Search for the Nuclear Symmetry Energy in Reaction Dynamics", "http://www.cenbg.in2p3.fr/heberge/EcoleJoliotCurie/coursannee/cours/Verde2010.pdf", last access date; August 2013

[7] B. A. Li et al., Phys. Rep. **464** (2008).

[8] E. Bonnet, et al., Phys. Rev. Lett. **105** (2010) 142701.

[9] H. Jaqaman, A.Z. Mekjian, and L.Zamick, Phys. Rev. **C 27** (1983) 2782.

[10] C. Wu and Z. Ren, Phys. Rev. **C 83** (2011) 044605.

[11] A. Carbone and A. Polis, Phys. Rev. **C 83** (2011) 024308.

[12] S. Ayik, O. Yilmaz, F. Acar, B. Danisman, N. Er and A. Gokalp, Nucl. Phys. **A 859** (2011) 73.

[13] Fatma Acar, "Spinodal Instabilities in Symmetric Nuclear Matter Within a Nonlinear Relativistic Approach", MsC Thesis, METU, 2011.

[14] H. Hofmann, "The Physics of Warm Nuclei", Oxford University Press, 2008

[15] V. Baran et al., Phys. Rep. **410** (2005).

[16] S. Ayik, N. Er, O. Yilmaz and A. Gokalp, Nucl. Phys. **A812** (2008) 44.

[17] K. Washiyama, S. Ayik and D. Lacroix, Phys. Rev. **C 80** (2009) 031602(R).

[18] S. Ayik, K. Washiyama and D. Lacroix, Phys. Rev. **C 79** (2009) 054606.

[19] Betul Danisman, "Spinodal Instabilities in Symmetric Nuclear Matter Within a Density Dependent Relativistic Mean-Field Approach", MsC Thesis, METU, 2011.

[20] Nuray Er, "Nuclear Spinodal Instabilities in Stochastic Mean-Field Approaches", PhD Thesis, METU, 2009.

[21] O. Yilmaz, S. Ayik, F. Acar, S. Saatci, A. Gokalp, Eur. Phys. **J A 49** (2013) 33.

[22] G. A. Lalazissis, J. Konig and P. Ring, Phys. Rev. **C 55** (1997) 540.

[23] B. K. Sharma, S. Pal, Phys. Rev. **C 81** (2010) 064304.

[24] G. Huo, L. Bo, M. Di Toro, Phys. Rev. **C 62** (2000) 035203.

[25] M. Colonna, Ph. Chomaz, **C 49** (1994) 4.

[26] B. Borderie, et al., Nucl. Phys. **A 734** (2004) 503.

[27] G. Sauer, H. Chandra, and U. Mosel, Nucl. Phys. **A 264** (1976) 221.

[28] G. Chaudhuri, S. Das Gupta, Phys. Rev. **C 80** (2009) 044609

[29] G. H. Zhang, W. Z. Jiang, Phys. Lett. **B 720** (2013) 148

[30] W. L. Qian, R. K. Su, P. Wang, Phys. Rev. **B 491** (2000) 90

[31] S. Ayik, Phys. Lett. **B 658** (2008) 174.

[32] S. Ayik, O. Yilmaz, N. Er, A. Gokalp, and P. Ring, Phys. Rev. **C 80** (2009) 034613.

[33] C. M. Ko, Qi Li, R. Wang, Phys. Rev. Lett. **59** (1987) 1084.

[34] A. Lopez, Revista Mexicana de Fisica **38** (1992) 95.

APPENDIX A

LINHARD FUNCTIONS IN THE SPINODAL REGION

In the spinodal region, the poles of the susceptibility is given as $\omega \to i\Gamma$ and $\omega \to -i\Gamma$ which correspond to the imaginary growing and decaying modes. Therefore, the components of the coefficient matrix in Eq. (3.61) can be determined for the spinodal region in terms of the imaginary poles.

The six equations presented in Eqs. (3.48, 3.49, 3.52, 3.53, 3.54) and (3.55) can be written in terms of the Linhard functions as

$$\begin{aligned} iS_B^n(\vec{k},\omega) &= \delta\rho_{B,p}(\vec{k},\omega)\left\{(G_\omega^2 - G_\rho^2)\chi_B^n(\vec{k},\omega)\right\} + \delta\rho_{B,n}(\vec{k},\omega)\left\{1 + (G_\omega^2 + G_\rho^2)\chi_B^n(\vec{k},\omega)\right\} \\ &+ \delta\rho_{s,p}(\vec{k},\omega)\left\{-G_\sigma^2\chi_s^n(\vec{k},\omega)\right\} + \delta\rho_{s,n}(\vec{k},\omega)\left\{-G_\sigma^2\chi_s^n(\vec{k},\omega)\right\} \\ &+ \delta\rho_{\mathrm{v},p}(\vec{k},\omega)\left\{-(G_\omega^2 - G_\rho^2)\chi_\mathrm{v}^n(\vec{k},\omega)\right\} + \delta\rho_{\mathrm{v},n}(\vec{k},\omega)\left\{-(G_\omega^2 + G_\rho^2)\chi_\mathrm{v}^n(\vec{k},\omega)\right\} \ , \end{aligned} \tag{A.1}$$

$$\begin{aligned} iS_B^p(\vec{k},\omega) &= \delta\rho_{B,p}(\vec{k},\omega)\left\{1 + (G_\omega^2 + G_\rho^2 + G_\gamma^2)\chi_B^p(\vec{k},\omega)\right\} + \delta\rho_{B,n}(\vec{k},\omega)\left\{(G_\omega^2 - G_\rho^2)\chi_B^p(\vec{k},\omega)\right\} \\ &+ \delta\rho_{s,p}(\vec{k},\omega)\left\{-G_\sigma^2\chi_s^p(\vec{k},\omega)\right\} + \delta\rho_{s,n}(\vec{k},\omega)\left\{-G_\sigma^2\chi_s^p(\vec{k},\omega)\right\} \\ &+ \delta\rho_{\mathrm{v},p}(\vec{k},\omega)\left\{-(G_\omega^2 + G_\rho^2 + G_\gamma^2)\chi_\mathrm{v}^p(\vec{k},\omega)\right\} + \delta\rho_{\mathrm{v},n}(\vec{k},\omega)\left\{-(G_\omega^2 - G_\rho^2)\chi_\mathrm{v}^p(\vec{k},\omega)\right\} \ , \end{aligned} \tag{A.2}$$

$$\begin{aligned} iS_s^n(\vec{k},\omega) &= \delta\rho_{B,p}(\vec{k},\omega)\left\{(G_\omega^2 - G_\rho^2)\chi_s^n(\vec{k},\omega)\right\} + \delta\rho_{B,n}(\vec{k},\omega)\left\{(G_\omega^2 + G_\rho^2)\chi_s^n(\vec{k},\omega)\right\} \\ &+ \delta\rho_{s,p}(\vec{k},\omega)\left\{G_\sigma^2\tilde{\chi}_s^n(\vec{k},\omega)\right\} + \delta\rho_{s,n}(\vec{k},\omega)\left\{1 + G_\sigma^2\tilde{\chi}_s^n(\vec{k},\omega)\right\} \\ &+ \delta\rho_{\mathrm{v},p}(\vec{k},\omega)\left\{-(G_\omega^2 - G_\rho^2)\tilde{\chi}_\mathrm{v}^n(\vec{k},\omega)\right\} + \delta\rho_{\mathrm{v},n}(\vec{k},\omega)\left\{-(G_\omega^2 + G_\rho^2)\tilde{\chi}_\mathrm{v}^n(\vec{k},\omega)\right\} \ , \end{aligned} \tag{A.3}$$

$$
\begin{aligned}
iS_s^p(\vec{k},\omega) &= \delta\rho_{B,p}(\vec{k},\omega)\left\{(G_\omega^2+G_\rho^2+G_\gamma^2)\chi_s^p(\vec{k},\omega)\right\}+\delta\rho_{B,n}(\vec{k},\omega)\left\{(G_\omega^2-G_\rho^2)\chi_s^p(\vec{k},\omega)\right\} \\
&+ \delta\rho_{s,p}(\vec{k},\omega)\left\{1+G_\sigma^2\tilde{\chi}_s^p(\vec{k},\omega)\right\}+\delta\rho_{s,n}(\vec{k},\omega)\left\{G_\sigma^2\tilde{\chi}_s^p(\vec{k},\omega)\right\} \\
&+ \delta\rho_{\mathrm{v},p}(\vec{k},\omega)\left\{-(G_\omega^2+G_\rho^2+G_\gamma^2)\tilde{\chi}_\mathrm{v}^p(\vec{k},\omega)\right\}+\delta\rho_{\mathrm{v},n}(\vec{k},\omega)\left\{-(G_\omega^2-G_\rho^2)\tilde{\chi}_\mathrm{v}^p(\vec{k},\omega)\right\}\ ,
\end{aligned}
\tag{A.4}
$$

$$
\begin{aligned}
iS_\nu^p(\vec{k},\omega) &= \delta\rho_{B,p}(\vec{k},\omega)\left\{(G_\omega^2+G_\rho^2+G_\gamma^2)\chi_\nu^p(\vec{k},\omega)\right\}+\delta\rho_{B,n}(\vec{k},\omega)\left\{(G_\omega^2-G_\rho^2)\chi_\nu^p(\vec{k},\omega)\right\} \\
&+ \delta\rho_{s,p}(\vec{k},\omega)\left\{-G_\sigma^2\tilde{\chi}_\mathrm{v}^p(\vec{k},\omega)\right\}+\delta\rho_{s,n}(\vec{k},\omega)\left\{-G_\sigma^2\tilde{\chi}_\mathrm{v}^p(\vec{k},\omega)\right\} \\
&+ \delta\rho_{\mathrm{v},p}(\vec{k},\omega)\left\{1+(G_\omega^2+G_\rho^2+G_\gamma^2)\tilde{\chi}_B^p(\vec{k},\omega)\right\}+\delta\rho_{\mathrm{v},n}(\vec{k},\omega)\left\{(G_\omega^2-G_\rho^2)\tilde{\chi}_B^p(\vec{k},\omega)\right\}
\end{aligned}
\tag{A.5}
$$

and

$$
\begin{aligned}
iS_\nu^n(\vec{k},\omega) &= \delta\rho_{B,p}(\vec{k},\omega)\left\{(G_\omega^2-G_\rho^2)\chi_\mathrm{v}^n(\vec{k},\omega)\right\}+\delta\rho_{B,n}(\vec{k},\omega)\left\{(G_\omega^2+G_\rho^2)\chi_\mathrm{v}^n(\vec{k},\omega)\right\} \\
&+ \delta\rho_{s,p}(\vec{k},\omega)\left\{-G_\sigma^2\tilde{\chi}_\nu^n(\vec{k},\omega)\right\}+\delta\rho_{s,n}(\vec{k},\omega)\left\{-G_\sigma^2\tilde{\chi}_\nu^n(\vec{k},\omega)\right\} \\
&+ \delta\rho_{\mathrm{v},p}(\vec{k},\omega)\left\{(G_\omega^2-G_\rho^2)\tilde{\chi}_B^n(\vec{k},\omega)\right\}+\delta\rho_{\mathrm{v},n}(\vec{k},\omega)\left\{1+(G_\omega^2+G_\rho^2)\tilde{\chi}_B^n(\vec{k},\omega)\right\}\ .
\end{aligned}
\tag{A.6}
$$

Previously, the Linhard functions are given as

$$
\begin{pmatrix} \chi_\mathrm{v}(\vec{k},\omega) \\ \chi_\mathrm{s}(\vec{k},\omega) \\ \chi_B(\vec{k},\omega) \end{pmatrix} = \gamma\int\frac{d^3p}{(2\pi\hbar)^3}\begin{pmatrix} c\vec{p}\cdot\hat{k}/\varepsilon_0^* \\ M_0^*c^2/\varepsilon_0^* \\ 1 \end{pmatrix}\frac{\vec{k}\cdot\vec{\nabla}_p f_0(\vec{p})}{\omega-\vec{\mathrm{v}}_0\cdot\vec{k}}
\tag{A.7}
$$

and

$$
\tilde{\chi}_\mathrm{s}(\vec{k},\omega)=\gamma\int\frac{d^3p}{(2\pi\hbar)^3}\left[\frac{(cp)^2}{\varepsilon_0^{*3}}f_0(\vec{p})-\left(\frac{M_0^*c^2}{\varepsilon_0^*}\right)^2\frac{\vec{k}\cdot\vec{\nabla}_p f_0(\vec{p})}{\omega-\vec{\mathrm{v}}_0\cdot\vec{k}}\right]\ ,
\tag{A.8}
$$

$$
\tilde{\chi}_\mathrm{v}(\vec{k},\omega)=\gamma\int\frac{d^3p}{(2\pi\hbar)^3}c\vec{p}\cdot\hat{k}\left[\frac{M_0^*c^2}{\varepsilon_0^{*2}}\frac{\vec{k}\cdot\vec{\nabla}_p f_0(\vec{p})}{\omega-\vec{\mathrm{v}}_0\cdot\vec{k}}\right]\ ,
\tag{A.9}
$$

$$
\tilde{\chi}_B(\vec{k},\omega)=\gamma\int\frac{d^3p}{(2\pi\hbar)^3}\left[\frac{\varepsilon_0^{*2}-(c\vec{p}\cdot\hat{k})^2}{\varepsilon_0^{*3}}f_0(\vec{p})-\frac{(c\vec{p}\cdot\hat{k})^2}{\varepsilon_0^{*2}}\frac{\vec{k}\cdot\vec{\nabla}_p f_0(\vec{p})}{\omega-\vec{\mathrm{v}}_0\cdot\vec{k}}\right]\ .
\tag{A.10}
$$

Therefore with the use of the relations $\vec{\nabla}_p \cdot \vec{k} = \frac{cp}{\varepsilon_0^*} kc \cos\theta \frac{\partial f_0}{\partial \varepsilon_0^*}$ and $\vec{v}_0 \cdot \vec{k} = c\frac{cp}{\varepsilon_0^*} k \cos\theta$ in the spinodal region where $\omega \to i\Gamma$, the first Linhard function in Eq. (A.7) can be found to be

$$\chi_{\rm v}^q(\vec{k},\omega) = \gamma \int \frac{d^3p}{(2\pi\hbar)^3} \left(\frac{cp\cos\theta}{\varepsilon_0^*}\right) \frac{\frac{cp}{\varepsilon_0^*} kc\cos\theta \frac{\partial f_0^q(\vec{p})}{\partial \varepsilon_0^*}}{\omega - c\frac{cp}{\varepsilon_0^*} k\cos\theta} \ . \tag{A.11}$$

We can introduce the short-hand notations $\cos\theta = x$, $cp = p^{'}$ and $kc\left(\frac{p^{'}}{\varepsilon_0^*}\right) = \alpha$, then the equation becomes

$$\begin{aligned} &= \gamma \frac{2\pi kc}{(2\pi\hbar c)^3} \int p^{'2} dp^{'} \left(\frac{p^{'}}{\varepsilon_0^*}\right)^2 \frac{\partial f_0^q(\vec{p})}{\partial \varepsilon_0^*} \int_{-1}^{1} dx \frac{x^2}{\omega - kc\frac{p^{'}}{\varepsilon_0^*} x} \\ &= \gamma \frac{2\pi kc}{(2\pi\hbar c)^3} \int p^{'2} dp^{'} \left(\frac{p^{'}}{\varepsilon_0^*}\right)^2 \frac{\partial f_0^q(\vec{p})}{\partial \varepsilon_0^*} \int_{-1}^{1} dx \frac{x^2}{\omega - \alpha x} \\ &= \gamma \frac{2\pi kc}{(2\pi\hbar c)^3} \int p^{'2} dp^{'} \left(\frac{p^{'}}{\varepsilon_0^*}\right)^2 \frac{\partial f_0^q(\vec{p})}{\partial \varepsilon_0^*} \int_{-1}^{1} dx \frac{x^2(-i\Gamma - \alpha x)}{\Gamma^2 + (\alpha x)^2} \ . \end{aligned} \tag{A.12}$$

Here, the integrals $\int_{-1}^{1} dx \frac{x}{\pi^2 + (\alpha x)^2} = 0$ and $\int_{-1}^{1} dx \frac{x^3}{\pi^2 + (\alpha x)^2} = 0$ can be used, then

$$\chi_{\rm v}^q(\vec{k},\omega) = \gamma \frac{2\pi kc}{(2\pi\hbar c)^3} \int p^{'2} dp^{'} \left(\frac{p^{'}}{\varepsilon_0^*}\right)^2 \frac{\partial f_0^q(\vec{p})}{\partial \varepsilon_0^*} \int_{-1}^{1} dx \frac{x^2(-i\Gamma)}{\Gamma^2 + (\alpha x)^2} \ . \tag{A.13}$$

By using the same notations, the other Linhard functions in the spinodal region where $\omega \to i\Gamma$, can be written as follows;

$$\begin{aligned} \chi_S^q(\vec{k},\omega) &= \gamma \int \frac{d^3p}{(2\pi\hbar)^3} \left(\frac{M_0^* c^2}{\varepsilon_0^*}\right) \frac{cp}{\varepsilon_0^*} kc \frac{\partial f_0^q(\vec{p})}{\partial \varepsilon_0^*} \frac{\cos\theta}{\omega - c\frac{cp}{\varepsilon_0^*} k\cos\theta} \\ &= \gamma \frac{2\pi kc}{(2\pi\hbar c)^3} \int p^{'2} dp^{'} \left(\frac{M_0^* c^2}{\varepsilon_0^*}\right) \left(\frac{p^{'}}{\varepsilon_0^*}\right) \frac{\partial f_0^q(\vec{p})}{\partial \varepsilon_0^*} \int_{-1}^{1} dx \frac{x(-\alpha x)}{\Gamma^2 + (\alpha x)^2} \ , \end{aligned} \tag{A.14}$$

$$\begin{aligned} \chi_B^q(\vec{k},\omega) &= \gamma \int \frac{d^3p}{(2\pi\hbar)^3} \left(\frac{cp}{\varepsilon_0^*}\right) kc \frac{\partial f_0^q(\vec{p})}{\partial \varepsilon_0^*} \frac{\cos\theta}{\omega - c\frac{cp}{\varepsilon_0^*} k\cos\theta} \\ &= \gamma \frac{2\pi kc}{(2\pi\hbar c)^3} \int p^{'2} dp^{'} \left(\frac{p^{'}}{\varepsilon_0^*}\right) \frac{\partial f_0^q(\vec{p})}{\partial \varepsilon_0^*} \int_{-1}^{1} dx \frac{x(-\alpha x)}{\Gamma^2 + (\alpha x)^2} \ , \end{aligned} \tag{A.15}$$

$$
\begin{aligned}
\tilde{\chi}_{\mathrm{v}}^{q}(\vec{k},\omega) &= \gamma \int \frac{d^3p}{(2\pi\hbar)^3} \left(\frac{M_0^* c^2}{\varepsilon_0^*}\right) \left(\frac{cp\cos\theta}{\varepsilon_0^*}\right) \frac{\frac{cp}{\varepsilon_0^*} kc\cos\theta \frac{\partial f_0^q(\vec{p})}{\partial \varepsilon_0^*}}{\omega - c\frac{cp}{\varepsilon_0^*} k\cos\theta} \\
&= \gamma \frac{2\pi kc}{(2\pi\hbar c)^3} \int p'^2 dp' \left(\frac{M_0^* c^2}{\varepsilon_0^*}\right) \left(\frac{p'}{\varepsilon_0^*}\right)^2 \frac{\partial f_0^q(\vec{p})}{\partial \varepsilon_0^*} \int_{-1}^{1} dx \frac{x^2(-i\Gamma)}{\Gamma^2 + (\alpha x)^2} \,,
\end{aligned}
\tag{A.16}
$$

$$
\begin{aligned}
\tilde{\chi}_{S}^{q}(\vec{k},\omega) &= \gamma \int \frac{d^3p}{(2\pi\hbar)^3} \left(\frac{1}{\varepsilon_0^*}\left(\frac{cp}{\varepsilon_0^*}\right)^2 f_0 - \left(\frac{M_0^* c^2}{\varepsilon_0^*}\right)^2 \frac{cp}{\varepsilon_0^*} kc \frac{\partial f_0^q(\vec{p})}{\partial \varepsilon_0^*} \frac{\cos\theta}{\omega - c\frac{cp}{\varepsilon_0^*} k\cos\theta}\right) \\
&= \gamma \frac{2\pi}{(2\pi\hbar c)^3} \int p'^2 dp' \left[\frac{1}{\varepsilon_0^*}\left(\frac{p'}{\varepsilon_0^*}\right)^2 f_0 \int_{-1}^{1} dx - kc\left(\frac{M_0^* c^2}{\varepsilon_0^*}\right)^2 \left(\frac{p'}{\varepsilon_0^*}\right) \frac{\partial f_0^q(\vec{p})}{\partial \varepsilon_0^*} \int_{-1}^{1} dx \frac{x}{\omega - \alpha x}\right] \\
&= \gamma \frac{2\pi}{(2\pi\hbar c)^3} \int p'^2 dp' \left[\frac{1}{\varepsilon_0^*}\left(\frac{p'}{\varepsilon_0^*}\right)^2 f_0 2 - kc\left(\frac{M_0^* c^2}{\varepsilon_0^*}\right)^2 \left(\frac{p'}{\varepsilon_0^*}\right) \frac{\partial f_0^q(\vec{p})}{\partial \varepsilon_0^*} \int_{-1}^{1} dx \frac{x(-\alpha x)}{\Gamma^2 + (\alpha x)^2}\right]
\end{aligned}
\tag{A.17}
$$

and

$$
\begin{aligned}
\tilde{\chi}_{B}^{q}(\vec{k},\omega) &= \gamma \int \frac{d^3p}{(2\pi\hbar)^3} \left[\frac{1}{\varepsilon_0^*} f_0 - \left(\frac{cp\cos\theta}{\varepsilon_0^*}\right)^2 f_0 - \left(\frac{cp\cos\theta}{\varepsilon_0^*}\right)^2 \frac{cp}{\varepsilon_0^*} kc \frac{\partial f_0^q(\vec{p})}{\partial \varepsilon_0^*} \frac{\cos\theta}{\omega - c\frac{cp}{\varepsilon_0^*} k\cos\theta}\right] \\
&= \gamma \frac{2\pi}{(2\pi\hbar c)^3} \int p'^2 dp' \left[\frac{1}{\varepsilon_0^*} f_0 \int_{-1}^{1} dx - \left(\frac{p'}{\varepsilon_0^*}\right)^2 f_0 \int_{-1}^{1} x^2 dx - \left(\frac{p'}{\varepsilon_0^*}\right)^3 kc \frac{\partial f_0^q(\vec{p})}{\partial \varepsilon_0^*} \int_{-1}^{1} dx \frac{x^3}{\omega - \alpha x}\right] \\
&= \gamma \frac{2\pi}{(2\pi\hbar c)^3} \int p'^2 dp' \left[\frac{1}{\varepsilon_0^*} f_0 \int_{-1}^{1} dx - \left(\frac{p'}{\varepsilon_0^*}\right)^2 f_0 \frac{2}{3} - \left(\frac{p'}{\varepsilon_0^*}\right)^3 kc \frac{\partial f_0^q(\vec{p})}{\partial \varepsilon_0^*} \int_{-1}^{1} dx \frac{-\alpha x^4}{\Gamma^2 + (\alpha x)^2}\right] .
\end{aligned}
\tag{A.18}
$$

Therefore, the elements of the coefficient matrix can be written in terms of the Linhard functions according to Eq. (3.62).

APPENDIX B

DERIVATIVE OF THE SUSCEPTIBILITY

In order to obtain the derivative of the susceptibility $\partial\varepsilon/\partial\omega$, the elements of the coefficient matrix should be derivated with respect to ω, one by one.

The susceptibility is given as

$$\varepsilon(\vec{k},\omega) = \begin{vmatrix} A_1^p & A_2^p & A_3^p & A_1^n & A_2^n & A_3^n \\ B_1^p & B_2^p & B_3^p & B_1^n & B_2^n & B_3^n \\ C_1^p & C_2^p & C_3^p & C_1^n & C_2^n & C_3^n \\ D_1^p & D_2^p & D_3^p & D_1^n & D_2^n & D_3^n \\ E_1^p & E_2^p & E_3^p & E_1^n & E_2^n & E_3^n \\ F_1^p & F_2^p & F_3^p & F_1^n & F_2^n & F_3^n \end{vmatrix} \tag{B.1}$$

and the derivation of the first element A_1^p yields,

$$\begin{aligned} \frac{\partial A_{11}}{\partial\omega} &= (G_\omega^2 - G_\rho^2)\frac{\partial\chi_B^n}{\partial\omega} = (G_\omega^2 - G_\rho^2)\gamma\int\frac{d^3p}{(2pi)^3}\frac{\partial}{\partial\omega}\left(\frac{\vec{k}\cdot\vec{\nabla}_p f_n^0(p)}{\omega - \vec{v_0}\cdot\vec{k}}\right) \\ &= (G_\omega^2 - G_\rho^2)\gamma\int\frac{d^3p}{(2pi)^3}\vec{k}\cdot\vec{\nabla}_p f_n^0(p)\left(-\frac{\omega}{(\omega - \vec{v_0}\cdot\vec{k})^2}\right) \\ &= -\gamma(G_\omega^2 - G_\rho^2)\int\frac{d^3p}{(2pi)^3}\frac{pk\cos\theta}{\varepsilon_0^*}\frac{\partial f_n^0}{\partial\varepsilon_0^*}\frac{\omega}{\left(\omega - \frac{pk\cos\theta}{\varepsilon_0^*}\right)^2} \ . \end{aligned} \tag{B.2}$$

For the other terms in the first row we obtain,

$$\begin{pmatrix} \frac{\partial A_{12}}{\partial\omega} \\ \frac{\partial A_{13}}{\partial\omega} \\ \frac{\partial A_{14}}{\partial\omega} \\ \frac{\partial A_{15}}{\partial\omega} \\ \frac{\partial A_{16}}{\partial\omega} \end{pmatrix} = \gamma\begin{pmatrix} -(G_\omega^2 + G_\rho^2) \\ G_\sigma^2 \\ G_\sigma^2 \\ (G_\omega^2 - G_\rho^2) \\ (G_\omega^2 + G_\rho^2) \end{pmatrix}\int\frac{d^3p}{(2pi)^3}\frac{pk\cos\theta}{\varepsilon_0^*}\frac{\partial f_n^0}{\partial\varepsilon_0^*}\frac{\omega}{\left(\omega - \frac{pk\cos\theta}{\varepsilon_0^*}\right)^2} \ . \tag{B.3}$$

Likewise, taking the derivatives of the elements in the second row yields,

$$\begin{pmatrix} \frac{\partial A_{21}}{\partial \omega} \\ \frac{\partial A_{22}}{\partial \omega} \\ \frac{\partial A_{23}}{\partial \omega} \\ \frac{\partial A_{24}}{\partial \omega} \\ \frac{\partial A_{25}}{\partial \omega} \\ \frac{\partial A_{26}}{\partial \omega} \end{pmatrix} = \gamma \begin{pmatrix} -(G_\omega^2 + G_\rho^2 + G_\gamma^2) \\ -(G_\omega^2 - G_\rho^2) \\ G_\sigma^2 \\ G_\sigma^2 \\ -(G_\omega^2 + G_\rho^2 + G_\gamma^2) \\ (G_\omega^2 - G_\rho^2) \end{pmatrix} \int \frac{d^3p}{(2pi)^3} \frac{pk\cos\theta}{\varepsilon_0^*} \frac{\partial f_n^0}{\partial \varepsilon_0^*} \frac{\omega}{\left(\omega - \frac{pk\cos\theta}{\varepsilon_0^*}\right)^2} . \tag{B.4}$$

The rest of the matrix elements can be derivated in a similar manner with the results,

$$\begin{pmatrix} \frac{\partial A_{31}}{\partial \omega} \\ \frac{\partial A_{32}}{\partial \omega} \\ \frac{\partial A_{33}}{\partial \omega} \\ \frac{\partial A_{34}}{\partial \omega} \\ \frac{\partial A_{35}}{\partial \omega} \\ \frac{\partial A_{36}}{\partial \omega} \end{pmatrix} = \gamma \begin{pmatrix} -(G_\omega^2 - G_\rho^2) \\ -(G_\omega^2 + G_\rho^2) \\ G_\sigma^2 \\ G_\sigma^2 \\ (G_\omega^2 - G_\rho^2) \\ (G_\omega^2 + G_\rho^2) \end{pmatrix} \int \frac{d^3p}{(2pi)^3} \frac{pk\cos\theta}{\varepsilon_0^*} \frac{\partial f_n^0}{\partial \varepsilon_0^*} \frac{\omega}{\left(\omega - \frac{pk\cos\theta}{\varepsilon_0^*}\right)^2} , \tag{B.5}$$

$$\begin{pmatrix} \frac{\partial A_{41}}{\partial \omega} \\ \frac{\partial A_{42}}{\partial \omega} \\ \frac{\partial A_{43}}{\partial \omega} \\ \frac{\partial A_{44}}{\partial \omega} \\ \frac{\partial A_{45}}{\partial \omega} \\ \frac{\partial A_{46}}{\partial \omega} \end{pmatrix} = \gamma \begin{pmatrix} -(G_\omega^2 + G_\rho^2 + G_\gamma^2) \\ -(G_\omega^2 - G_\rho^2) \\ G_\sigma^2 \\ G_\sigma^2 \\ (G_\omega^2 + G_\rho^2 + G_\gamma^2) \\ (G_\omega^2 - G_\rho^2) \end{pmatrix} \int \frac{d^3p}{(2pi)^3} \frac{pk\cos\theta}{\varepsilon_0^*} \frac{\partial f_n^0}{\partial \varepsilon_0^*} \frac{\omega}{\left(\omega - \frac{pk\cos\theta}{\varepsilon_0^*}\right)^2} , \tag{B.6}$$

$$\begin{pmatrix} \frac{\partial A_{51}}{\partial \omega} \\ \frac{\partial A_{52}}{\partial \omega} \\ \frac{\partial A_{53}}{\partial \omega} \\ \frac{\partial A_{54}}{\partial \omega} \\ \frac{\partial A_{55}}{\partial \omega} \\ \frac{\partial A_{56}}{\partial \omega} \end{pmatrix} = \gamma \begin{pmatrix} -(G_\omega^2 - G_\rho^2) \\ -(G_\omega^2 + G_\rho^2) \\ G_\sigma^2 \\ G_\sigma^2 \\ (G_\omega^2 - G_\rho^2) \\ (G_\omega^2 + G_\rho^2) \end{pmatrix} \int \frac{d^3p}{(2pi)^3} \frac{pk\cos\theta}{\varepsilon_0^*} \frac{\partial f_n^0}{\partial \varepsilon_0^*} \frac{\omega}{\left(\omega - \frac{pk\cos\theta}{\varepsilon_0^*}\right)^2} , \tag{B.7}$$

$$\begin{pmatrix} \frac{\partial A_{61}}{\partial \omega} \\ \frac{\partial A_{62}}{\partial \omega} \\ \frac{\partial A_{63}}{\partial \omega} \\ \frac{\partial A_{64}}{\partial \omega} \\ \frac{\partial A_{65}}{\partial \omega} \\ \frac{\partial A_{66}}{\partial \omega} \end{pmatrix} = \gamma \begin{pmatrix} -(G_\omega^2 + G_\rho^2 + G_\gamma^2) \\ -(G_\omega^2 - G_\rho^2) \\ G_\sigma^2 \\ G_\sigma^2 \\ (G_\omega^2 + G_\rho^2 + G_\gamma^2) \\ (G_\omega^2 - G_\rho^2) \end{pmatrix} \int \frac{d^3p}{(2pi)^3} \frac{pk\cos\theta}{\varepsilon_0^*} \frac{\partial f_n^0}{\partial \varepsilon_0^*} \frac{\omega}{\left(\omega - \frac{pk\cos\theta}{\varepsilon_0^*}\right)^2} \,. \tag{B.8}$$

APPENDIX C

BARYON DENSITY CORRELATION FUNCTIONS

The spectral intensity of the baryon density correlation function is given as $\tilde{\sigma}(\vec{k},t) = \tilde{\sigma}_{pp}(\vec{k},t) + \tilde{\sigma}_{np}(\vec{k},t) + \tilde{\sigma}_{pn}(\vec{k},t) + \tilde{\sigma}_{nn}(\vec{k},t)$. We can write the elements of this expression in terms of the growing and decaying poles as

$$\begin{aligned}\tilde{\sigma}^{BB}_{ab}(\vec{k},t)(2\pi)^3\delta^3(\vec{k}-\vec{k}') &= \overline{\delta\rho^{B+}_a(\vec{k})(\delta\rho^{B+}_b(\vec{k}))^*}e^{2\Gamma_k t} + \overline{\delta\rho^{B-}_a(\vec{k})(\delta\rho^{B-}_b(\vec{k}))^*}e^{-2\Gamma_k t} \\ &+\overline{\delta\rho^{B+}_a(\vec{k})(\delta\rho^{B-}_b(\vec{k}))^*} + \overline{\delta\rho^{B-}_a(\vec{k})(\delta\rho^{B+}_b(\vec{k}))^*} \qquad \text{(C.1)}\end{aligned}$$

where a and b stands for the neutron of the proton. The growing and decaying unstable modes are defined for neutron and proton respectively as follows,

$$\delta\rho^{p\mp}_B(\vec{k}) = -\hbar\frac{\left[N^p_1\tilde{S}^p_B - N^p_2\tilde{S}^p_s + N^p_3\tilde{S}^p_V - N^p_4\tilde{S}^n_B + N^p_5\tilde{S}^n_s - N^p_6\tilde{S}^n_V\right]}{\partial\varepsilon(\vec{k},\omega)/\partial\omega}\Big|_{\omega=\mp i\Gamma_k} \qquad \text{(C.2)}$$

$$\delta\rho^{n\mp}_B(\vec{k}) = -\hbar\frac{\left[-N^n_1\tilde{S}^p_B + N^n_2\tilde{S}^p_s - N^n_3\tilde{S}^p_V + N^n_4\tilde{S}^n_B - N^n_5\tilde{S}^n_s + N^n_6\tilde{S}^n_V\right]}{\partial\varepsilon(\vec{k},\omega)/\partial\omega}\Big|_{\omega=\mp i\Gamma_k} . \qquad \text{(C.3)}$$

The elements of Eq. (C.1) should be calculated seperately. First, let us evaluate the term $\tilde{\sigma}^{BB}_{pp}(\vec{k},t)$ for $a = b = p$. If we employ Eqs. (C.2) and (C.3) we get

$$\begin{aligned}\tilde{\sigma}^{BB}_{pp}(\vec{k},t)(2\pi)^3\delta^3(\vec{k}-\vec{k}') &= \overline{\delta\rho^{B+}_p(\vec{k})(\delta\rho^{B+}_p(\vec{k}))^*}e^{2\Gamma_k t} + \overline{\delta\rho^{B-}_p(\vec{k})(\delta\rho^{B-}_p(\vec{k}))^*}e^{-2\Gamma_k t} \\ &+\overline{\delta\rho^{B+}_p(\vec{k})(\delta\rho^{B-}_p(\vec{k}))^*} + \overline{\delta\rho^{B-}_p(\vec{k})(\delta\rho^{B+}_p(\vec{k}))^*} \qquad \text{(C.4)}\end{aligned}$$

in terms of the growing and decaying poles.

Here, the correlations of the growing and decaying unstable modes can be written in terms of

the source terms as

$$
\begin{aligned}
& \left[\overline{(\delta\rho_p^B(\vec{k}))^{\pm}}\right]\left[\overline{(\delta\rho_p^B(\vec{k}'))^{\pm}}\right]^* \frac{d_\varepsilon^{\pm} d_\varepsilon^{\pm *}}{\hbar^2} \\
= \; & \overline{\tilde{S}_p^{B\pm}(\vec{k},\omega)\tilde{S}_p^{B\pm}(\vec{k}',\omega)^*}|N_{1p}^{\pm}|^2 - \overline{\tilde{S}_p^{B\pm}(\vec{k},\omega)\tilde{S}_p^{S\pm}(\vec{k}',\omega)^*}N_{1p}^{\pm}N_{2p}^{\pm *} + \overline{\tilde{S}_p^{B\pm}(\vec{k},\omega)\tilde{S}_p^{V\pm}(\vec{k}',\omega)^*}N_{1p}^{\pm}N_{3p}^{\pm *} \\
- \; & \overline{\tilde{S}_p^{S\pm}(\vec{k},\omega)\tilde{S}_p^{B\pm}(\vec{k}',\omega)^*}N_{2p}^{\pm}N_{1p}^{\pm *} + \overline{\tilde{S}_p^{S\pm}(\vec{k},\omega)\tilde{S}_p^{S\pm}(\vec{k}',\omega)^*}|N_{2p}^{\pm}|^2 - \overline{\tilde{S}_p^{S\pm}(\vec{k},\omega)\tilde{S}_p^{V\pm}(\vec{k}',\omega)^*}N_{2p}^{\pm}N_{3p}^{\pm *} \\
+ \; & \overline{\tilde{S}_p^{B\pm}(\vec{k},\omega)\tilde{S}_p^{B\pm}(\vec{k}',\omega)^*}N_{3p}^{\pm}N_{1p}^{\pm *} - \overline{\tilde{S}_p^{V\pm}(\vec{k},\omega)\tilde{S}_p^{S\pm}(\vec{k}',\omega)^*}N_{3p}^{\pm}N_{2p}^{\pm *} + \overline{\tilde{S}_p^{V\pm}(\vec{k},\omega)\tilde{S}_p^{V\pm}(\vec{k}',\omega)^*}|N_3^{\pm}|^2 \\
+ \; & \overline{\tilde{S}_n^{B\pm}(\vec{k},\omega)\tilde{S}_n^{B\pm}(\vec{k}',\omega)^*}|N_{4p}^{\pm}|^2 - \overline{\tilde{S}_n^{B\pm}(\vec{k},\omega)\tilde{S}_n^{S\pm}(\vec{k}',\omega)^*}N_{4p}^{\pm}N_{5p}^{\pm *} + \overline{\tilde{S}_n^{B\pm}(\vec{k},\omega)\tilde{S}_n^{V\pm}(\vec{k}',\omega)^*}N_{4p}^{\pm}N_{6p}^{\pm *} \\
- \; & \overline{\tilde{S}_n^{S\pm}(\vec{k},\omega)\tilde{S}_n^{B\pm}(\vec{k}',\omega)^*}N_{5p}^{\pm}N_{4p}^{\pm *} + \overline{\tilde{S}_n^{S\pm}(\vec{k},\omega)\tilde{S}_n^{S\pm}(\vec{k}',\omega)^*}|N_{5p}^{\pm}|^2 - \overline{\tilde{S}_n^{S\pm}(\vec{k},\omega)\tilde{S}_n^{V\pm}(\vec{k}',\omega)^*}N_{5p}^{\pm}N_{6p}^{\pm *} \\
+ \; & \overline{\tilde{S}_n^{B\pm}(\vec{k},\omega)\tilde{S}_n^{B\pm}(\vec{k}',\omega)^*}N_{6p}^{\pm}N_{4p}^{\pm *} - \overline{\tilde{S}_n^{V\pm}(\vec{k},\omega)\tilde{S}_n^{S\pm}(\vec{k}',\omega)^*}N_{6p}^{\pm}N_{5p}^{\pm *} + \overline{\tilde{S}_n^{V\pm}(\vec{k},\omega)\tilde{S}_n^{V\pm}(\vec{k}',\omega)^*}|N_{6p}^{\pm}|^2
\end{aligned}
\tag{C.5}
$$

with using the short-hand notations $d_\epsilon^+ = \frac{\partial\varepsilon(\vec{k},\omega)}{\partial\omega}|_{\omega=i\Gamma}$ and $d_\epsilon^- = \frac{\partial\varepsilon(\vec{k},\omega)}{\partial\omega}|_{\omega=-i\Gamma}$ for the growing and decaying modes respectively.

Similarly, for the cross terms we can find,

$$
\begin{aligned}
& \left[\overline{(\delta\rho_p^B(\vec{k}))^{\pm}}\right]\left[\overline{(\delta\rho_p^B(\vec{k}'))^{\mp}}\right]^* \frac{d_\varepsilon^{\pm} d_\varepsilon^{\mp *}}{\hbar^2} \\
= \; & \overline{\tilde{S}_p^{B\pm}(\vec{k},\omega)\tilde{S}_p^{B\mp}(\vec{k}',\omega)^*}N_{1p}^{\pm}N_{1p}^{\mp *} - \overline{\tilde{S}_p^{B\pm}(\vec{k},\omega)\tilde{S}_p^{S\mp}(\vec{k}',\omega)^*}N_{1p}^{\pm}N_{2p}^{\mp *} + \overline{\tilde{S}_p^{B\pm}(\vec{k},\omega)\tilde{S}_p^{V\mp}(\vec{k}',\omega)^*}N_{1p}^{\pm}N_{3p}^{\mp *} \\
- \; & \overline{\tilde{S}_p^{S\pm}(\vec{k},\omega)\tilde{S}_p^{B\mp}(\vec{k}',\omega)^*}N_{2p}^{\pm}N_{1p}^{\mp *} + \overline{\tilde{S}_p^{S\pm}(\vec{k},\omega)\tilde{S}_p^{S\mp}(\vec{k}',\omega)^*}N_{2p}^{\pm}N_{2p}^{\mp *} - \overline{\tilde{S}_p^{S\pm}(\vec{k},\omega)\tilde{S}_p^{V\mp}(\vec{k}',\omega)^*}N_{2p}^{\pm}N_{3p}^{\mp *} \\
+ \; & \overline{\tilde{S}_p^{B\pm}(\vec{k},\omega)\tilde{S}_p^{B\mp}(\vec{k}',\omega)^*}N_{3p}^{\pm}N_{1p}^{\mp *} - \overline{\tilde{S}_p^{V\pm}(\vec{k},\omega)\tilde{S}_p^{S\mp}(\vec{k}',\omega)^*}N_{3p}^{\pm}N_{2p}^{\mp *} + \overline{\tilde{S}_p^{V\pm}(\vec{k},\omega)\tilde{S}_p^{V\mp}(\vec{k}',\omega)^*}N_{3p}^{\pm}N_{3p}^{\mp *} \\
+ \; & \overline{\tilde{S}_n^{B\pm}(\vec{k},\omega)\tilde{S}_n^{B\mp}(\vec{k}',\omega)^*}N_{4p}^{\pm}N_{4p}^{\mp *} - \overline{\tilde{S}_n^{B\pm}(\vec{k},\omega)\tilde{S}_n^{S\mp}(\vec{k}',\omega)^*}N_{4p}^{\pm}N_{5p}^{\mp *} + \overline{\tilde{S}_n^{B\pm}(\vec{k},\omega)\tilde{S}_n^{V\mp}(\vec{k}',\omega)^*}N_{4p}^{\pm}N_{6p}^{\mp *} \\
- \; & \overline{\tilde{S}_n^{S\pm}(\vec{k},\omega)\tilde{S}_n^{B\mp}(\vec{k}',\omega)^*}N_{5p}^{\pm}N_{4p}^{\mp *} + \overline{\tilde{S}_n^{S\pm}(\vec{k},\omega)\tilde{S}_n^{S\mp}(\vec{k}',\omega)^*}N_{5p}^{\pm}N_{5p}^{\mp *} - \overline{\tilde{S}_n^{S\pm}(\vec{k},\omega)\tilde{S}_n^{V\mp}(\vec{k}',\omega)^*}N_{5p}^{\pm}N_{6p}^{\mp *} \\
+ \; & \overline{\tilde{S}_n^{B\pm}(\vec{k},\omega)\tilde{S}_n^{B\mp}(\vec{k}',\omega)^*}N_{6p}^{\pm}N_{4p}^{\mp *} - \overline{\tilde{S}_n^{V\pm}(\vec{k},\omega)\tilde{S}_n^{S\mp}(\vec{k}',\omega)^*}N_{6p}^{\pm}N_{5p}^{\mp *} + \overline{\tilde{S}_n^{V\pm}(\vec{k},\omega)\tilde{S}_n^{V\mp}(\vec{k}',\omega)^*}N_{6p}^{\pm}N_{6p}^{\mp *} \; .
\end{aligned}
\tag{C.6}
$$

Previously, the following definitions for the stochastic source terms are used,

$$
\begin{pmatrix} \tilde{S}_{\mathrm{v}}(\vec{k},\omega) \\ \tilde{S}_{\mathrm{s}}(\vec{k},\omega) \\ \tilde{S}_B(\vec{k},\omega) \end{pmatrix} = \gamma \int \frac{d^3p}{(2\pi\hbar)^3} \begin{pmatrix} c\vec{p}\cdot\vec{k}/\varepsilon_0^* \\ M_0^* c^2/\varepsilon_0^* \\ 1 \end{pmatrix} \frac{\delta\tilde{f}(\vec{k},\vec{p},0)}{\omega - \vec{\mathrm{v}}_0\cdot\vec{k}} \; . \tag{C.7}
$$

With the use of the relation

$$
\overline{\delta}\tilde{f}(\vec{k},\vec{p},0)f(\vec{k},\vec{p},0)^* = (2\pi)^3\delta^3(\vec{k}-\vec{k}')(2\pi\hbar)^3\delta^3(\vec{p}-\vec{p}')f(p)(1-f(p)) \tag{C.8}
$$

the correlations of the source terms can be obtained. The first term in the above Eq. (C.4) becomes,

$$
\begin{aligned}
& \overline{\tilde{S}_p^{B+}(\vec{k},\omega)\tilde{S}_p^{B+}(\vec{k}',\omega)^*} \\
= \; & \gamma^2 \int \frac{d^3p'}{(2\pi)^3}\frac{d^3p}{(2\pi)^3}\frac{\delta f_p(\vec{k},\vec{p},0)\delta f_p(\vec{k}',\vec{p}',0)^*}{(i\Gamma-\vec{v}_0\cdot\vec{k})(i\Gamma-\vec{v}_0\cdot\vec{k}')^*} \\
= \; & \gamma^2(2\pi\hbar)^3\delta^3(\vec{k}-\vec{k}')\int \frac{d^3p}{(2\pi)^3}\frac{f_p(p)(1-f_p(p))}{\Gamma^2+(\vec{v}_0\cdot\vec{k})^2} \\
= \; & \gamma^2(2\pi\hbar)^3\delta^3(\vec{k}-\vec{k}')\int \frac{d^3p}{(2\pi)^3}\frac{f_p(p)(1-f_p(p))}{\Gamma^2+(\alpha x)^2} \; . \qquad \text{(C.9)}
\end{aligned}
$$

Likewise, the other correlations for the source terms can be given as

$$
\begin{pmatrix}
\overline{\tilde{S}_p^{B+}(\vec{k},\omega)\tilde{S}_p^{S+}(\vec{k}',\omega)^*} \\
\overline{\tilde{S}_p^{S+}(\vec{k},\omega)\tilde{S}_p^{B+}(\vec{k}',\omega)^*} \\
\overline{\tilde{S}_p^{S+}(\vec{k},\omega)\tilde{S}_p^{S+}(\vec{k}',\omega)^*} \\
\overline{\tilde{S}_p^{V+}(\vec{k},\omega)\tilde{S}_p^{V+}(\vec{k}',\omega)^*}
\end{pmatrix}
= \gamma^2(2\pi\hbar)^3\delta^3(\vec{k}-\vec{k}')\int \frac{d^3p}{(2\pi)^3}
\begin{pmatrix}
M_0^*c^2/\varepsilon_0^* \\
M_0^*c^2/\varepsilon_0^* \\
\left(M_0^*c^2/\varepsilon_0^*\right)^2 \\
\left(c\vec{p}\cdot\vec{k}/\varepsilon_0^*\right)^2
\end{pmatrix}
\frac{f_p(p)(1-f_p(p))}{\Gamma^2+(\alpha x)^2} \; . \qquad \text{(C.10)}
$$

and

$$
\begin{pmatrix}
\overline{\tilde{S}_n^{B+}(\vec{k},\omega)\tilde{S}_n^{B+}(\vec{k}',\omega)^*} \\
\overline{\tilde{S}_n^{B+}(\vec{k},\omega)\tilde{S}_n^{S+}(\vec{k}',\omega)^*} \\
\overline{\tilde{S}_n^{S+}(\vec{k},\omega)\tilde{S}_n^{B+}(\vec{k}',\omega)^*} \\
\overline{\tilde{S}_n^{S+}(\vec{k},\omega)\tilde{S}_n^{S+}(\vec{k}',\omega)^*} \\
\overline{\tilde{S}_n^{V+}(\vec{k},\omega)\tilde{S}_n^{V+}(\vec{k}',\omega)^*}
\end{pmatrix}
= \gamma^2(2\pi\hbar)^3\delta^3(\vec{k}-\vec{k}')\int \frac{d^3p}{(2\pi)^3}
\begin{pmatrix}
1 \\
M_0^*c^2/\varepsilon_0^* \\
M_0^*c^2/\varepsilon_0^* \\
\left(M_0^*c^2/\varepsilon_0^*\right)^2 \\
\left(c\vec{p}\cdot\vec{k}/\varepsilon_0^*\right)^2
\end{pmatrix}
\frac{f_n(p)(1-f_n(p))}{\Gamma^2+(\alpha x)^2} \; . \qquad \text{(C.11)}
$$

The rest of the terms read zero where the odd integral over p gives zero in the calculations as

$$
\overline{\tilde{S}_p^{B+}(\vec{k},\omega)\tilde{S}_p^{V+}(\vec{k}',\omega)^*} = \gamma^2(2\pi\hbar)^3\delta^3(\vec{k}-\vec{k}')\int \frac{d^3p}{(2\pi)^3}\left(\frac{c\vec{p}\cdot\vec{k}}{\varepsilon_0^*}\right)\frac{f_p(p)(1-f_p(p))}{\Gamma^2+(\alpha x)^2} = 0 \qquad \text{(C.12)}
$$

and

$$
\begin{aligned}
&\overline{\tilde{S}_p^{V+}(\vec{k},\omega)\tilde{S}_p^{B+}(\vec{k}',\omega)^*} = 0 \\
&\overline{\tilde{S}_p^{S+}(\vec{k},\omega)\tilde{S}_p^{V+}(\vec{k}',\omega)^*} = \overline{\tilde{S}_p^{V+}(\vec{k},\omega)\tilde{S}_p^{S+}(\vec{k}',\omega)^*} = 0 \\
&\overline{\tilde{S}_n^{B+}(\vec{k},\omega)\tilde{S}_n^{V+}(\vec{k}',\omega)^*} = \overline{\tilde{S}_n^{V+}(\vec{k},\omega)\tilde{S}_n^{B+}(\vec{k}',\omega)^*} = 0 \\
&\overline{\tilde{S}_n^{S+}(\vec{k},\omega)\tilde{S}_n^{V+}(\vec{k}',\omega)^*} = \overline{\tilde{S}_n^{V+}(\vec{k},\omega)\tilde{S}_n^{S+}(\vec{k}',\omega)^*} = 0 \ .
\end{aligned}
\tag{C.13}
$$

We can define the following integrals

$$
\begin{pmatrix} K_{BB}^{++q} \\ K_{BS}^{++q} \\ K_{SB}^{++q} \\ K_{SS}^{++q} \\ K_{VV}^{++q} \end{pmatrix} = \gamma^2 \int \frac{d^3p}{(2\pi)^3} \begin{pmatrix} 1 \\ M_0^* c^2/\varepsilon_0^* \\ M_0^* c^2/\varepsilon_0^* \\ \left(M_0^* c^2/\varepsilon_0^*\right)^2 \\ \left(c\vec{p}\cdot\vec{k}/\varepsilon_0^*\right)^2 \end{pmatrix} \frac{f_q(p)(1-f_q(p))}{\Gamma^2 + (\alpha x)^2}
\tag{C.14}
$$

and express the source term correlations as

$$
\begin{pmatrix} \overline{\tilde{S}_q^{B+}(\vec{k},\omega)\tilde{S}_q^{B+}(\vec{k}',\omega)^*} \\ \overline{\tilde{S}_q^{B+}(\vec{k},\omega)\tilde{S}_q^{S+}(\vec{k}',\omega)^*} \\ \overline{\tilde{S}_q^{S+}(\vec{k},\omega)\tilde{S}_q^{B+}(\vec{k}',\omega)^*} \\ \overline{\tilde{S}_q^{S+}(\vec{k},\omega)\tilde{S}_q^{S+}(\vec{k}',\omega)^*} \\ \overline{\tilde{S}_q^{V+}(\vec{k},\omega)\tilde{S}_q^{V+}(\vec{k}',\omega)^*} \end{pmatrix} = (2\pi\hbar)^3\delta^3(\vec{k}-\vec{k}') \begin{pmatrix} K_{BB}^{++q} \\ K_{BS}^{++q} \\ K_{SB}^{++q} \\ K_{SS}^{++q} \\ K_{VV}^{++q} \end{pmatrix}
\tag{C.15}
$$

where q denotes the proton or neutron.

By using this definitions, the correlation of the growing mode in Eq. (C.5) is found as,

$$
\begin{aligned}
&\left\{\overline{\left(\delta\rho_p^B(\vec{k})\right)^+}\right\}\left\{\overline{\left(\delta\rho_p^B(\vec{k})\right)^+}\right\}^* \\
= \quad & (2\pi\hbar)^3\delta^3(\vec{k}-\vec{k}')\frac{\hbar^2}{d_\varepsilon^+ d_\varepsilon^{+*}}\Big\{K_{BB}^{++p}|N_1^+|^2 - K_{BS}^{++p}(N_1^+N_2^- + N_2^+N_1^-) + K_{SS}^{++p}|N_2^+|^2 \\
+ \quad & K_{VV}^{++p}|N_3^+|^2 + K_{BB}^{++n}|N_4^+|^2 - K_{BS}^{++n}(N_4^+N_5^- + N_5^+N_4^-) + K_{SS}^{++n}|N_5^+|^2 + K_{VV}^{++n}|N_6^+|^2\Big\} \ .
\end{aligned}
\tag{C.16}
$$

The correlation of the decaying mode can be obtained in a similar manner by using the following relations;

$$\begin{pmatrix} \overline{\tilde{S}_q^{B-}(\vec{k},\omega)\tilde{S}_q^{B-}(\vec{k}',\omega)^*} \\ \overline{\tilde{S}_q^{B-}(\vec{k},\omega)\tilde{S}_q^{S-}(\vec{k}',\omega)^*} \\ \overline{\tilde{S}_q^{S-}(\vec{k},\omega)\tilde{S}_q^{B-}(\vec{k}',\omega)^*} \\ \overline{\tilde{S}_q^{S-}(\vec{k},\omega)\tilde{S}_q^{S-}(\vec{k}',\omega)^*} \\ \overline{\tilde{S}_q^{V-}(\vec{k},\omega)\tilde{S}_q^{V-}(\vec{k}',\omega)^*} \end{pmatrix} = \gamma^2(2\pi\hbar)^3\delta^3(\vec{k}-\vec{k}')\int\frac{d^3p}{(2\pi)^3}\begin{pmatrix} 1 \\ M_0^*c^2/\varepsilon_0^* \\ M_0^*c^2/\varepsilon_0^* \\ \left(M_0^*c^2/\varepsilon_0^*\right)^2 \\ \left(c\vec{p}\cdot\vec{k}/\varepsilon_0^*\right)^2 \end{pmatrix}\frac{f_q(p)(1-f_q(p))}{\Gamma^2+(\alpha x)^2}\ , \tag{C.17}$$

and

$$\begin{aligned} \overline{\tilde{S}_q^{B-}(\vec{k},\omega)\tilde{S}_q^{V-}(\vec{k}',\omega)^*} &= \overline{\tilde{S}_q^{V-}(\vec{k},\omega)\tilde{S}_q^{B-}(\vec{k}',\omega)^*} = 0 \\ \overline{\tilde{S}_q^{S-}(\vec{k},\omega)\tilde{S}_q^{V-}(\vec{k}',\omega)^*} &= \overline{\tilde{S}_q^{V-}(\vec{k},\omega)\tilde{S}_q^{S-}(\vec{k}',\omega)^*} = 0\ . \end{aligned} \tag{C.18}$$

By using the definitions of the K integrals, it can be observed that the correlation of the decaying mode is equal with that of the growing mode,

$$\begin{aligned} &\left\{\overline{\left(\delta\rho_p^B(\vec{k})\right)^+}\right\}\left\{\overline{\left(\delta\rho_p^B(\vec{k})\right)^+}\right\}^* = \left\{\overline{\left(\delta\rho_p^B(\vec{k})\right)^-}\right\}\left\{\overline{\left(\delta\rho_p^B(\vec{k})\right)^-}\right\}^* \\ = \quad & (2\pi\hbar)^3\delta^3(\vec{k}-\vec{k}')\frac{\hbar^2}{d_\varepsilon^+ d_\varepsilon^{+*}}\left\{K_{BB}^{++p}|N_1^+|^2 - K_{BS}^{++p}(N_1^+N_2^- + N_2^+N_1^-) + K_{SS}^{++p}|N_2^+|^2\right. \\ + \quad & \left. K_{VV}^{++p}|N_3^+|^2 + K_{BB}^{++n}|N_4^+|^2 - K_{BS}^{++n}(N_4^+N_5^- + N_5^+N_4^-) + K_{SS}^{++n}|N_5^+|^2 + K_{VV}^{++n}|N_6^+|^2\right\}\ . \end{aligned} \tag{C.19}$$

The same procedure is implemented in order to find the correlations for the mixed modes. The correlations of the source terms are,

$$\begin{pmatrix} \overline{\tilde{S}_q^{B+}(\vec{k},\omega)\tilde{S}_q^{B-}(\vec{k}',\omega)^*} \\ \overline{\tilde{S}_q^{B+}(\vec{k},\omega)\tilde{S}_q^{S-}(\vec{k}',\omega)^*} \\ \overline{\tilde{S}_q^{S+}(\vec{k},\omega)\tilde{S}_q^{B-}(\vec{k}',\omega)^*} \\ \overline{\tilde{S}_q^{S+}(\vec{k},\omega)\tilde{S}_q^{S-}(\vec{k}',\omega)^*} \\ \overline{\tilde{S}_q^{V+}(\vec{k},\omega)\tilde{S}_q^{V-}(\vec{k}',\omega)^*} \end{pmatrix} = \gamma^2(2\pi\hbar)^3\delta^3(\vec{k}-\vec{k}')\int\frac{d^3p}{(2\pi)^3}\begin{pmatrix} 1 \\ M_0^*c^2/\varepsilon_0^* \\ M_0^*c^2/\varepsilon_0^* \\ \left(M_0^*c^2/\varepsilon_0^*\right)^2 \\ \left(c\vec{p}\cdot\vec{k}/\varepsilon_0^*\right)^2 \end{pmatrix}\frac{f_q(p)(1-f_q(p))}{\Gamma^2+(\alpha x)^2}\ , \tag{C.20}$$

and

$$\overline{\tilde{S}_q^{B+}(\vec{k},\omega)\tilde{S}_q^{V-}(\vec{k}',\omega)^*} = \overline{\tilde{S}_q^{V+}(\vec{k},\omega)\tilde{S}_q^{B-}(\vec{k}',\omega)^*} = 0$$
$$\overline{\tilde{S}_q^{S+}(\vec{k},\omega)\tilde{S}_q^{V-}(\vec{k}',\omega)^*} = \overline{\tilde{S}_q^{V+}(\vec{k},\omega)\tilde{S}_q^{S-}(\vec{k}',\omega)^*} = 0\ . \tag{C.21}$$

Then the expressions are found for the mixed terms as

$$\begin{aligned}
&\left\{\overline{\left(\delta\rho_p^B(\vec{k})\right)^+}\right\}\left\{\overline{\left(\delta\rho_p^B(\vec{k})\right)^-}\right\}^* \\
= \quad & \frac{\hbar^2}{d_\varepsilon^+ d_\varepsilon^{+*}}\left\{K_{BB}^{+-p}N_1^+N_1^+ - 2K_{BS}^{+-p}N_1^+N_2^+ + K_{SS}^{+-p}N_2^+N_2^+ + K_{VV}^{+-p}N_3^+N_3^+\right. \\
+ \quad & \left. K_{BB}^{+-n}N_4^+N_4^+ - 2K_{BS}^{+-n}N_4^+N_5^+ + K_{SS}^{+-n}N_5^+N_5^+ + K_{VV}^{+-n}N_6^+N_6^+\right\}
\end{aligned} \tag{C.22}$$

and

$$\begin{aligned}
&\left\{\overline{\left(\delta\rho_p^B(\vec{k})\right)^-}\right\}\left\{\overline{\left(\delta\rho_p^B(\vec{k})\right)^+}\right\}^* \\
= \quad & \frac{\hbar^2}{d_\varepsilon^+ d_\varepsilon^{+*}}\left\{K_{BB}^{+-p}N_1^-N_1^- - 2K_{BS}^{+-p}N_1^-N_2^- + K_{SS}^{+-p}N_2^-N_2^- + K_{VV}^{+-p}N_3^-N_3^-\right. \\
+ \quad & \left. K_{BB}^{+-n}N_4^-N_4^- - 2K_{BS}^{+-n}N_4^-N_5^- + K_{SS}^{+-n}N_5^-N_5^- + K_{VV}^{+-n}N_6^-N_6^-\right\}
\end{aligned} \tag{C.23}$$

with the use of the integrals

$$\begin{pmatrix} K_{BB}^{+-q} \\ K_{SS}^{+-q} \\ K_{VV}^{+-q} \\ K_{BS}^{+-q} \end{pmatrix} = \gamma^2 \int \frac{d^3p}{(2\pi\hbar)^3} \begin{pmatrix} 1 \\ \left(M_0^* c^2/\varepsilon_0^*\right)^2 \\ \left(c\vec{p}\cdot\vec{k}/\varepsilon_0^*\right)^2 \\ M_0^* c^2/\varepsilon_0^* \end{pmatrix} \frac{-\Gamma^2 + (\alpha x)^2}{\left[-\Gamma^2 + (\alpha x)^2\right]^2} f_q(p)\left[1 - f_q(p)\right]\ . \tag{C.24}$$

Now we can write the first term of the spectral intensity of the baryon density correlation function as

$$\tilde{\sigma}_{pp}(\vec{k},t) = \hbar^2 \frac{E_{pp}^+}{\left(\frac{\partial\varepsilon(k,\omega)}{\partial\omega}\right)_{\omega=i\Gamma_k}}(e^{2\Gamma t} + e^{-2\Gamma t}) + \hbar^2 \frac{E_{pp}^{+-} + E_{pp}^{-+}}{\left(\frac{\partial\varepsilon(k,\omega)}{\partial\omega}\right)_{\omega=-i\Gamma_k}} \tag{C.25}$$

where the short-hand notations are used for

$$
\begin{aligned}
E^{+}_{pp} = E^{-}_{pp} &= K^{++p}_{BB}|N^{+}_{1}|^2 - K^{++p}_{BS}(N^{+}_{1}N^{-}_{2} + N^{+}_{2}N^{-}_{1}) + K^{++p}_{SS}|N^{+}_{2}|^2 + K^{++p}_{VV}|N^{+}_{3}|^2 \\
&+ K^{++n}_{BB}|N^{+}_{4}|^2 - K^{++n}_{BS}(N^{+}_{4}N^{-}_{5} + N^{+}_{5}N^{-}_{4}) + K^{++n}_{SS}|N^{+}_{5}|^2 + K^{++n}_{VV}|N^{+}_{6}|^2 \\
\\
E^{+-}_{pp} &= K^{+-p}_{BB}N^{+}_{1}N^{+}_{1} - 2K^{+-p}_{BS}N^{+}_{1}N^{+}_{2} + K^{+-p}_{SS}N^{+}_{2}N^{+}_{2} + K^{+-p}_{VV}N^{+}_{3}N^{+}_{3} \\
&+ K^{+-n}_{BB}N^{+}_{4}N^{+}_{4} - 2K^{+-n}_{BS}N^{+}_{4}N^{+}_{5} + K^{+-n}_{SS}N^{+}_{5}N^{+}_{5} + K^{+-n}_{VV}N^{+}_{6}N^{+}_{6} \\
\\
E^{-+}_{pp} &= K^{+-p}_{BB}N^{-}_{1}N^{-}_{1} - 2K^{+-p}_{BS}N^{-}_{1}N^{-}_{2} + K^{+-p}_{SS}N^{-}_{2}N^{-}_{2} + K^{+-p}_{VV}N^{-}_{3}N^{-}_{3} \\
&+ K^{+-n}_{BB}N^{-}_{4}N^{-}_{4} - 2K^{+-n}_{BS}N^{-}_{4}N^{-}_{5} + K^{+-n}_{SS}N^{-}_{5}N^{-}_{5} + K^{+-n}_{VV}N^{-}_{6}N^{-}_{6} \ .
\end{aligned}
\tag{C.26}
$$

Secondly, we can write the spectral intensity for $\tilde{\sigma}^{BB}_{nn}(\vec{k},t)$ in Eq. (C.1) as

$$
\begin{aligned}
\tilde{\sigma}^{BB}_{nn}(\vec{k},t)(2\pi)^3\delta^3(\vec{k}-\vec{k}') &= \overline{\delta\rho^{B+}_{n}(\vec{k})(\delta\rho^{B+}_{n}(\vec{k}))^*}e^{2\Gamma_k t} + \overline{\delta\rho^{B-}_{n}(\vec{k})(\delta\rho^{B-}_{n}(\vec{k}))^*}e^{-2\Gamma_k t} \\
&+\overline{\delta\rho^{B+}_{n}(\vec{k})(\delta\rho^{B-}_{n}(\vec{k}))^*} + \overline{\delta\rho^{B-}_{n}(\vec{k})(\delta\rho^{B+}_{n}(\vec{k}))^*} \ .
\end{aligned}
\tag{C.27}
$$

By using Eq. (C.3) and the same definitions for the K integrals in Eqs. (C.14) and (C.24), the four terms in this relation can be obtained with the same procedure for $a = b = p$ case. Furthermore, the correlations are found for the growing, decaying and the mixed terms respectively as,

$$
\begin{aligned}
&\left\{\overline{\left(\delta\rho^{B}_{n}(\vec{k})\right)^{+}}\right\}\left\{\overline{\left(\delta\rho^{B}_{n}(\vec{k})\right)^{+}}\right\}^{*} = \left\{\overline{\left(\delta\rho^{B}_{n}(\vec{k})\right)^{-}}\right\}\left\{\overline{\left(\delta\rho^{B}_{n}(\vec{k})\right)^{-}}\right\}^{*} \\
= \ & \frac{\hbar^2}{d^{+}_{\varepsilon}d^{+*}_{\varepsilon}}\left\{K^{++p}_{BB}|N^{+}_{7}|^2 - K^{++p}_{BS}(N^{+}_{7}N^{-}_{8} + N^{+}_{8}N^{-}_{7}) + K^{++p}_{SS}|N^{+}_{8}|^2 + K^{++p}_{VV}|N^{+}_{9}|^2\right. \\
+ \ & \left. K^{++n}_{BB}|N^{+}_{10}|^2 - K^{++n}_{BS}(N^{+}_{10}N^{-}_{11} + N^{+}_{11}N^{-}_{10}) + K^{++n}_{SS}|N^{+}_{11}|^2 + K^{++n}_{VV}|N^{+}_{12}|^2\right\} \ ,
\end{aligned}
\tag{C.28}
$$

$$
\begin{aligned}
&\left\{\overline{\left(\delta\rho^{B}_{n}(\vec{k})\right)^{+}}\right\}\left\{\overline{\left(\delta\rho^{B}_{n}(\vec{k})\right)^{-}}\right\}^{*} \\
= \ & \frac{\hbar^2}{d^{+}_{\varepsilon}d^{+*}_{\varepsilon}}\left\{K^{+-p}_{BB}N^{+}_{7}N^{+}_{7} - 2K^{+-p}_{BS}N^{+}_{7}N^{+}_{8} + K^{+-p}_{SS}N^{+}_{8}N^{+}_{8} + K^{+-p}_{VV}N^{+}_{9}N^{+}_{9}\right. \\
+ \ & \left. K^{+-n}_{BB}N^{+}_{10}N^{+}_{10} - 2K^{+-n}_{BS}N^{+}_{10}N^{+}_{11} + K^{+-n}_{SS}N^{+}_{11}N^{+}_{11} + K^{+-n}_{VV}N^{+}_{12}N^{+}_{12}\right\}
\end{aligned}
\tag{C.29}
$$

and

$$
\begin{aligned}
& \left\{\overline{\left(\delta\rho_n^B(\vec{k})\right)^-}\right\}\left\{\overline{\left(\delta\rho_n^B(\vec{k})\right)^+}\right\}^* \\
= & \frac{\hbar^2}{d_\varepsilon^+ d_\varepsilon^{+*}}\left\{K_{BB}^{+-p}N_7^-N_7^- - 2K_{BS}^{+-p}N_7^-N_8^- + K_{SS}^{+-p}N_8^-N_8^- + K_{VV}^{+-p}N_9^-N_9^-\right. \\
+ & \left. K_{BB}^{+-n}N_{10}^-N_{10}^- - 2K_{BS}^{+-n}N_{10}^-N_{11}^- + K_{SS}^{+-n}N_{11}^-N_{11}^- + K_{VV}^{+-n}N_{12}^-N_{12}^-\right\} .
\end{aligned}
\tag{C.30}
$$

Then $\tilde{\sigma}_{nn}(\vec{k},t)$ can be written as

$$
\tilde{\sigma}_{nn}(\vec{k},t) = \hbar^2\frac{E_{nn}^+}{\left(\frac{\partial\varepsilon(k,\omega)}{\partial\omega}\right)_{\omega=i\Gamma_k}}(e^{2\Gamma t}+e^{-2\Gamma t}) + \hbar^2\frac{E_{nn}^{+-}+E_{nn}^{-+}}{\left(\frac{\partial\varepsilon(k,\omega)}{\partial\omega}\right)_{\omega=-i\Gamma_k}} \tag{C.31}
$$

where

$$
\begin{aligned}
E_{nn}^+ = E_{nn}^- &= K_{BB}^{++p}|N_7^+|^2 - K_{BS}^{++p}(N_7^+N_8^- + N_8^+N_7^-) + K_{SS}^{++p}|N_8^+|^2 + K_{VV}^{++p}|N_9^+|^2 \\
&+ K_{BB}^{++n}|N_{10}^+|^2 - K_{BS}^{++n}(N_{10}^+N_{11}^- + N_{11}^+N_{10}^-) + K_{SS}^{++n}|N_{11}^+|^2 + K_{VV}^{++n}|N_{12}^+|^2 \\
\\
E_{nn}^{+-} &= K_{BB}^{+-p}N_7^+N_7^+ - 2K_{BS}^{+-p}N_7^+N_8^+ + K_{SS}^{+-p}N_8^+N_8^+ + K_{VV}^{+-p}N_9^+N_9^+ \\
&+ K_{BB}^{+-n}N_{10}^+N_{10}^+ - 2K_{BS}^{+-n}N_{10}^+N_{11}^+ + K_{SS}^{+-n}N_{11}^+N_{11}^+ + K_{VV}^{+-n}N_{12}^+N_{12}^+ \\
\\
E_{nn}^{-+} &= K_{BB}^{+-p}N_7^-N_7^- - 2K_{BS}^{+-p}N_7^-N_8^- + K_{SS}^{+-p}N_8^-N_8^- + K_{VV}^{+-p}N_9^-N_9^- \\
&+ K_{BB}^{+-n}N_{10}^-N_{10}^- - 2K_{BS}^{+-n}N_{10}^-N_{11}^- + K_{SS}^{+-n}N_{11}^-N_{11}^- + K_{VV}^{+-n}N_{12}^-N_{12}^- .
\end{aligned}
\tag{C.32}
$$

Finally, let us indicate the spectral intensities for the cross terms $\tilde{\sigma}_{pn}^{BB}(\vec{k},t)$ and $\tilde{\sigma}_{np}^{BB}(\vec{k},t)$. In terms of the growing and decaying modes, they can be shown as

$$
\begin{aligned}
\tilde{\sigma}_{pn}^{BB}(\vec{k},t)(2\pi)^3\delta^3(\vec{k}-\vec{k}') &= \overline{\delta\rho_p^{B+}(\vec{k})(\delta\rho_n^{B+}(\vec{k}))^*}e^{2\Gamma_k t} + \overline{\delta\rho_p^{B-}(\vec{k})(\delta\rho_n^{B-}(\vec{k}))^*}e^{-2\Gamma_k t} \\
&+\overline{\delta\rho_p^{B+}(\vec{k})(\delta\rho_n^{B-}(\vec{k}))^*} + \overline{\delta\rho_p^{B-}(\vec{k})(\delta\rho_n^{B+}(\vec{k}))^*}
\end{aligned}
\tag{C.33}
$$

and

$$
\begin{aligned}
\tilde{\sigma}_{np}^{BB}(\vec{k},t)(2\pi)^3\delta^3(\vec{k}-\vec{k}') &= \overline{\delta\rho_n^{B+}(\vec{k})(\delta\rho_p^{B+}(\vec{k}))^*}e^{2\Gamma_k t} + \overline{\delta\rho_n^{B-}(\vec{k})(\delta\rho_p^{B-}(\vec{k}))^*}e^{-2\Gamma_k t} \\
&+\overline{\delta\rho_n^{B+}(\vec{k})(\delta\rho_p^{B-}(\vec{k}))^*} + \overline{\delta\rho_n^{B-}(\vec{k})(\delta\rho_p^{B+}(\vec{k}))^*} .
\end{aligned}
\tag{C.34}
$$

Furthermore,

$$
\begin{aligned}
& \left\{\overline{\left(\delta\rho_p^B(\vec{k})\right)^+}\right\}\left\{\overline{\left(\delta\rho_n^B(\vec{k})\right)^+}\right\}^* = \left\{\overline{\left(\delta\rho_n^B(\vec{k})\right)^+}\right\}\left\{\overline{\left(\delta\rho_p^B(\vec{k})\right)^+}\right\}^* \\
= & \left\{\overline{\left(\delta\rho_p^B(\vec{k})\right)^-}\right\}\left\{\overline{\left(\delta\rho_n^B(\vec{k})\right)^-}\right\}^* = \left\{\overline{\left(\delta\rho_n^B(\vec{k})\right)^-}\right\}\left\{\overline{\left(\delta\rho_p^B(\vec{k})\right)^-}\right\}^* \\
= & \frac{\hbar^2}{d_\varepsilon^+ d_\varepsilon^{+*}}\left\{K_{BB}^{++p}|N_7^+||N_1^-| - K_{BS}^{++p}(N_7^+N_2^- + N_8^+N_1^-) + K_{SS}^{++p}|N_8^+||N_2^-| + K_{VV}^{++p}|N_9^+||N_3^-|\right. \\
- & \left. K_{BB}^{++n}|N_{10}^+||N_4^-| - K_{BS}^{++n}(N_{10}^+N_5^- + N_{11}^+N_4^-) + K_{SS}^{++n}|N_{11}^+||N_5^-| + K_{VV}^{++n}|N_{12}^+||N_6^-|\right\}
\end{aligned}
\tag{C.35}
$$

and

$$
\begin{aligned}
& \left\{\overline{\left(\delta\rho_p^B(\vec{k})\right)^+}\right\}\left\{\overline{\left(\delta\rho_n^B(\vec{k})\right)^-}\right\}^* = \left\{\overline{\left(\delta\rho_n^B(\vec{k})\right)^+}\right\}\left\{\overline{\left(\delta\rho_p^B(\vec{k})\right)^-}\right\}^* \\
= & \left\{\overline{\left(\delta\rho_p^B(\vec{k})\right)^-}\right\}\left\{\overline{\left(\delta\rho_n^B(\vec{k})\right)^+}\right\}^* = \left\{\overline{\left(\delta\rho_n^B(\vec{k})\right)^-}\right\}\left\{\overline{\left(\delta\rho_p^B(\vec{k})\right)^+}\right\}^* \\
= & \frac{\hbar^2}{d_\varepsilon^+ d_\varepsilon^{+*}}\left\{K_{BB}^{+-p}|N_7^+||N_1^-| - K_{BS}^{+-p}(N_7^+N_2^+ + N_8^+N_1^+) + K_{SS}^{+-p}|N_8^+||N_2^+| + K_{VV}^{+-p}|N_9^+||N_3^+|\right. \\
- & \left. K_{BB}^{+-n}|N_{10}^+||N_4^+| - K_{BS}^{+-n}(N_{10}^+N_5^+ + N_{11}^+N_4^+) + K_{SS}^{+-n}|N_{11}^+||N_5^+| + K_{VV}^{+-n}|N_{12}^+||N_6^+|\right\} \ .
\end{aligned}
\tag{C.36}
$$

Then we obtained the cross term spectral intensities as

$$
\tilde{\sigma}_{pn}(\vec{k},t) = \tilde{\sigma}_{np}(\vec{k},t) = \hbar^2 \frac{E_{pn}^+}{\left(\frac{\partial\varepsilon(k,\omega)}{\partial\omega}\right)_{\omega=i\Gamma_k}}(e^{2\Gamma t} + e^{-2\Gamma t}) + \hbar^2 \frac{2E_{pn}^{+-}}{\left(\frac{\partial\varepsilon(k,\omega)}{\partial\omega}\right)_{\omega=-i\Gamma_k}} \tag{C.37}
$$

with the short-hand notations

$$
\begin{aligned}
E_{pn}^+ = E_{np}^+ &= K_{BB}^{++p}N_7^+N_1^- - K_{BS}^{++p}(N_7^+N_2^- + N_8^+N_1^-) + K_{SS}^{++p}N_8^+N_2^- + K_{VV}^{++p}N_9^+N_3^- \\
&- K_{BB}^{++n}N_{10}^+N_4^- - K_{BS}^{++n}(N_{10}^+N_5^- + N_{11}^+N_{4^-}) + K_{SS}^{++n}N_{11}^+N_5^- + K_{VV}^{++n}N_{12}^+N_6^-
\end{aligned}
$$

$$
\begin{aligned}
E_{pn}^{+-} = E_{np}^{+-} &= K_{BB}^{+-p}N_7^+N_1^+ - K_{BS}^{+-p}(N_7^+N_2^+ + N_8^+N_1^+) + K_{SS}^{+-p}N_8^+N_2^+ + K_{VV}^{+-p}N_9^+N_3^+ \\
&- K_{BB}^{+-n}N_{10}^+N_4^+ - K_{BS}^{+-n}(N_{10}^+N_5^+ + N_{11}^+N_{4^+}) + K_{SS}^{+-n}N_{11}^+N_5^+ + K_{VV}^{+-n}N_{12}^+N_6^+ \ .
\end{aligned}
\tag{C.38}
$$